MONITORING AN INDUSTRIAL HYDROCYCLONE USING FREQUENCY DOMAIN MULTIPLEXING ELECTRICAL IMPEDANCE TOMOGRAPHY

Prepared For: The Department of Electrical Engineering at the University of Cape Town

Prepared By: V. C. Capindissa

Date: May 3, 2005

Keywords: Tomography, Hydrocyclone

Dissertation submitted in partial fulfilment of the requirements of the degree of Master of Science (MSc) in Electrical Engineering at the University of Cape Town

DECLARATION

I, VLADIMIR C. CAPINDISSA, declare that this dissertation is my own work. It is being submitted for the degree of Master of Science in Electrical Engineering at the University of Cape Town. It has not been submitted before for any degree, examination or university.

Signature---------- on the 3rd day of May 2005

ACKNOWLEDGMENTS

In loving memory of my brother, Edson Calazange Capindissa Nobre, you will always be remembered.

The author wishes to thank Prof. Jonathan Tapson for his knowledgeable supervision, continuous guidance and assistance. The author would also like to express thanks to Mr. Glen Newins from UCT Mechanical Engineering Department workshop for his work in built the cylindrical and conical section of the hydrocyclone, Mr Robert Oliver UCT Geology Department's workshop for manufacturing and supplying the gravel samples and Mr. Kenneth Maseko from UCT Chemical Engineering Department workshop for all help his with the hydrocyclone.

Special thanks to Professor Rubens Sampaio - Mechanical Engineering Department Catholic University of Rio de Janeiro, PUC-RIO, RJ Brasil, for all your attention.

Mr. Aubrey Mainza, from UCT Chemical Engineering Department. Thank you for the insightful discussions.

David Sharp thanks for the friendship and support.

Finally all students and staff not mentioned here that made this work possible thank you very much.

Last but not least Liv for all your stressing on my behalf thank you.

TERMS OF REFERENCE

Professor Jonathan Tapson, the coordinator of the tomography group for the Department of Electrical Engineering of the University of Cape Town, commissioned this project on July 14 2003. This thesis will be used as the first approach on monitoring and controlling hydrocyclones at University of Cape Town.

His specific instructions were to:

- To design sensors that can be used on the tomographic system.
- To describe the criteria that plays a role in determining the use of the sensors on the tomography system.
- To set out a comprehensive manner of analysing a hydrocyclone.
- To propose technique(s) of monitoring a hydrocyclone.
- To make recommendations for possible new designs of sensors and circuitries for future use in the University of Cape Town tomography research group.

SYNOPSIS

This thesis describes the implementation of an Electrical Impedance Tomography (EIT) system using Frequency Domain Multiplexing (FDM) to monitor an industrial hydrocyclone.

In order to utilise resources more effectively, to reduce negative environmental impact, to satisfy demands and legislations on product quality, there has been a rapid increase in research for optimisation and control of hydrocyclones, as industries consistently demand new and more cost effective ways of production.

In an industrial setup, it is very difficult to determine the optimal operating point of a hydrocyclone. Tomography offers an exceptional opportunity to untangle the intricacies of the separation process structures without the intrusion of the sensing equipment or having to interfere with the process.

The use of an Electrical Resistance Tomography (ERT) system with Time Domain Multiplexing (TDM) is one method used to try and solve this optimisation problem. At the University of Cape Town (UCT), an innovative Electrical Impedance Tomography (EIT) system using Frequency Domain Multiplexing (FDM) which is inherently faster than ERT TDM. This system increased the likelihood that a faster frame rate may be achieved for image reconstruction.

To gain in-depth understanding of the several aspects involved in this research project, books, articles and internet sites on the design, construction, control of hydrocyclones and the different types of tomography schemes were consulted; as well as interviews and discussions with staff and students from University of Cape Town.

This project focuses on the size and stability of the air core. An 8 electrode FDM EIT was used on a 50 mm diameter Krebs hydrocyclone to monitor the behaviour of the air core. Results from the dynamic performance have shown that volume fraction prediction is a good indicator to observe the behaviour of the air core, as it allows for quantitative, numeric interpretation or comparison of the data.

LIST OF ILLUSTRATIONS

Equations **page**

Figures **page**

Tables **page**

TABLE OF CONTENTS

CHAPTER 1

INTRODUCTION

1.1. SUBJECT

This thesis describes the implementation of an Electrical Impedance Tomography (EIT) system using Frequency Domain Multiplexing (FDM) to monitor an industrial hydrocyclone.

1.2. BACKGROUND TO THE THESIS

In an industrial setup, it is very difficult to determine the optimal operating point of a hydrocyclone. This is due to the complex parameters associated with the process while pursuing a good quality, quantity and size of the final product demanded. These parameters are determined by the size of hydrocyclone and the pressure of the feed to the hydrocyclone; the last factor in turn is determined by the pump size and speed.

These conditions introduce an operating cost for the use of hydrocyclones in industrial plants. Furthermore, the absence of strategies for controlling hydrocyclones restricts the use of remote monitoring.

To address the problem a research project on operating conditions of a hydrocyclone was initiated. The aim was to find ways to introduce online measurement to acquire data to be used in monitoring and control strategies, also with possible use to model the fluid dynamics inside the hydrocyclone.

The use of an Electrical Resistance Tomography (ERT) system with Time Domain Multiplexing (TDM) [2] is one method used to try and solve this optimisation problem. At the University of Cape Town (UCT), Teague [25] and Giannopoulos [26], under the guidance of professor Tapson, developed an innovative Electrical Impedance Tomography (EIT) system using Frequency

Domain Multiplexing (FDM) which is inherently faster than ERT TDM. This system increased the likelihood that a faster frame rate may be achieved for image reconstruction.

The project was divided into five parts:

1. The study of tomography schemes.
2. The study of hydrocyclone operating conditions.
3. The design and construction of the sensors to capture the necessary data.
4. The implementation of an 8 electrode FDM EIT on a hydrocyclone and image reconstruction of the data.
5. Extension of the design to a 16 electrode FDM EIT.

1.3. CORE ASPECT OF THIS THESIS

The main purpose this thesis is to design and implement sensors that are able to perform at a satisfactory level on a tomographic system, as well as to theorise on possible effective methods and procedures to monitor and control an industrial hydrocyclone.

1.4. OBJECTIVES

The objectives of this thesis include:

- To design sensors to be used on the tomographic system.
- To describe the criteria that plays a role in determining the use of the sensors on the tomographic system.
- To set out a comprehensive manner of analysing a hydrocyclone.
- To propose technique(s) of monitoring and controlling a hydrocyclone.
- To make recommendations for possible new designs of sensors and circuitries for future use in the University of Cape Town tomography research group.

1.5. METHODS USED TO GATHER INFORMATION

The information, on which this report is based, was gathered by means of:

- Lecture notes from the University of Cape Town on sensor and circuitry design.
- Books on tomography, circuitry, measurements, sensors and electronics.
- Articles and thesis on tomography and hydrocyclones.
- The use of internet sites with relevant information on tomography, hydrocyclones, sensors and circuitry design.
- Information obtained from staff and students through discussions at the University of Cape Town.
- Discussions of the UCT tomography research group.

1.6. SCOPE AND LIMITATIONS

The information is restricted to electrical tomography systems, whereby emphasis is placed on FDM EIT.

This thesis is part of a larger project for the University; therefore some facets were designed and developed by other members of the UCT tomography research group and only their results are described here, in order to present a more complete picture of the project.

The focus on FDM EIT and dependence on preceding results from the group has resulted in a few minor negative complications during various design, development and implementation stages of this project.

Testing of hydrocyclones was limited to the only available hydrocyclone, which was a 50 mm diameter one, due to unavailability of a larger size one for this particular use.

1.7. PLAN OF DEVELOPMENT

This thesis begins by reviewing the literature review in chapter 2. It then describes the implementation of an 8 electrode circuit and image reconstruction in chapter 3. This is followed by in-depth explanation of the design of the sensor unit in the form of conductive probes and capacitor plates in chapter 4.

Then a discussion of the performance of the system is done in chapter 5. The description of monitoring an operating hydrocyclone followed in chapter 6.

In chapter 7 conclusions based on the performance of the FDM EIT system and on the research are drawn. Finally, based on the performance of the FDM EIT system and on the conclusions, recommendations to current and future works of the University of Cape Town's tomography research group are made in chapter 8.

CHAPTER 2

LITERATURE REVIEW

2. LITERATURE REVIEW

To gain in-depth knowledge of the several aspects involved in this research project, the work done by previous researchers had to be consulted. Investigation was conducted on the design, construction and control of hydrocyclones as well as a study on the different types of tomography schemes.

2.1. THE HYDROCYCLONE

In recent years, there has been a rapid increase in research for optimisation and control of hydrocyclones as industries consistently demand new and more cost effective ways of production.

A hydrocyclone is a density separator that uses the principle of centrifugal sedimentation to remove or classify particles from a fluid by converting pressure energy into rotational moment. The rotational moment provides the necessary centrifugal force required to separate particular matters from a primary liquid on the basis of size, shape and density.

Due to their simple physical design and robustness while in operation, hydrocyclones have a wide use in industry. Hydrocyclones are designed to perform specific functions, and therefore differ from one another according to what is expected during their operating life span. Over time, different shapes have been proposed, but only the conical and cylindrical shapes are commonly used in industry, with the conical being the most common one [12].

Although there might be differences between hydrocyclone designs, a few common features are expected across all hydrocyclones. These include the following:

- high separation performance;
- controllability and
- cost effectiveness.

Due to its interdisciplinary nature, the study of the properties and fluid dynamics of the conical hydrocyclones, first patented in 1891 by Bretney [12], has been one with a lot of input from a variety of researchers in different fields.

Most of the studies performed were to try to understand and model the fluid dynamics inside the hydrocyclone, and thereafter to understand its separation efficiency. Even though a lot of time and thought has been put into these studies, the ability to understand the separation efficiency of the hydrocyclone is still incomplete [6, 22]. This is because hydrocyclones operate under a very large number of parameters that operate simultaneously [5, 10]. However, researchers tend to investigate one or more of those parameters that determine separation efficiency, while assuming that the others are constant or ignoring them completely [1].

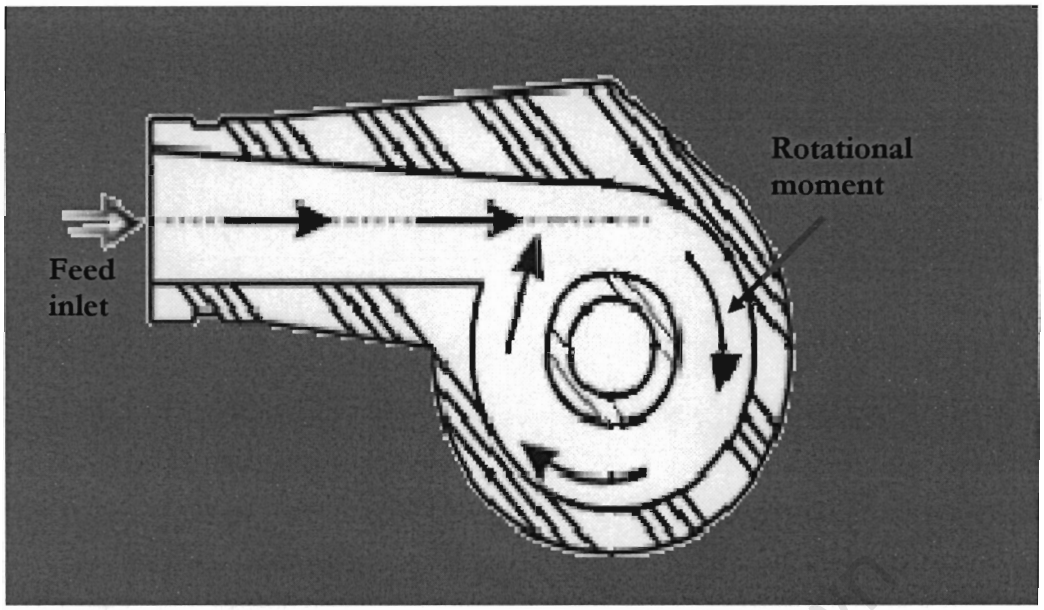

Fig. 2.1 Rotational Moment created from the tangential feed (Adapted from the web page: Spintophydrocyclone.htm [35])

A hydrocyclone operates as follows: the pressurised slurry is fed tangentially into the hydrocyclone creating a rotational moment [4, 13], as shown in fig 2.1. The centrifugal force generated causes the heavier suspended particles to move to the wall [4], while the radial velocity forces the liquid and lighter gravity particles to move inward toward the centre.

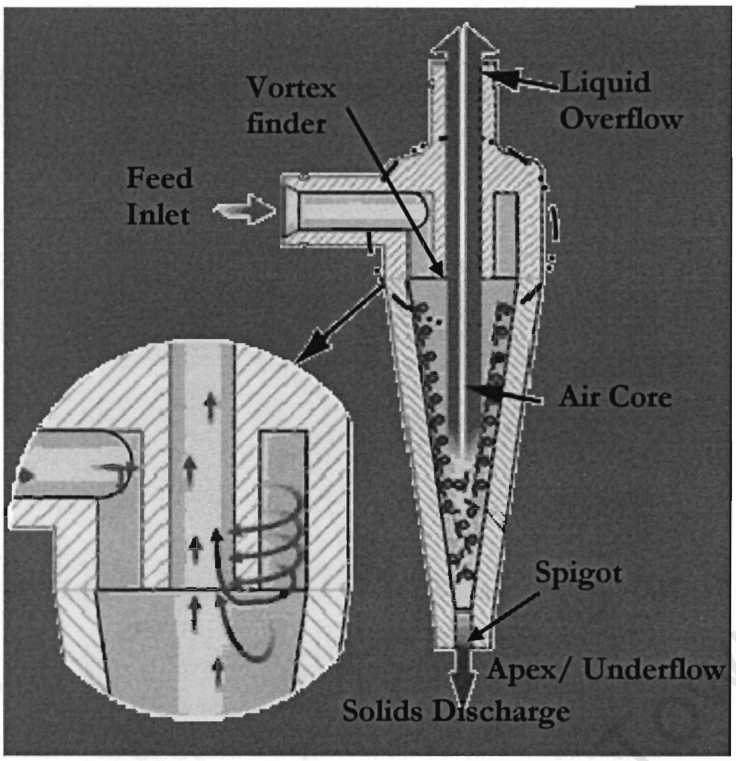

Fig. 2.2 Side cross-section of an operating hydrocyclone (Adapted from the web page: Spintophydrocyclone.htm [35])

Two vortexes are formed [12, 13]; one carries the heavy particles to the apex (this is also known as the underflow). The spigot orifice (see fig. 2.2) permits the heavier particles and a small amount of the liquid to be discharged. Air is drawn through the apex and the second developing vortex carries the cleaned liquid and lighter gravity particles out through the vortex finder tube, also known as the overflow.

The pressure in the central part of the hydrocyclone decreases to a level smaller than the atmospheric pressure [4], due to high tangential velocity of the fluid. The low pressure region created causes the formation of an air core about the central line along the entire body [4, 9, 13], as seen in fig 2.2.

2.1.1. The Air Core

For many years this air core, in the internal flow of the hydrocyclone, was elusive to many researchers. Due to the nature of the process, most hydrocyclones are made out of metal, and also the slurry is often dense [6], making the air core dynamics the least observable factor governing the flow split [1, 4, 6, 13, 17].

Recently the importance of the air core has been acknowledged by all major institutions which are engaged in the study of flow patterns and efficiency of hydrocyclones [5, 13]. They have come to agree that both the air core size and its stability are of extreme importance when trying to describe the fluid mechanics inside of hydrocyclones.

Predictions of the diameter of an air core are given as a function of various hydrocyclone geometries and operational conditions [3, 4, 5, and 13]. Under operating conditions many researchers [1, 3, 4, 5, and 6] have concluded that the pressure of the feed is the primary element in the creation of an air core i.e. an increase in the pressure of the feed flow causes the diameter of the air core in the hydrocyclone to increase. Nevertheless it is also known that the pressure of the feed can only be increased up to a specific point, and beyond this critical point the air core decreases and collapses [5]. Cullivan et. al. [9] went further and attributed the creation and stability (or collapse) of an air core as a function of transport, hence negating pressure driven theory.

It is also believed that the shape of the discharge at the underflow determines the separation performance of the hydrocyclones [3, 8, and 13]. Moreover it is stated that the presence or rather the disappearance of the air core is associated with a transition from a spray to a roping type underflow discharge [3, 6, and 8].
An underflow discharge in the form of roping flow is characterized by high slurry viscosity [5], and for such viscous slurry the air is not inhaled through the apex [3]. According to Romero et. al. [4] the addition of solid particles to the fluid medium causes a change in viscosity, so the

presence of solid particles increases the viscosity of the suspension significantly in relation to the viscosity of the pure fluid.

However spray/roping discharges are more of an effect than a cause of an air core. Therefore they can be used as a guideline for visual monitoring [1, 6], or for setup of the equipment. As spray discharge exists when the air core is present and the roping discharge will appear as the air core collapses [1, 3, and 8].

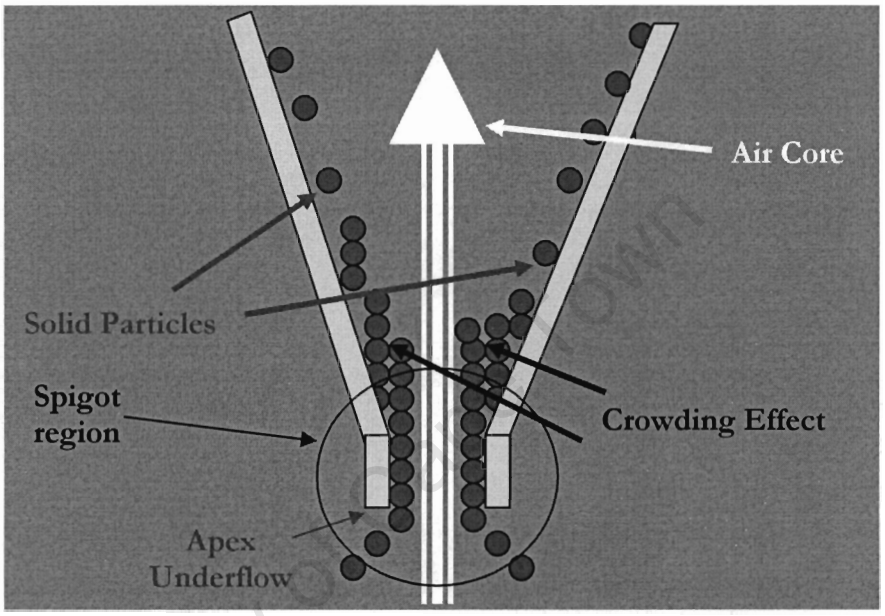

Fig. 2.3 The crowding effect at the spigot region

The collapse of the air core can be explained by the crowding effect theory [33]. The crowding effect (fig. 2.3) refers to the crowding of particles between the air core and the conical wall near the spigot region as a function of the pressure feed and slurry concentration (viscosity).

The crowding effect is directly proportional to the pressure of the feed; an increase in the pressure of the feed leads to an increase in the tangential velocity which in turn causes the flow of solids along the conical wall to increase.

The crowding effect varies with the slurry concentration. The more concentrated the slurry the faster the air core will collapse because more particles exist in the suspension, therefore more particles will move to the spigot region (apex or underflow) [1, 6]. The moment the bulk of

solids in the spigot becomes greater than the solids capacity of the spigot pipe, there is saturation at the spigot region. Consequently a portion of the coarse particles are carried upwards to the overflow collapsing the separation process of the hydrocyclone. As Firth [10] stated, the separation capability of a cyclone is strongly determined by the capacity of the spigot to handle the amount of material moving through the underflow, and the size distribution of the feed.

Initially it was assumed that the air core was cylindrical and symmetrical at the center of the hydrocyclone [4, 5, and 6]. However later results from Dyakowski and Williams [3] have demonstrated the existence of a conical air core, and that the angle of the cone is dependent on the concentration of the slurry. They also observed that an increase in the slurry viscosity causes a decrease in the diameter of the air core. i.e. air core stability decays with high slurry viscosities [3].

Firth [10] observed that while in operation the conical vessel experiences more intense turbulence near the spigot than anywhere else. Monredon [14] discovered that by varying the size of the diameter of the spigot while working with a fixed slurry concentration, the stability of the air core improved with the increase in size of the spigot.

These experiments take into account the geometrical properties of the hydrocyclone and how it plays a role in the prediction of the appearance and stability of the air core; and provide an alternative if not a holistic view on the air core compared to previous theories discussed.

Concha et al [16] went as far as to conclude that the feed and the concentration of the slurry alone are not enough to determine the type of the discharge in a hydrocyclone. This also means that the cause of the appearance of the air core is not linked to the feed and concentration of the slurry alone.

Furthermore, Concha et al [16] state that, with a given feed or concentration of the slurry, any type of discharge can be obtained by changing the spigot and/or the vortex finder size.

The work of Concha et al [16], following the work of Plitt et al [23] and Bustamente et al (as stated in the work of Concha et. al. [16]), resulted in the development of a formula to calculate the size of the diameter of the air core based on the ratio of the underflow diameter (apex) to the overflow diameter (vortex) (d_u/d_o).

Bustamente et al study (as stated in the work of Concha et. al. [16]) state that the ratio of the underflow diameter to overflow diameter (d_u/d_o) separates the region of rope and spray discharge as follows:

For values of $d_u/d_o < 0.34$ only spray discharge is obtained i.e. the air core exists.

For values of $0.34 < d_u/d_o < 0.50$ spray, semi-rope or rope can occur depending on pressure and other variables i.e. the air core may or may not exist.

For values of $0.50 < d_u/d_o < 0.90$ only rope discharge is obtained i.e. the air core does not exist.

In their work Concha et al [16] the limit numbers were different from Bustamente et al study (as stated in the work of Concha et. al. [16]), whereby the range for spray and rope discharges were as follows:

For values of $d_u/d_o > 0.56$ only spray discharge is obtained i.e. the air core exist.

For values of $0.56 > d_u/d_o > 0.45$ spray, semi-rope or rope can occur depending on other variables i.e. the air core may or may not exist.

For values of $d_u/d_o < 0.45$ only rope discharge is obtained i.e. the air core does not exist.

Among researchers there is a common sense that the air core diameter size and stability are good indicators of the flow conditions in a hydrocyclone, therefore, if the air core can be controlled, the flow conditions in the hydrocyclone can be controlled [3, 4].

2.2. TOMOGRAPHY SCHEMES

In order to utilise resources more effectively, to reduce negative environmental impact, to satisfy demands and legislations on product quality, industry has been put under pressure to find new ways of production [29]. Hence it has become most important to gain in-depth knowledge about the exact internal flow behaviour of the process equipment.

Tomography offers an exceptional opportunity to untangle the intricacies of the separation process structures without the intrusion of the sensing equipment or having to interfere with the experiment. Tomographic technologies involve acquisition of measurement signals from sensors located on the periphery of an object such as a process vessel or pipeline [29, 32].

Most tomographic technologies are concerned with extraction of information from a process or subject, to form a cross-sectional image [32]. One such method utilises an array of sensors placed in parallel so that their sensing field interrogates a projection of a suitable signal across the subject, which is assumed to be circular in cross-section. In order to explore the entire cross section it is necessary to obtain the other projections by rotating the subject in the direction normal to the direction of the sensor field, or preferably to rotate the measurement sensor, around the subject. It may not always be possible to adopt such methodology since it may be physically impractical to rotate the subject, or the sensors, and the time required to rotate the assembly may be too long compared to changes occurring within the subject under the investigation [29, 32].

A good tomographic system should possess two important qualities, which are non-invasive and non-intrusive. On the non-invasive front a tomographic system should not necessitate any breach on the walls of the process vessel, for instance, by the introduction of conductive probes; and to satisfy the non-intrusive quality it should not disturb the nature of the process being examined. It is not always feasible to satisfy both requirements although the latter can be satisfied to a higher degree [29, 32].

The vital part of any tomographic technique is the sensor system that is deployed. The bases of any measurement are to discern and make the most of the differences in the properties of the process being examined. A variety of sensing methods can be employed based on measurements of transmission, diffraction or electrical phenomena [29, 32]. The table 2.1 below shows a selection of possible sensing methods and their principal attributes.

Table 2.1 Sensors for Process Tomography (adapted from M.S. Beck and R.A. Williams [29, 32])

Principle	Spatial resolution (percentage of diameter of cross section)	Practical realization	Comments
Electromagnetic Radiation	1%	Optical	-Fast -Optical access required
		X-ray and γ-ray	-Slow -Radiation containment
		Position emission	-Labeled particles -Not on-line
		Magnetic resonance	-Fast -Expensive for large vessels
Acoustics	3%	Ultrasonic	-Sonic speed limitations -Complex use
Measurement of electrical properties	10%	Capacitive Conductive Inductive	-Fast -Low cost -Suitable for small or large vessels

However it should be bared in mind that obtaining a high quality computed "image" represents only the initial stage of information input to the process engineer. The ultimate goal is to provide process engineer with a quantitative, numeric, interpretation of an image. Dependency on visual diagnosis based on glancing at the images will be, in most cases inadequate, except perhaps to diagnose gross malfunction during a process [29, 32].

This thesis concentrates on the measurement of the electrical properties of the subjects under the investigation by applying capacitive and conductive tomographic techniques as subsequently discussed.

2.2.1 ELECTRICAL CAPACITANCE TOMOGRAPHY

In electrical capacitance tomography (ECT) the measurement principle is based on the principle that the capacitance between two plates is a function of the permittivity of the components in the measurement volume as well as of their distribution. The relationship between the permittivity, the spatial distribution of the permittivity and the resulting capacitance can be derived from Maxwell's equations [30].

An ECT system consists of the primary sensor system, the sensor electronics and capacitance measurement instrument, and a computer for the image reconstruction [30]. The sensor(s) are often made of copper foils and generally consists of peripherally mounted electrodes which are non-invasive and non-intrusive. The sensors also have a casing that provides mechanical stability and electromagnetic stray immunity [30].

Sampling of electrodes is conducted by the use of sensor electronics, whereas the measurement instrument is used for measurement of the capacitance between the electrodes [30]. The set of measurements is transmitted to a computer, in which the reconstruction is done. To avoid outside electromagnetic interference with the measurements, an earthed radial shield guards the measurement electrodes [30].

A signal generator is applied to drive one electrode of the unknown capacitance. The resulting current on the other electrode is converted to voltage and then amplified. By using a 90° phase-shifted reference voltage a demodulation is possible and a capacitance-proportional analogue signal is available [30].

2.2.2 ELECTRICAL RESISTANCE TOMOGRAPHY

In contrast to electrical capacitance tomography systems (ECT), the sensors in electrical resistance tomography (ERT) system are required to be in permanent contact with the conductive liquid inside the process vessel [27, 31], in some cases making them both intrusive and invasive. In addition the sensors have to be more conductive than the liquid, to avoid problems from contact impedance [32], and also to obtain reliable measurements [27, 31]. For the majority of process applications, the electrodes are metallic and are typically fabricated from brass, stainless steel, silver, gold, platinum, silver palladium or any other suitable material that demonstrate a number of properties. These properties in non-inferred order of priority are: low cost, ease of fabrication and installation, good electrical conduction and resistance to abrasion and corrosion. The electrodes are placed equally distant around the process vessel to map resistivity changes across the plane or planes of interest [31].

The size of the electrodes is an important factor, because considerations must be given to the largely used current- injection and voltage measuring ERT system. Hence a large surface area is required for the current-injecting electrodes, to ensure that an even current density is generated within the vessel. However when detecting the resultant equi-potential a small surface area, ideally a needle point, is optimal to avoid averaging several equi-potentials [27, 31].

Finally, also requiring consideration is the signal-carrying cables between the electrodes and the current injection/voltage measurement circuitry when building the sensors into the vessel. Longer cables are associated with bigger stray capacitance and the current leakage, which consequently result in highly undesirable phase shifting signals. In addition the cabling can act as an antenna and is affected by electromagnetic interference which is prevalent in process environments with heavy duty electrical machinery (such as pumps) and associated equipment [27, 31].

2.2.3 ELECTRICAL IMPEDANCE TOMOGRAPHY

Given that in capacitance tomography, the difference in relative permittivity is imaged, it can not be determined whether one phase with a certain permittivity or a mixture of two phases yielding the same permittivity is present. In order to distinguish between more than two phases present in the measurement volume, either all phases but the two phases need to be immobile, or an additional imaging system has to be employed [30].

The use of an additional imaging system also includes a vast variety of different impedance tomography systems, whereby in addition to the permittivity, the conductivity of the phase is imaged [30]. This is also known as a dual modality measurement system. At UCT it is known as impedance measurement as the permittivity and conductivity are treated as impedances.

2.2.4 TIME DOMAIN MULTIPLEXING

In time domain multiplexing, electrical impedance tomography (EIT), a signal with a fixed frequency is injected through one electrode and is measured on the other remaining electrodes.

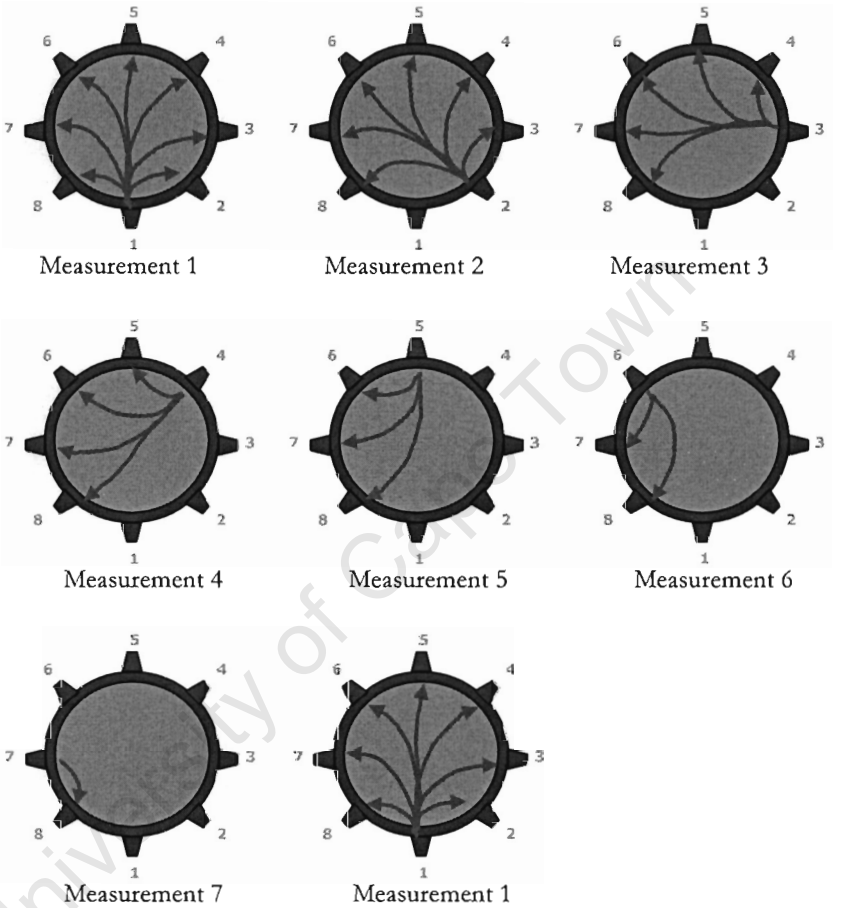

Fig. 2.4 A set of time domain measurements scheme (the numbers 1 to 8 around the vessel are bi-directional electrodes, the arrows indicate the direction of the signal)

The signal is then shifted to the next electrode and a similar measurement to the previous one is taken ignoring the already taken one. This is done until all electrodes are covered giving 28 independent measurement paths, and that forms the first set of readings. One such set is shown in the fig 2.4 above which is an illustration adapted from Smit [27].

2.2.5 FREQUENCY DOMAIN MULTIPLEXING

In frequency domain multiplexing there are dedicated transmitters and dedicated receivers. Each transmitter has a fixed frequency so at any one moment all the frequencies are present. The set of signal paths are shown in fig. 2.5 below.

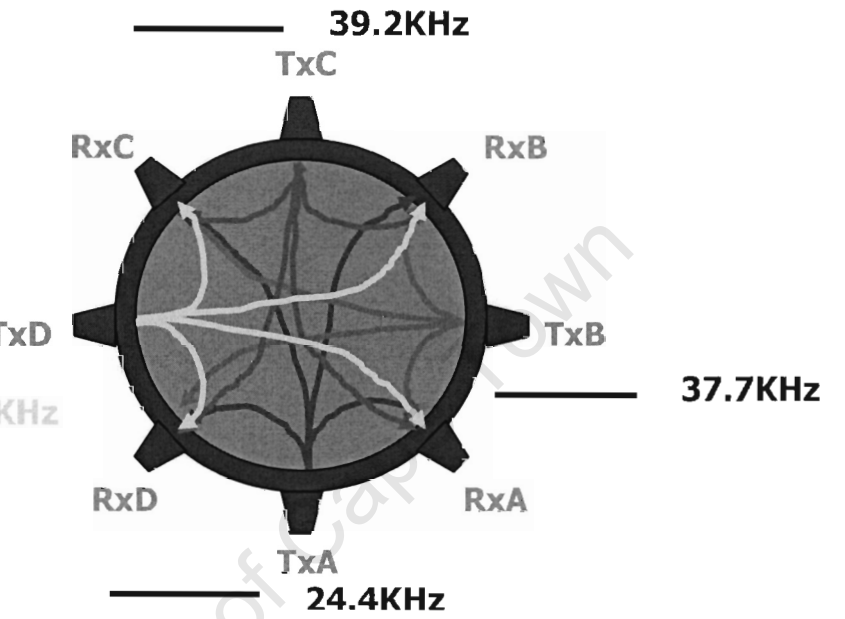

Fig. 2.5 A set of frequency domain measurement scheme

The figure shows an example of an 8 electrode system where there are four fixed transmitter channels and four fixed receiver channels. The four transmitter frequencies are 24.4 kHz on channel A (TxA), 37.7 kHz on channel B (TxB), 39.2 kHz on channel C (TxC) and 46.5 kHz on channel D (TxD). The receivers are: RxA on channel A, RxB on channel B, RxC on channel C and RxD on channel D. Each receiver captures signals from all four transmitters.

CHAPTER 3

THE 8 ELECTRODE FDM EIT SYSTEM

3. THE 8 ELECTRODE FDM EIT SYSTEM

This chapter describes how the Electrical Impedance Tomography (EIT) system using Frequency Domain Multiplexing (FDM) system monitors the changes in capacitance and resistance resulting from the insertion (appearance) of air and/or gravel in a water medium, and then how the information is handled in a computer as databases used by the neural network for training and testing itself.

3.1. THE SYSTEM

The FDM EIT system was first developed by G. Teague in his PhD study [25] following the work of Q. Smit in his MSc. study [27] and then the FDM EIT system was improved by A. Giannopoulos in his MSc. study [26]. The difference between Smit's [27], Teague's [25] and Giannopoulos's [26] studies is that Smit's [27] used single frequency (time domain multiplexing) while Teague [25] and Giannopoulos [26] used multiple frequencies (frequency domain multiplexing). The main difference between Teague's [25] and Giannopoulos's [26] studies is Teague [25] used square waves as his injected signals, and Giannopoulos [26] used sine waves. For this application the improved system by Giannopoulos [26] was used, however all other aspects from Teague, Tapson and Smit [11] and Teague [25] were used, such as the air and gravel placement system as well as the reconstruction system.

The FDM EIT system consists of:

- The primary sensor
- The frequency generating boards
- The transmitter and receiver boards
- The synchronous detection boards
- The sampler controller board
- The reconstruction software

The figure below shows the interactions of the different parts of the system.

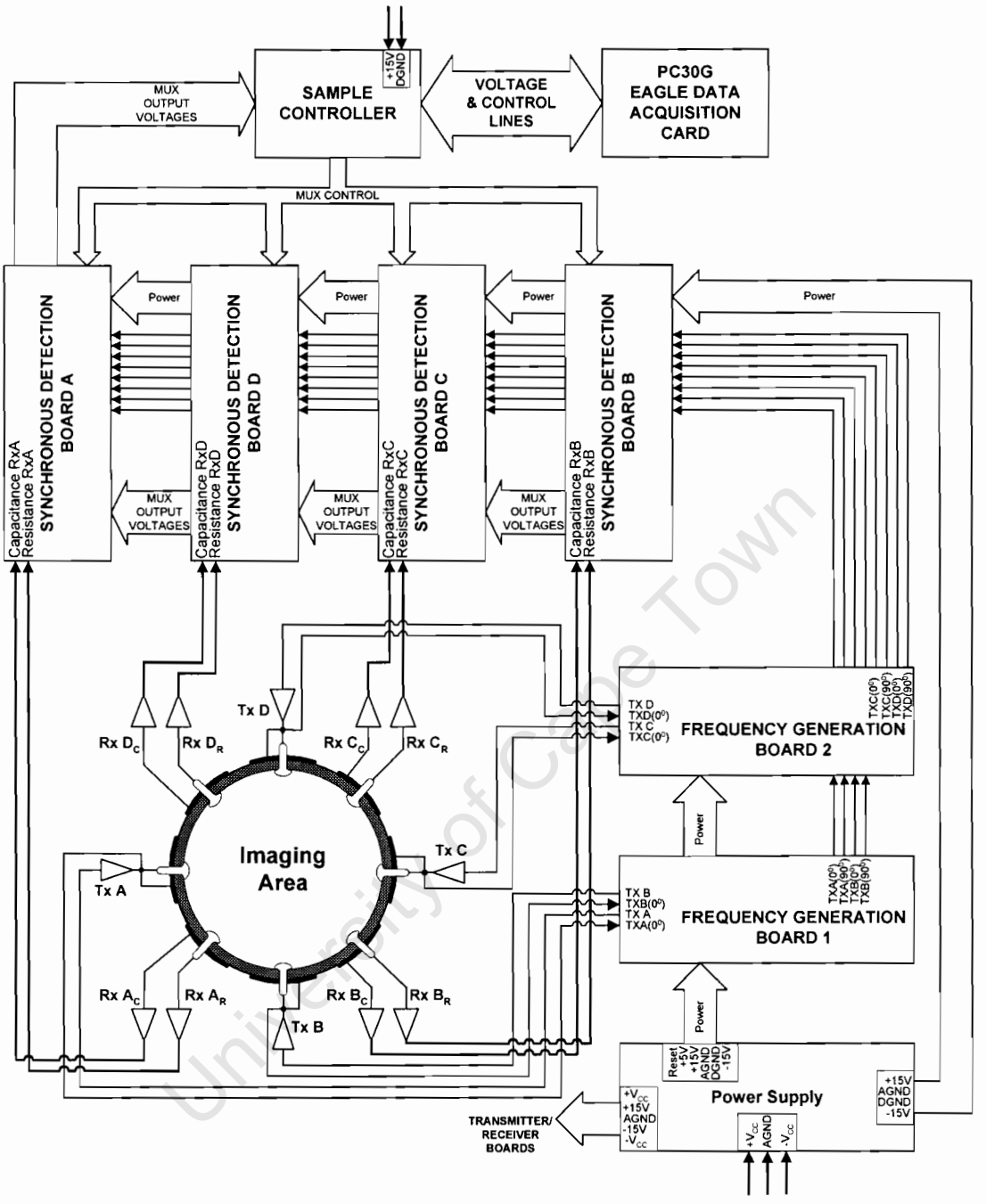

Fig. 3.1 Eight electrodes FDM EIT system (picture from Giannopoulos [26])

In the figure 3.1, the power supply unit regulates the voltage and supplies power to all other units. The frequency generating board generates the four frequencies and their quadratures; the frequencies are sent to the transmitter boards while the frequencies and their quadratures are sent to the synchronous detection boards. The transmitter boards (Tx A, Tx B, Tx C and Tx D) inject the signals to the process vessel through two (capacitance and resistance) joined electrodes, while the

receiver boards extract the signals from the process vessel via two (capacitance and resistance) separated electrodes and send them to the synchronous detection boards, note that the receiver boards for each channel is divided into two paths (Rx A_C and Rx A_R); (Rx B_C and Rx B_R); (Rx C_C and Rx C_R); (Rx D_C and Rx D_R); the subscript are: C - for capacitance path and R - for resistance path. On the synchronous detection boards demodulation and multiplexing of signals is performed. The outcome signals are sent to the sampler controller board, which connects the EIT system to the reconstruction computer via a PC30G Eagle data acquisition card.

3.1.1. The primary sensor system

The primary sensor system consists of the electrodes which have a direct contact with the process under investigation. Its main aspects are the combination, and placement of the conductive probes and capacitive plates around the boundary of the vessel. This section is dealt with in more detail in Chapter 4 where the apparatus is described.

3.1.2. Frequency generation

Unlike square waves, using sine wave excitations in process vessels has been shown to be a far more effective method, especially when more than four different frequencies are used, as the sine waves keep the signal clean [26]. This means that there is less harmonic distortion, and therefore fewer crossover demodulation terms.

Each sine wave and its quadrature are generated independently of all other frequencies and their quadratures by using a PIC16F84A microcontroller, therefore four PIC16F84A microcontrollers are used to generate four sine waves and their quadratures in the system.

A wide variety of sine waves and their 90° phase shifted versions can be generated on a PIC16F84A microcontroller, either by modifying the code or by changing the external crystal on the microcontroller. This is because it is accurate, simple and very easy to program [26].

The frequencies are limited from 15 kHz to 78.125 kHz, because 15 kHz is the lowest frequency where useful capacitance and resistance results were obtained by Giannopoulos for the 8 electrode FDM EIT system, and the highest frequency that the PIC16F84A microcontroller can generate in this method is 78.125 kHz.

Table 3.1 The four frequencies and the crystal used by the FDM EIT system (from Giannopoulos [26])

The Sine-Wave Frequencies for a 8-Electrode FDM Electrical Impedance Tomography		
Numbers	**Frequencies (Hz)**	**Crystals (MHz)**
1st	24375	16.38
2nd	37500	12
3rd	39375	16.38
4th	46875	12

The frequencies shown on table 3.1 were obtained by using an optimisation search algorithm employing Population Based Incremental Learning, PBIL, written by Teague [25] that produce optimal frequency separation and hence minimal output ripple [26].

3.1.3. Signal injection into the vessel

From the generating boards the signals are conveyed to the transmitter boards (four in total), which amplify and inject the signals into the process vessel. A LM1875T power opamp is used to perform the driving of the signal and is preceded by a buffer to avoid stray capacitance from the cables transporting the signals [26] as shown in the figure 3.2.

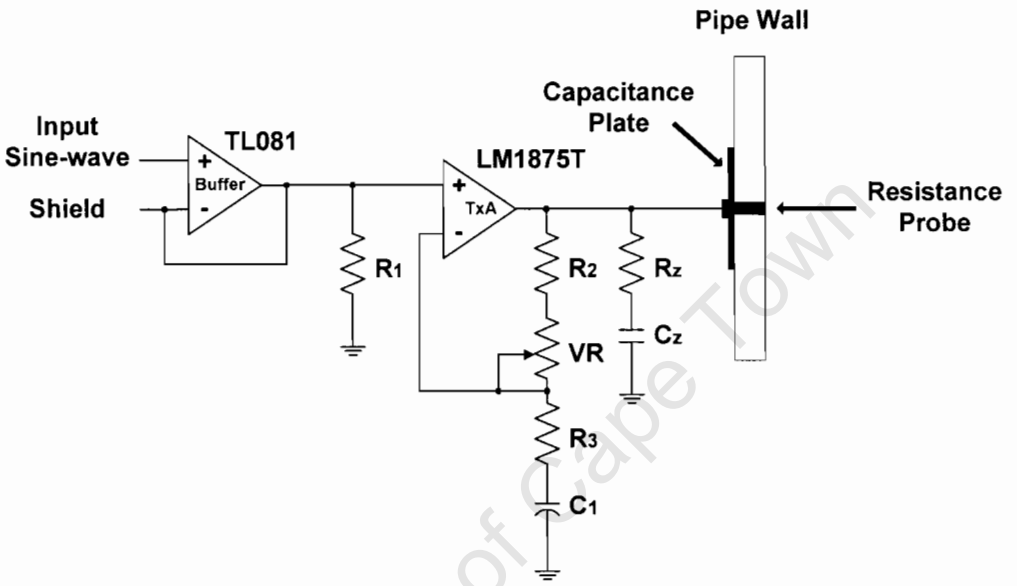

Fig. 3.2 Transmitter board circuit diagram (from Giannopoulos [26])

Since the transmitter path for the capacitance and for the resistance is the same, the transmitter capacitor plate and the conductive probes are in direct contact with each other [25, 26].

3.1.4. Signal extracting from the vessel

The signals from the inside of the process vessel are collected by the receiver boards (four in total). Each board is connected to a receiver capacitance plate and to the receiver conductive probes. The capacitance and resistance paths are isolated [25, 26], as shown in fig. 3.3 below.

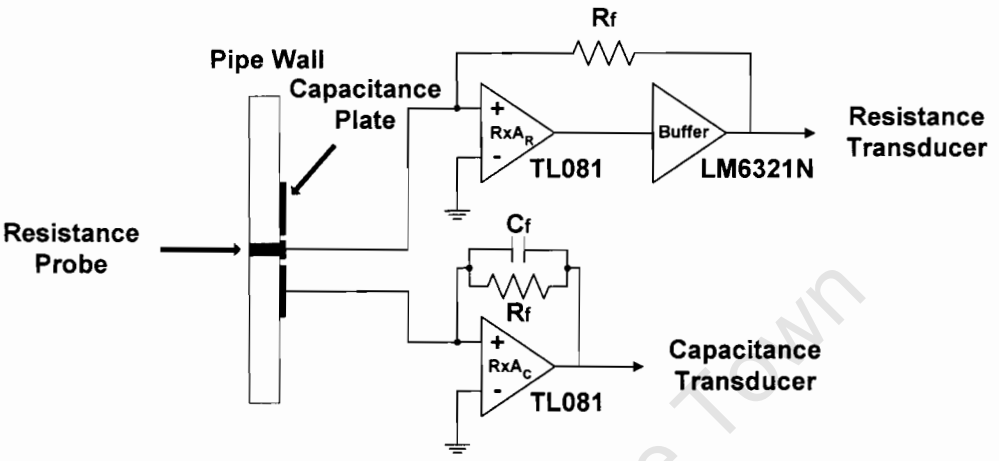

Fig. 3.3 Receiver board circuit diagram (from Giannopoulos [26])

In the receivers, the capacitor plates have larger holes and an isolating material to ensure there is no electrical contact between them and the conductive probes.

The resistance path in the board consists of an opamp and a buffer with a high current output. The buffer provides the required current to the feed back resistor so that the opamp does not saturate. For this application the R_f resistor used by Giannopoulos [26], was substituted with a 100 kΩ potentiometer to increase the gain. The resistance transducer operates by monitoring resistance changes between the electrode pairs due to the appearance of a non-conductive phase which causes an increase in the resistance and a decrease in the amplitude of the waveform [26]. It is effectively an inverting amplifier with the electrolyte as the input resistance.

The capacitance path in the receiver's boards consists of a single opamp. The output of the capacitance transducer is governed by equation 3.1 (from Giannopoulos [26]), where the output voltage V_O is obtained by relating the feedback capacitance C_F to the unknown capacitance C_X for a transmitted voltage V_E [26].

$$V_O = -\frac{C_X}{C_F} * V_E \qquad \textbf{Equation 3.1}$$

To ensure that the opamp does not saturate, a feedback resistance R_F is connected in parallel with C_F. For this application the R_F resistance was substituted with a 500 kΩ potentiometer to increase the gain.

The receiver board detects and conveys any capacitance and/or resistance fluctuations that occur in the measurement volume to the synchronous detection module. The signals consist of a superposition of components signals from the different transmitters [26].

3.1.5. Synchronous detection system

The synchronous detection system of the FDM EIT consists of four synchronous detection boards, each board performing synchronous detection for one complete channel, where a channel accommodates both the capacitance and the resistance signals from a specific receiver board [26], as shown in the figure below.

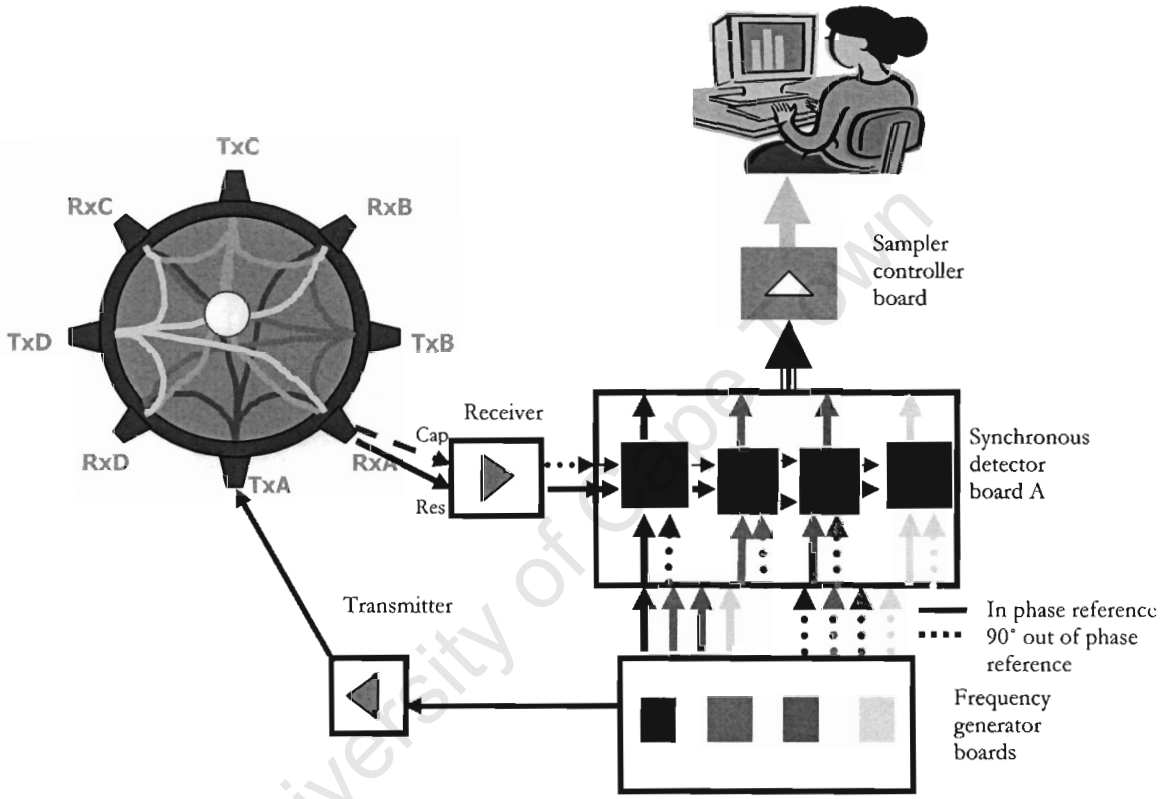

Fig. 3.4 Synchronised detection on channel A

In fig. 3.4 the signal, from the frequency generating board, is sent to transmitter A (TxA) and injected to the process vessel through two (capacitance and resistance) joined electrodes, then the receiver A (RxA) extract the signals (the signals from all transmitters) from the process vessel via two (capacitance and resistance) isolated electrodes and send them to the synchronous detection board A. On the synchronous detection board A, demodulation is performed using the reference signals from the frequency generating boards. The signals are then multiplexed, and the outcome signals are sent to the sampler controller board, which connects the EIT system to the reconstruction computer.

A very important aspect of synchronous detection is that it does not make use of the polarity of the actual signal, which often carries a lot of noise, to determine when the inversion must occur [25, 26]. It only requires that the reference signal, in this case a sine wave, be clean. This reference signal is in phase for an output signal proportional to the change in resistance, and 90° out of phase for an output signal proportional to the change in capacitance on the path of the original signal from the frequency generating board [26].

The outputs of the synchronous detection board are d.c. signals whose magnitudes are proportional to the capacitance and resistance of the specific path [25, 26].

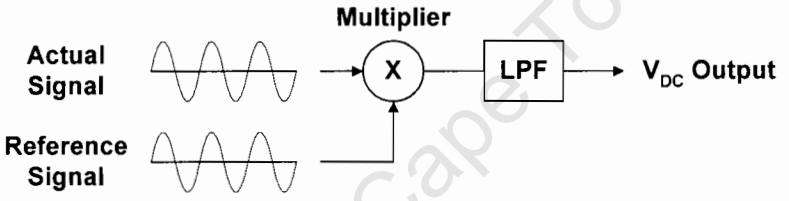

Fig. 3.5 The multiplication and filtering stages (from Giannopoulos [26])

These d.c. signals are obtained by multiplying the signal from the receiver board with a reference signal coherent with the signal applied on the transmitter boards, in order to extract the signal proportional to the resistance of a specific channel, as shown in fig. 3.5 above. In the case of the capacitance in the same channel a 90° phase shifted version of the same reference signal is used. An AD633J analogue multiplier is used to do the multiplications.

The signals are then amplified individually by opamps with variable gains to optimise their dynamic ranges. Finally the signals are low pass filtered by 4th order Butterworth filters with cut off frequencies of 200 Hz [26].

Since the data acquisition card in use (Eagle PC30G) only has 16 analogue input channels, and the FDM EIT system output has 32 output voltages, multiplexing of the output voltage is done after the measurements are performed, thus isolating the data acquisition process from the transducer systems. Therefore the system does not affect the capacitance or the resistance readings and does not have to wait between each sample [26].

The multiplexing of the four capacitance and four resistance signals are done by using a single DG406CJ 16 input CMOS analogue switch on each synchronous detection board. The address lines of these multiplexers are driven by the sample controller board, which also stores temporarily all the outputs of the multiplexer [26].

3.1.6. Sample controller

To make the capturing process faster a sample controller is used. The sample controller allows streaming to be employed which permits a very high amount of data to be transferred, resulting in higher sampling rates [26]. The idea behind it is that the address lines of the analogue multiplexers are driven by a separate source, thus the sampling rate does not depend on the software through the PC30G card on the computer. Therefore the software was only used to configure the sampler controller board, before and after a complete set of data is acquired [26]. The software was written by Teague [25] and modified by Giannopoulos [26] to suit the sine wave signal handling.

3.2. NEURAL NETWORKS

A neural network is a highly parameterized mathematical function that offers a general framework for representing non-linear function mapping from several input variables to several output variables [11].

Teague, Tapson and Smit [11] investigated two types of neural networks, the multi-layer perceptron and the radial basis function. For the reconstruction algorithm the multi-layer perceptron was used, because it consistently out performed the radial basis function neural network, and this out performance was due to the limited amount of training data available [11].

A multi-layer perceptron is a densely interconnected, layered network of neurons. Each neuron consists of a combined function which forms the weighted sum of the neuron input, and an activation function, which introduces a non-linearity into the network and confines the output to lie with a specific range [11].

In order to obtain an image or volume fraction reconstruction of the various phases inside the vessel, a pixel image of the cross section of the vessel is first constructed; where each pixel, in the image, can be considered the output of an individual neural network, performing a classification function for that particular pixel.

Teague, Tapson and Smit [11] defined:

$$\text{Pixel} = f[\text{classify}(C, G)] \qquad C - \text{Capacitance; } G - \text{Conductance}$$

where

$$\text{pixel} \in (\text{air, gravel, water})$$

By combining the neural network outputs in parallel, an image of the contents of the vessel is obtained. By letting the algorithm proceed to sum the air, gravel and water in the image then an estimate of the individual component volume fraction inside the vessels cross section can be obtained [11, 25].

3.3. IMAGE RECONSTRUCTION

An image is obtained by looking at the 88 output neurons such that each neuron corresponds to a pixel within the cross section of the vessel [11, 25, and 26]. To match a circular vessel the 12 pixels in the corners were ignored.

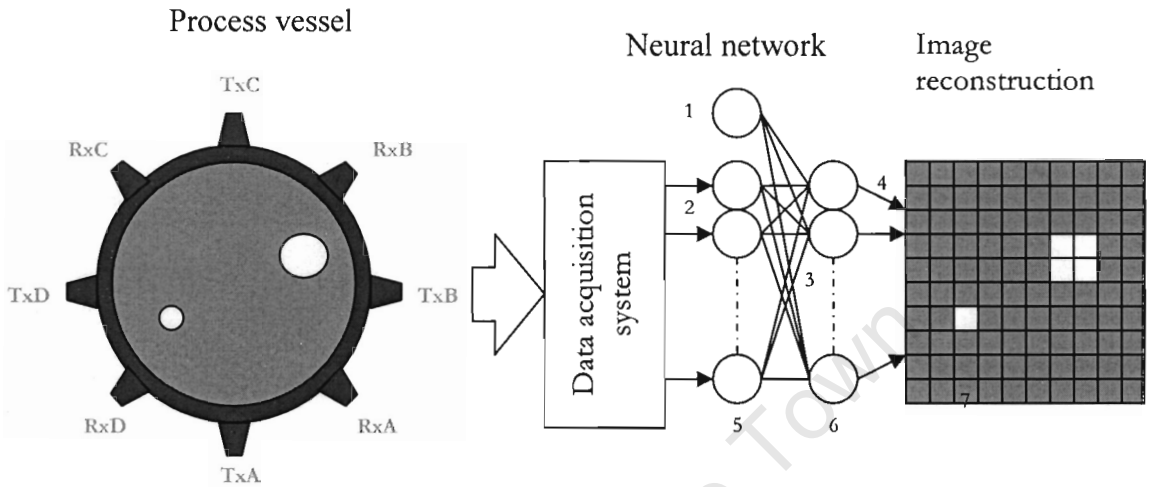

1 – the offset neuron; 2 – the voltage readings proportional to capacitance and conductance; 3 – the network weights; 4 – the Tanh activation function; 5 – the input layer neurons; 6 – the output layer neurons; 7 – a pixel.

Fig. 3.6 Single-layer feed forward neural network (Adapted from G. Teague [25])

Teague, Tapson and Smit [11] and Teague [25] used a single-layer feed forward neural network to obtain a two-phase image reconstruction as shown in the figure 3.6. The signals are taken from the vessel to the data acquisition system and are then fed to the neural network. The numbers indicate the different parts of a single-layer feed forward neural network: 1 – the offset neuron; 2 – the voltage readings proportional to capacitance and conductance; 3 – the network weights; 4 – the Tanh activation function; 5 – the input layer neurons; 6 – the output layer neurons; 7 – a pixel.

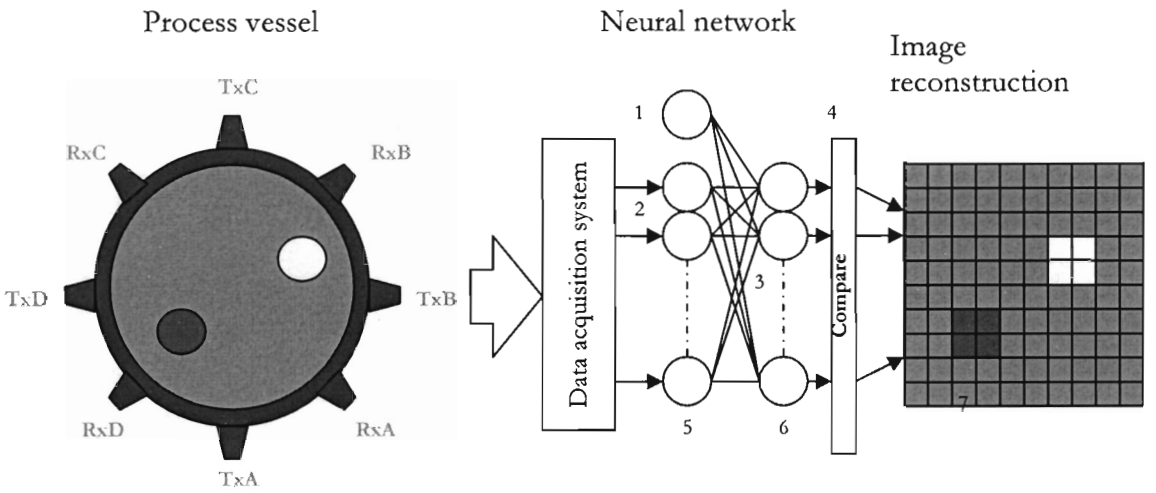

1 – the offset neuron; 2 – the voltage readings proportional to capacitance and conductance; 3 – the network weights; 4 – 1-of-C output encoding; 5 – the input layer neurons; 6 – the output layer neurons; 7 – a pixel

Fig. 3.7 Single-layer feed forward with a 1-of-C output encoding neural network (Adapted from G. Teague [25])

For a three-phase mixture Teague, Tapson and Smit [11] and Teague [25] used a single-layer feed forward network with a 1-of-C output encoding neural network as shown in fig. 3.7. The signals are taken from the vessel to the data acquisition system and are then fed to the neural network. The numbers indicate the different parts of a single-layer feed forward with a 1-of-C output encoding neural network: 1 – the offset neuron; 2 – the voltage readings proportional to capacitance and conductance; 3 – the network weights; 4 – 1-of-C output encoding; 5 – the input layer neurons; 6 – the output layer neurons; 7 – a pixel.

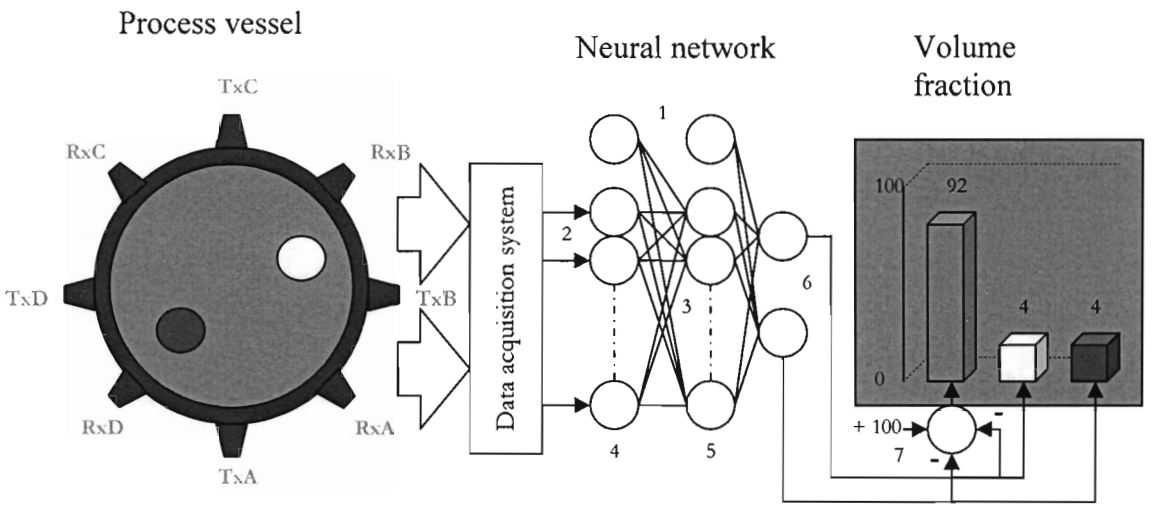

1 – the offset neurons; 2 – the voltage readings proportional to capacitance and conductance; 3 – the network weights; 4 – the input layer neurons; 5 – the hidden layer neurons; 6 – the output layer neurons; 7– the addition function

Fig. 3.8 Double-layer feed forward neural network (Adapted from G. Teague [25])

To perform a volume fraction prediction, Teague, Tapson and Smit [11] and Teague [25] used a double-layer feed forward neural network as shown in the fig. 3.8. The signals are taken from the vessel to the data acquisition system and are then fed to the neural network. The numbers indicate the different parts of a double-layer feed forward neural network: 1 – the offset neurons; 2 – the voltage readings proportional to capacitance and conductance; 3 – the network weights; 4 – the input layer neurons; 5 – the hidden layer neurons; 6 – the output layer neurons; 7– the addition function (+100 - 4 - 4 = 92).

3.4. TRAINING THE SYSTEM

The multi-layer perceptron neural network has to be trained to obtain the adjustable parameters, or weights, of the network that controls the functional mapping. Training a neural network is done by presentation of known input-output pairs to the network and adjustment of the network weights until the error is satisfactorily small, which is achieved by a large quantity of representative data [11].

Training was done by placing samples of sandstone (as gravel objects) and polystyrene (as air bubbles) on a grid inside the cylindrical section of the hydrocyclone, and recording electrical properties for each different set, using the reconstruction software.

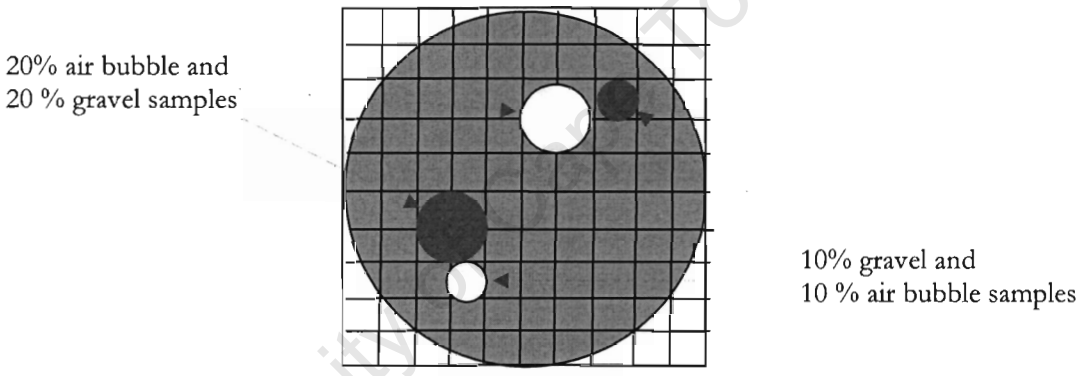

Fig. 3.9 Ten-by ten mapping grid

Figure 3.9 shows how the placement grid was mapped to the cylindrical section and how the different samples were positioned

The placement grid was changed from the "Bed of Nails" placement grid, used by Teague, Tapson and Smit [11], Teague [25] and Giannopoulos [26], to a placement grid with holes on it, in a way the opposite to a bed of nails. This was because it was very difficult to construct a bed of nails for a grid of less than 50 mm total diameter. Therefore the samples were fitted with (nail like) sharp ends to fit the holes of the placement grid so as to stabilise them.

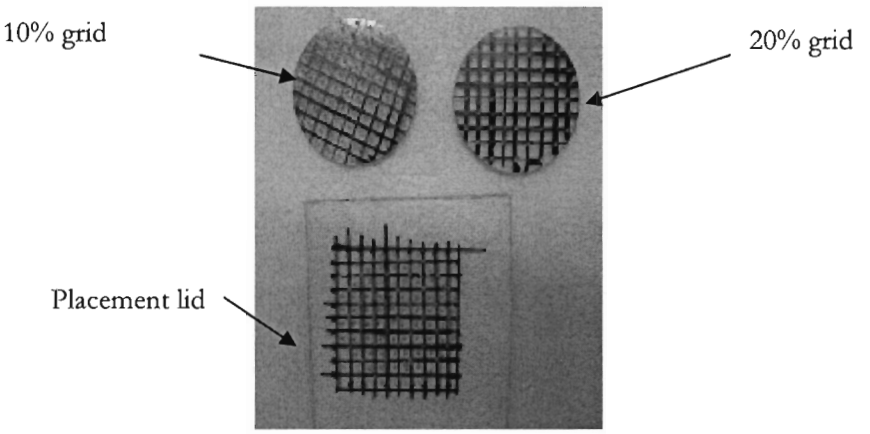

Fig. 3.10 Set of grids for system training

Two different grids to train bubbles with 10% and 20% of the diameter of the hydrocyclone were available as in fig 3.1; the figure shows the two placement grids and the placement lid. The placement lid was used to keep the samples from floating out of place.

Table 3.2 Grid positions to train bubbles with 10% and 20% of the diameter of the hydrocyclone

Grid	Available positions	# of sets readings
10%	76	222
20%	37	456

Table 3.2 shows grid positions to train bubbles with size equal to 10% and 20% of the diameter of the hydrocyclone. On average each grid had sets equal to the number of positions, multiplied by two different bubbles (gravel and air). Each set of readings was performed three times to improve the noise performance of the neural network [11].

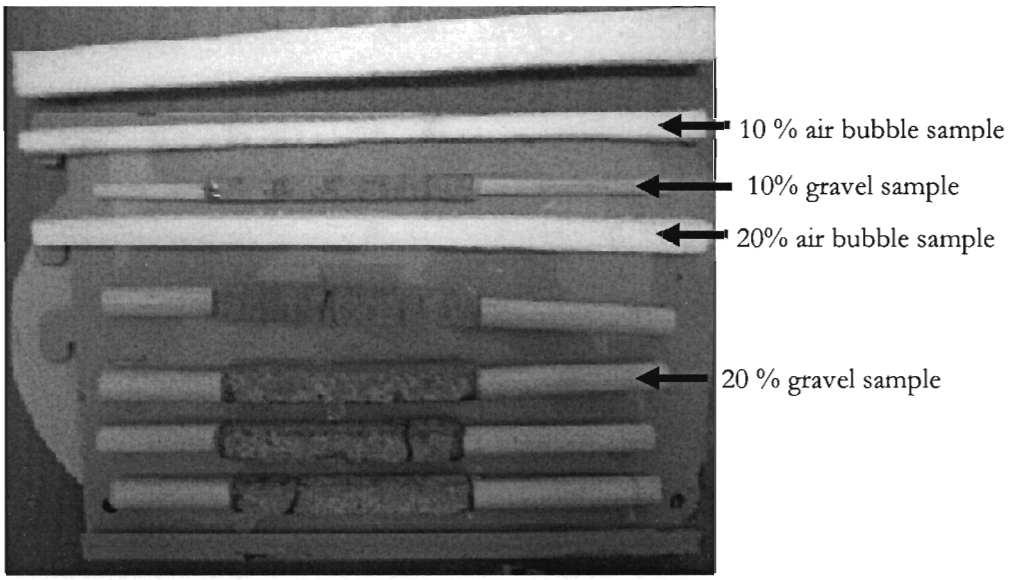

Fig. 3.11 Set of Air and Gravel Samples

Figure 3.11 is a picture showing the different gravel objects and air bubbles. Gravel samples supplied and manufactured by the UCT Geology Department's workshop.

3.5. OBTAINING DATABASES

A database is a collection of different sets of readings for particular positions of air bubble or gravel objects.

Databases were obtained by placing a specimen (air bubble or gravel object) on a placement grid and recording the electrical properties (dielectric properties shown on table 3.3) of that position using the reconstruction software; after which the specimen is moved to a new position on the placement grid and a new sample is taken. The process is continued until all the intended positions are sampled. This database is stored as a training database and is used to train the reconstruction algorithm of the neural network [25].

Table 3.3 Dielectric constants of phases (from Teague [25] and Smit [27])

Phase	Dielectric medium
Polystyrene	2.56
Air	1.00054
Water	78.54
Gravel	3 to 5

Table 3.3 shows the dielectric constants for the different phases.

The same steps are repeated to create a second database, which is recorded as a testing database and is used to test the reconstruction algorithm of the neural network.

It is important that obtaining the databases is done in as short a time as possible in order to avoid the electrical properties of the water from drifting, as its properties change with time.

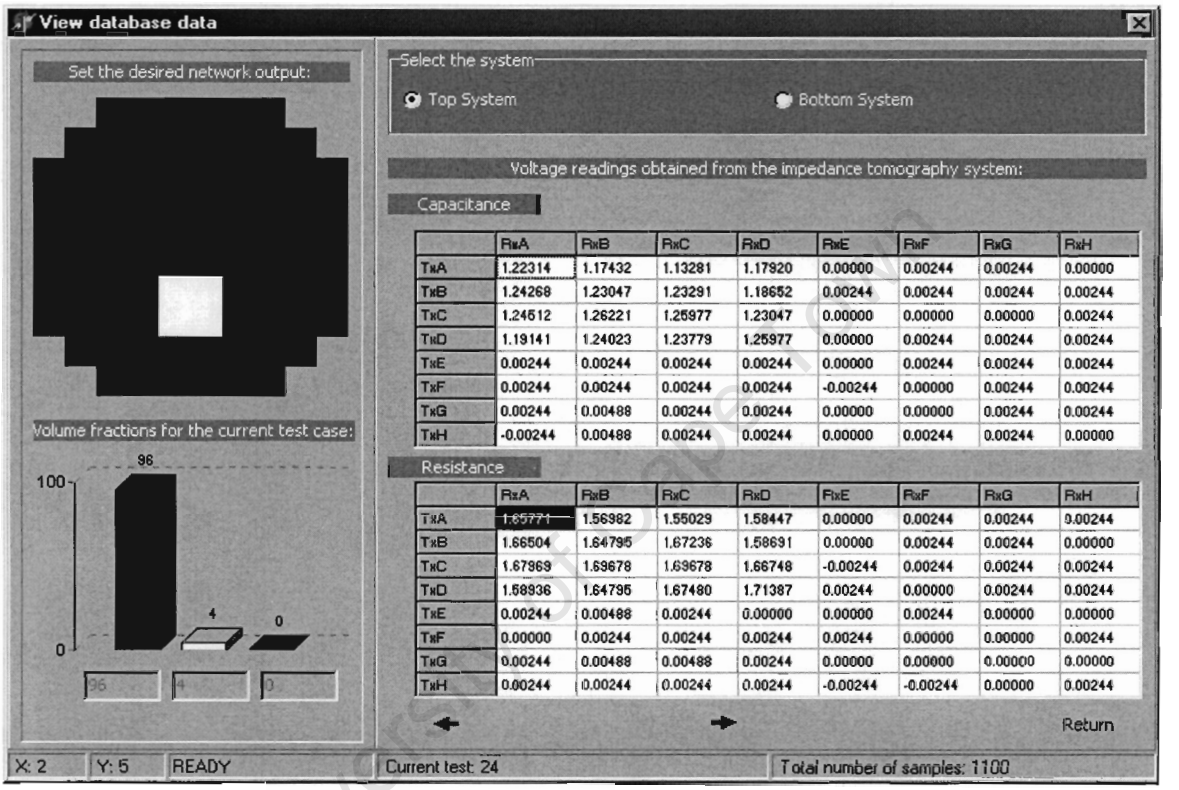

Fig. 3.12 An air bubble at a particular testing position

Figure 3.12 shows entry number 24 of the testing database of a two phase mixture (water and air). It contains the actual image position as well as the volume fraction and the voltages that represent this position. For capacitance the voltages are around 1.2 volts, while for resistance the voltages are around 1.6 volts.

Note that the only transmitters in use are TxA, TxB, TxC and TxD; and the receivers are RxA, RxB, RxC and RxD.

CHAPTER 4

APPARATUS DESIGN AND CONSTRUCTION

4. APPARATUS DESIGN AND CONSTRUCTION

A 50 mm diameter Krebs hydrocyclone was available for testing for a period of 10 months.

4.1. THE HYDROCYCLONE

The hydrocyclone is composed of two parts with three sections; the top part fig 4.1 a), which supports the inlet and the vortex finder, and the bottom part fig 4.1 b) which supports the cylindrical and conical sections. The hydrocyclone has a vortex finder diameter of 22.5 mm and a spigot of 5.4 mm.

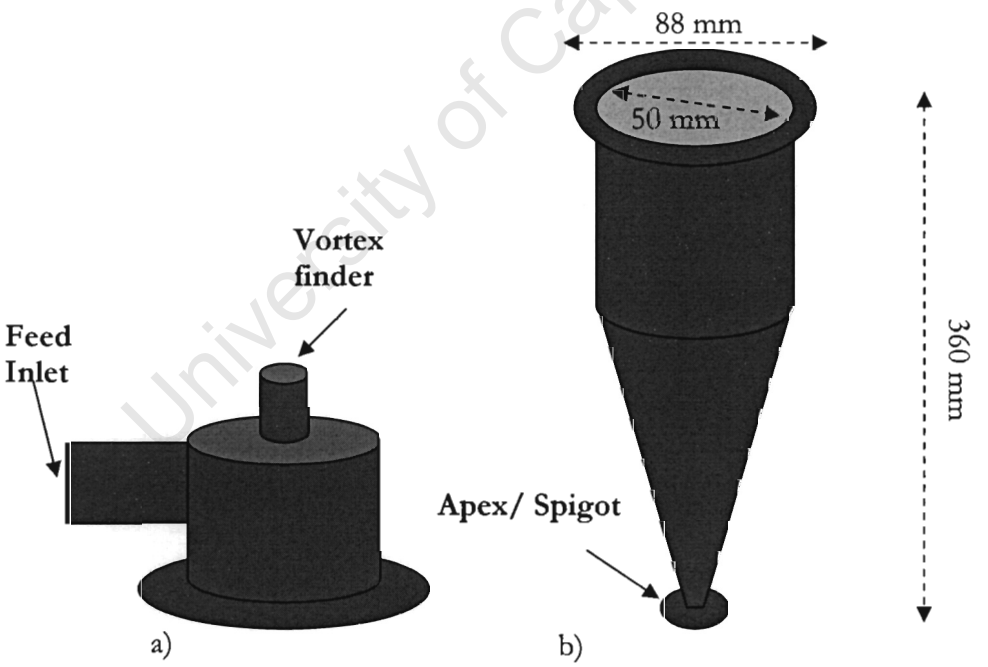

Fig. 4.1 The top and the bottom parts of the hydrocyclone

The cylindrical section is where the centrifugal forces act, and the conical section is where the spigot is situated. The cylindrical section was found to be the ideal area to position the sensor unit, since its geometry allows placement of rectangular capacitor plates.

Due to the invasive nature of the FDM EIT system (conductive probes have to be drilled through to make contact with the fluid) on the existing hydrocyclone, a separate cylindrical and conical section of the hydrocyclone had to be redesigned (see Appendix A for the designs), and were built by the UCT Mechanical Engineering Department's workshop.

4.1.1. THE CYLINDRICAL SECTION

The cylindrical section connects above with the top part where the inlet and the vortex finder are located, and below with the conical section.

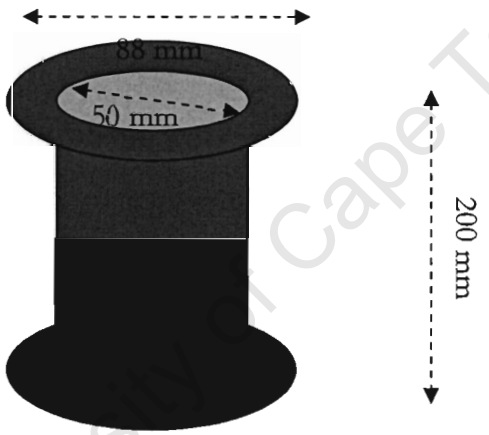

Fig. 4.2 Cylindrical section of the hydrocyclone

The cylindrical section fig. 4.2 was made of Perspex acrylic plastic and has as dimensions: an inner diameter of 50 mm, an outer diameter of 60 mm and height of 200 mm. It was fitted at both ends with an outer disk of 88 mm diameter, tapered at 15 degrees to give an edge of 6 mm thickness. These outer disks were used to connect to the other parts of the hydrocyclone using Krebs clamps.

4.1.2. THE CONICAL SECTION

The conical section connects at the top with the cylindrical section where the electrodes are located and at the bottom with the spigot.

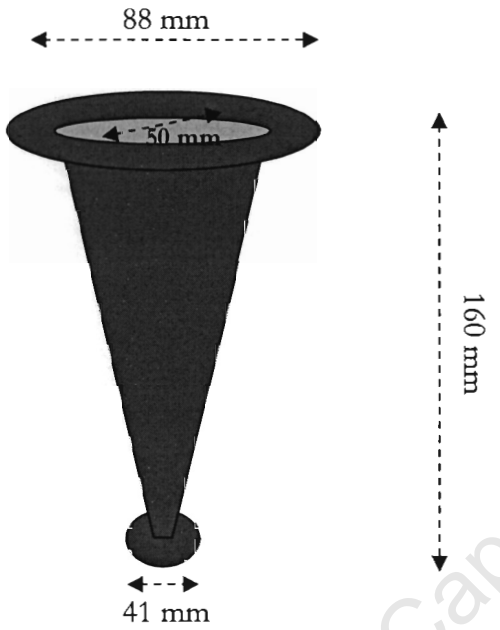

Fig. 4.3 The conical section of the hydrocyclone

The conical section fig. 4.3 was also made of Perspex acrylic plastic and has as dimensions: an inner diameter of 50 mm at the top and 13 mm at the bottom, an outer diameter of 60 mm at the top and 23 mm at the bottom. It has a height of 160 mm. It was fitted at the upper end with an outer disk of 88 mm diameter tapered at 15 degrees to give an edge of 4.52 mm thickness, and at the lower end it was fitted with an outer disk of 41 mm diameter tapered at 15 degrees to give an edge of 2.86 mm thickness. These outer disks were used to connect to the other parts of the hydrocyclones using Krebs clamps.

4.2. THE SENSOR UNIT

The sensor unit is where all data collection from the inside of the hydrocyclone happens. The data is then sent to the FDM EIT system; from there the data goes to the reconstruction computer. The sensor unit is a combination of mechanical structures and electronic blocks, working together to produce analogue outputs according to the contents of the hydrocyclone.

The sensor unit is composed of: the capacitor sensors and three layers of conductive sensors.

4.2.1. THE CAPACITOR SENSORS

The capacitive sensors were built by arranging electrodes around the boundary of the cylindrical part of the hydrocyclone.

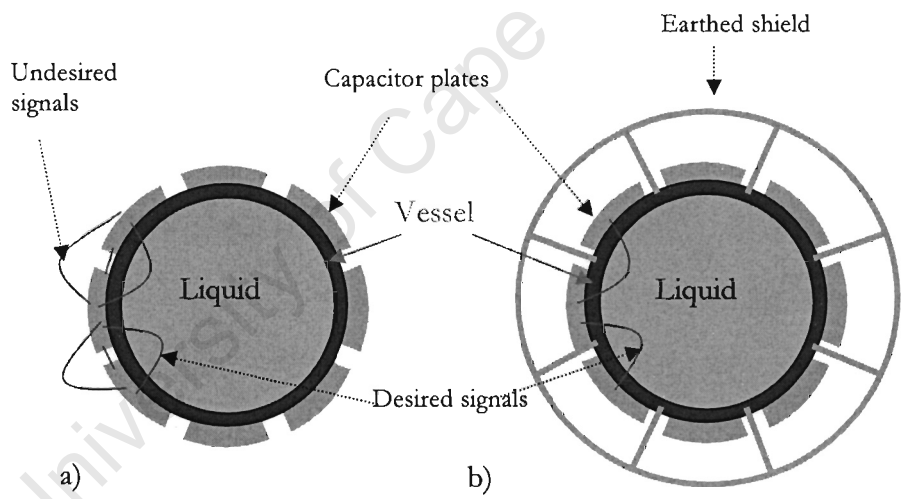

Fig. 4.4 Shielding arrangement for capacitor plates

On fig.4.4 a) it can be seen that the emitting signal can travel in different directions, therefore an earthed shield similar to the one developed by Xie et. al. [32] was added to avoid the electrodes from attaining a short path and to make sure only the relevant signal are captured, i.e. no outside electromagnetic interference. For this application it was necessary that only the signals going through the liquid, seen in fig. 4.4 b), were captured.

When in place the electrode of the capacitor sensor gives a sensing volume as shown in fig 4.5.

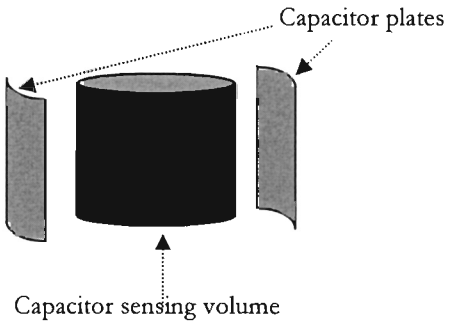

Fig. 4.5 Capacitor sensing volume

The materials considered for the capacitor electrodes were aluminium and copper. Aluminium so far has been the material mostly used for this application at UCT; however copper will be the first choice. The reason for use of copper rather than aluminium is because copper, being more conductive than aluminium, will relay the transmitted and received signals better, therefore improving the signal-to-noise ratio (SNR) of the measurements.

It was found that for a 20 mm by 50 mm capacitor copper plate pair of transmitter and receiver (fig. 4.6) a signal could still be captured in air with up to 65 mm distance between the plates. The hydrocyclone maximum distance is 60 mm (being its outside diameter).

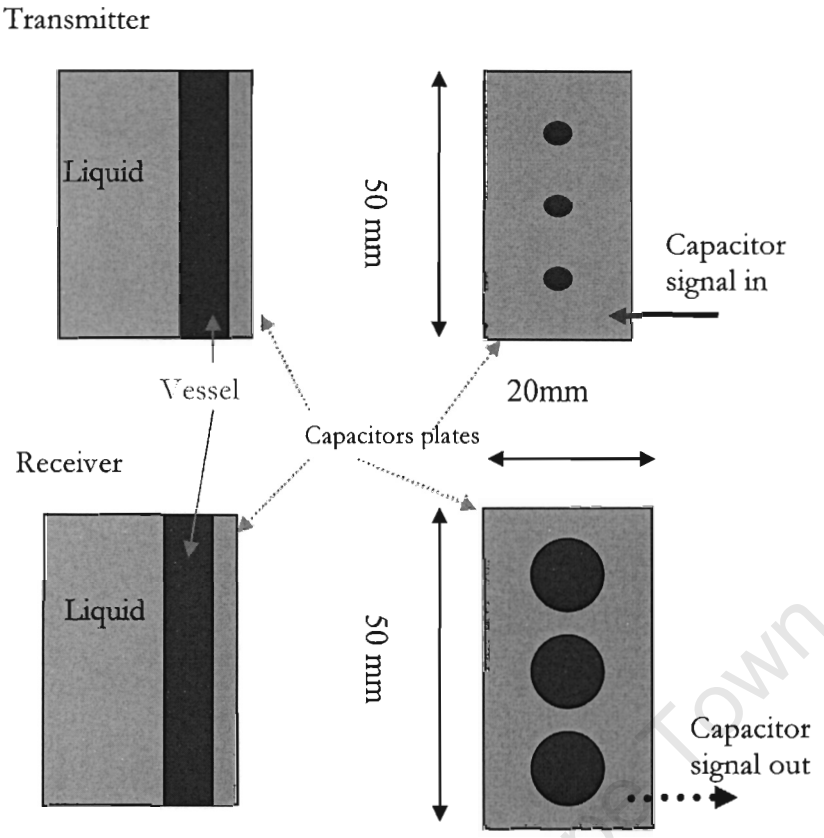

Fig. 4.6 Capacitor plates

In fig. 4.6 the design and size for the transmitter and receiver capacitor plates are shown. The plates have holes on them to allow the conductive probes to be placed. The plates are attached to the walls of the vessel.

4.2.1.1. ARRANGING THE ELECTRODES

Arranging the electrodes around the circular perimeter of the vessel proved to be rather intricate. This was because the area of the capacitor plates is small, and therefore extra screws could not be added to attach capacitor plates to the vessel. The way to attach the capacitor plates onto the boundary was done by using the resistance probes as fasteners by screwing nuts on them.

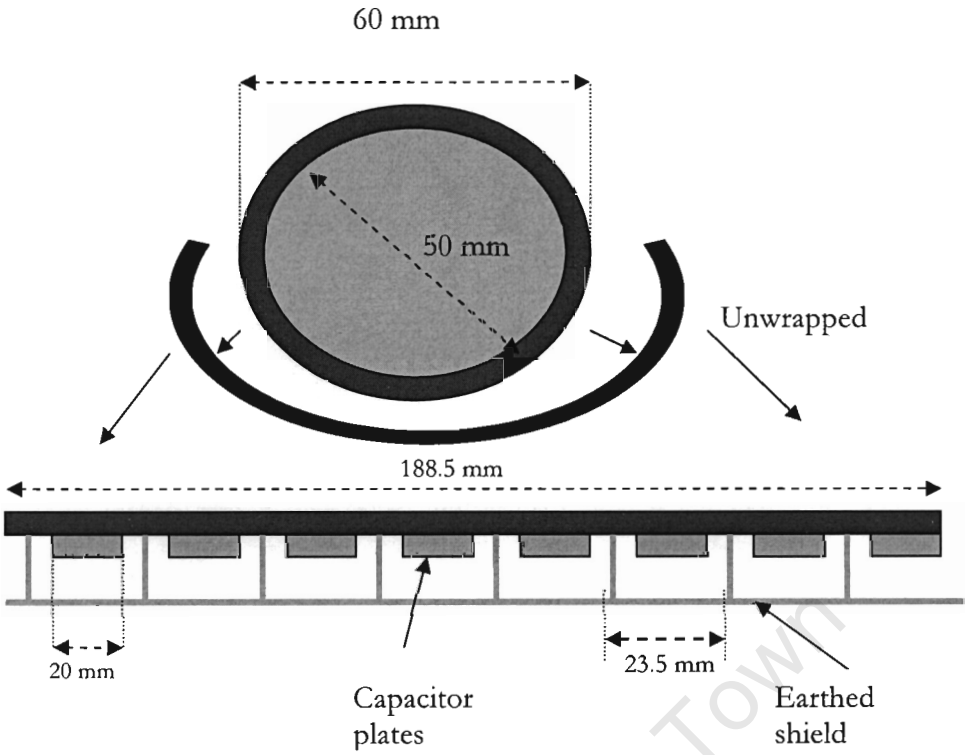

Fig. 4.7 Arrangement of capacitor plates around the parameter

For a 60 mm outside diameter cylinder the surface perimeter is given by $P = \pi * d$ which gives a perimeter of 188.5 mm as shown in fig.4.7. The 8 capacitor electrodes are 20 mm wide, therefore 160 mm of the perimeter is used by the 8 capacitor plates, leaving 28.5 mm which gets used in between plates. Each gap is 3.5 mm, and the shield rests on a 1 mm groove about 1.2 mm away from each capacitor plate.

It is part of this study to extend the 8 electrode Frequency Domain Multiplexing (FDM) Electrical Impedance Tomography (EIT) system to a 16 FDM EIT system. However from figure 4.7, it can be seen that to fit 16 electrodes in a space of 188.5 mm would work out to very small dimensions. The capacitor plates would be too narrow and too long, in the order of 8 mm wide to 125 mm in length, in order to obtain an area of 1000 mm^2, which is the minimal area for the capacitor plates to give a sensible reading [32]. Moreover the sensing volume would be too long, and the air core diameter would not be accurate.

4.2.2. THE CONDUCTIVE SENSORS

The design for the conductive sensor was to have the electrodes placed on the periphery of the cylindrical part of the hydrocyclone, right in the middle of the capacitive plates. They are positioned equidistantly around the boundary. The materials considered were brass and stainless steel threaded rods. Here all that needs to be avoided is the problem arising due to contact impedance [25], therefore the material used must be more conductive than the fluid being imaged. The first choice was stainless steel. The reason for the use of stainless steel was because brass failed to withstand the corrosive or abrasive nature of the mixture under investigation. For resistance probes, 2 mm diameter stainless steel threaded rods were found to be best for this application and design as shown in fig.4.8.

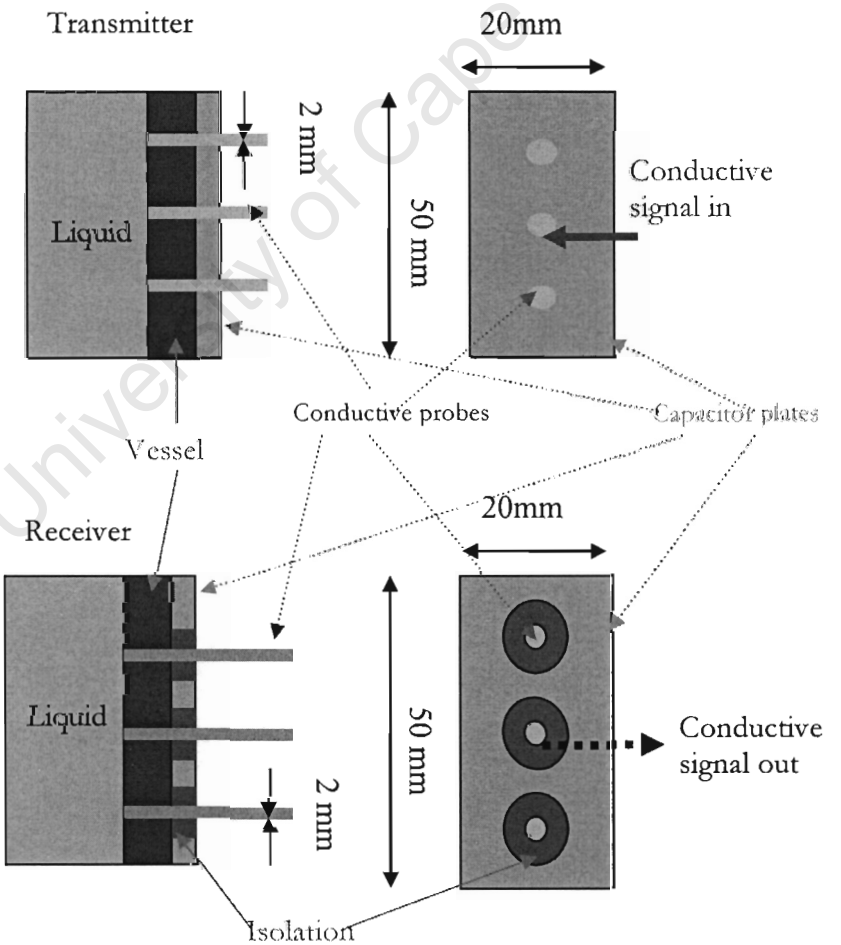

Fig. 4.8 Conductive probes

In fig. 4.8 the design and size for the transmitter and receiver conductive probes are shown. The probes are in contact with the capacitor plates on the transmitter setup, and the probes are isolated from the capacitor plates on the receiver setup by placing a non-conductive material between the plate and the probes.

4.3. THE THREE LAYER CONDUCTIVE SENSORS

Instead of using only one conductive electrode through the capacitive plate, as shown in fig. 4.9, three are used (see fig. 4.10); this is because the capacitor sensing region is a volume, while the conductive image would be captured from a plane if only one conductive electrode was used.

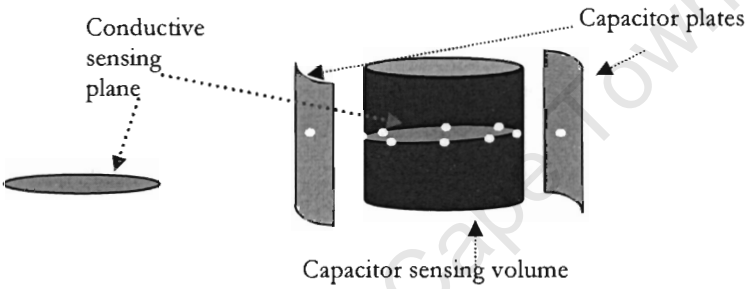

Fig. 4.9 Single-layer conducting sensing plane

Therefore, three sets are used, giving a volumetric sensing region as shown in fig. 4.10. The information from the capacitance sensing volume and the conductive sensing planes were combined to reconstruct a 2-D image of the region or a volume fraction prediction.

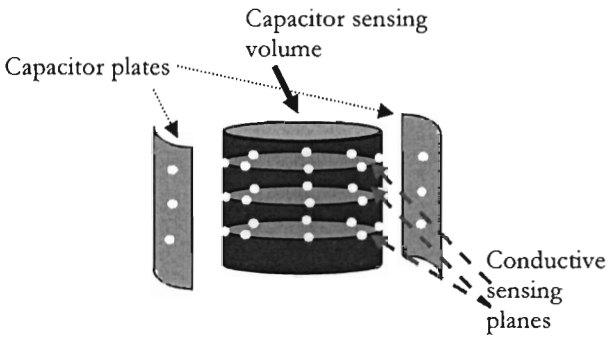

Fig. 4.10 Triple-layer conducting sensing planes

CHAPTER 5

THE 8 ELECTRODE FDM EIT SYSTEM PERFORMANCE

5. THE 8 ELECTRODE FDM EIT SYSTEM PERFORMANCE

In this chapter two types of performance are discussed: the static and dynamic performances.

5.1. STATIC PERFORMANCE

Under static performance, tests and results achieved in a stationary tank are discussed.

Training and testing of the neural network was conducted with the use of air bubbles only; as the research at this point had shown that to understand the air core dynamics and stability, a hydrocyclone operating with water only could be used, as described by Concha et. al. [16] and also by Wanwilai [34].

In training and testing of the neural network, databases were obtained using the same method as Giannopoulos [26] and Teague [25]. That is, by placing 10% or 20% of the diameter of the hydrocyclone polystyrene samples (as air bubbles) in the stationary tank by means of the placement grids, and taking readings using the reconstruction software.

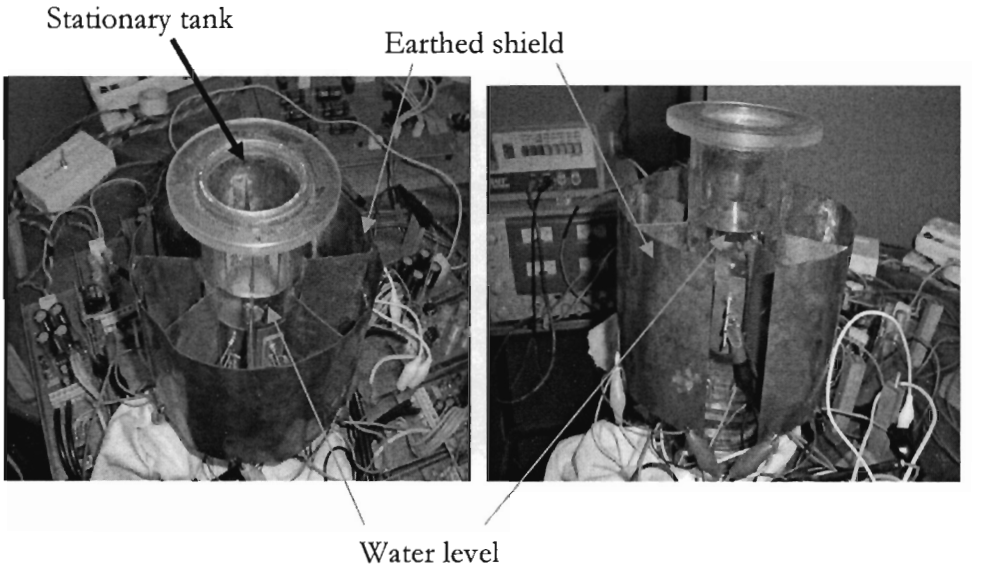

Fig. 5.1 The stationary tank (see appendix B for system pictures)

The stationary tank is the cylindrical section of the hydrocyclone, which contains the sensor unit, with one of its ends closed and full of water, as seen in the figure 5.1 above.

Once the training and testing databases for the static conditions were recorded, the image reconstruction and the volume fraction prediction could be started. The first attempts at the image reconstruction and volume fraction predictions gave results that were unimpressive and far from expected. This was because the input gain from the data acquisition system was set to very low levels, and the time taken to complete the databases was relatively long, allowing the electrical properties of the water to drift a lot.

The gain was improved by increasing the R_f resistor for the capacitance and conductance paths on the receiver board (see section 3.1.4) by introducing 500kΩ and 100kΩ potentiometers respectively. The necessary gain was 277kΩ for the capacitance and 56KΩ for the conductance; however the potentiometers were introduced to easily facilitate any future changes.

The image reconstruction and the volume fraction prediction improved significantly. Below are shown three typical entries of image reconstruction and their volume fraction predictions.

Figure 5.2 shows an image reconstruction for case 1101, which represents the tank with 100% water.

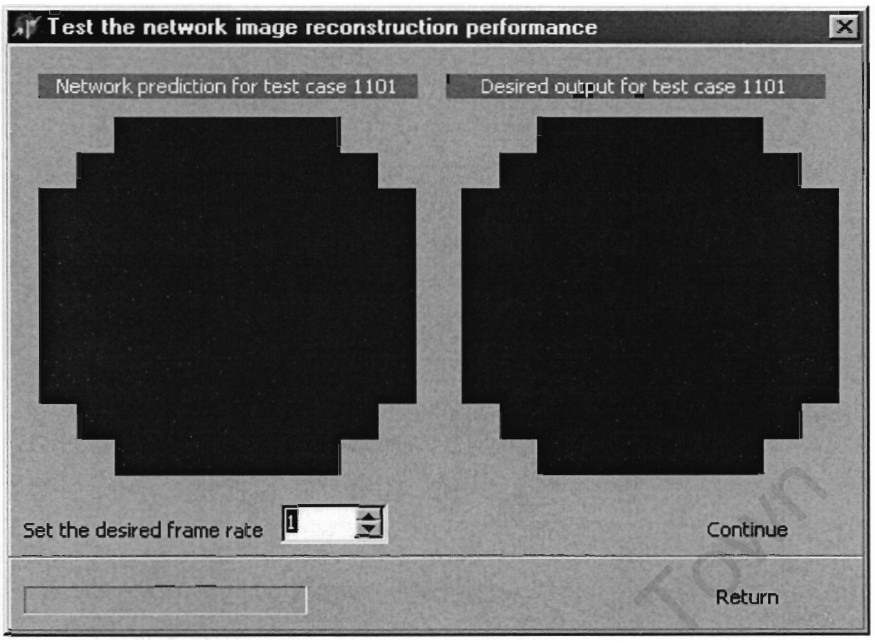

Fig. 5.2 An image reconstruction for case 1101

In figure 5.2 a typical image reconstruction of the static tank full of water is shown. The case number is 1101. The frame rate at which the database was viewed had to be slowed down to one frame per second, to allow the picture to be taken. In the picture the network prediction image is the one on the left and the desired output image is the one on the right, so that a visual comparison can be done.

Figure 5.3 shows a volume fraction for the same case 1101, which represents the tank with 100% water.

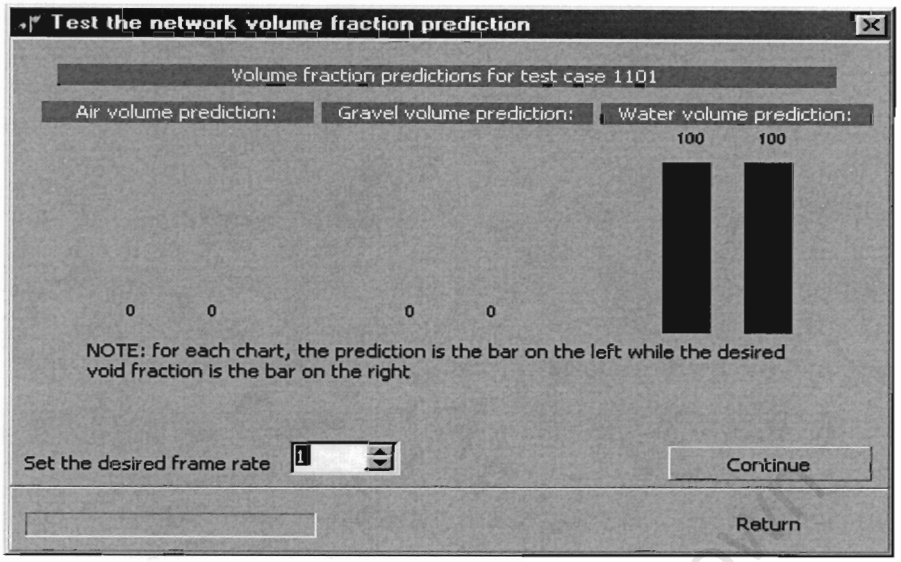

Fig. 5.3 A volume fraction prediction for case 1101

In figure 5.3 a volume fraction prediction of the static tank full of water is shown, the case number is 1101. The frame rate at which the database was viewed had to be slowed down to one frame per second, to allow the picture to be taken. The picture shows two bars side by side for each case (air, gravel and water volume prediction). The network prediction bar is the one on the left and the desired output bar is the one on the right; in this case a quantitative, numeric interpretation or comparison can be done. This picture shows that: the volume prediction of air is 0, when the desired output of air is 0; the volume prediction of gravel is 0, when the desired output of gravel is 0; and the volume prediction of water is 100, when the desired output of water is 100.

Figure 5.4 shows an image reconstruction for case 1123, which represents an air bubble of size equal to 20% of the diameter of the tank.

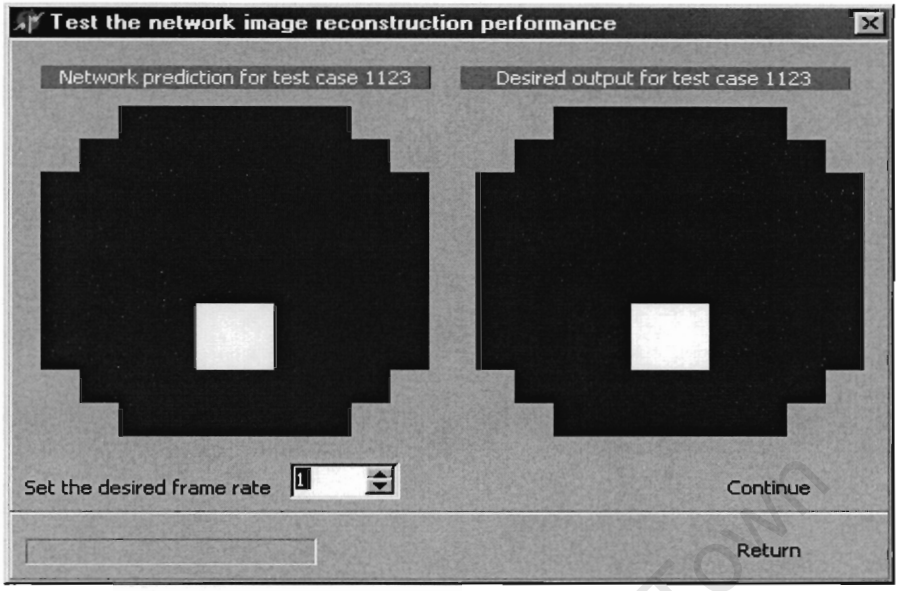

Fig. 5.4 An image reconstruction for case 1123, which was a 20% air bubble

In figure 5.4 an image reconstruction of the static tank with an air bubble size of 20% of the diameter of the tank, at a particular position is shown. The case number is 1123. The frame rate at which the database was viewed had to be slowed down to one frame per second, to allow the picture to be taken. In the picture the network prediction image is the one on the left and the desired output image is the one on the right. A visual comparison can be done to see the position of the air bubble.

Figure 5.5 shows a volume fraction for the same case 1123, which represents an air bubble of size equal to 20% of the diameter of the tank.

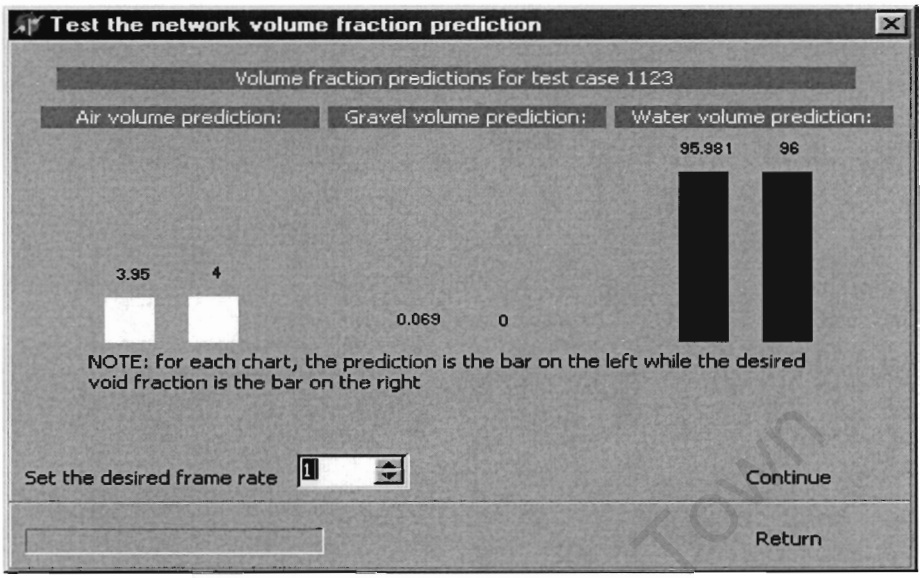

Fig. 5.5 A volume fraction prediction for case 1123

In figure 5.5 a volume fraction prediction of the static tank with 4% air and 96% water is shown. The case number is 1123. The frame rate at which the database was viewed had to be slowed down to one frame per second, to allow the picture to be taken. The picture shows two bars side by side for each case (air, gravel and water volume prediction). The network prediction bar is the one on the left and the desired output bar is the one on the right; in this case a quantitative, numeric interpretation or comparison can be done.

This picture shows that: the volume prediction of air is 3.95%, when the desired output of air is 4%; the volume prediction of gravel is 0.069, when the desired output of gravel is 0; and the volume prediction of water is 95.981%, when the desired output of water is 96%.

Figure 5.6 shows an image reconstruction for case 1154, which represents an air bubble of size equal to 20% of the diameter of the tank.

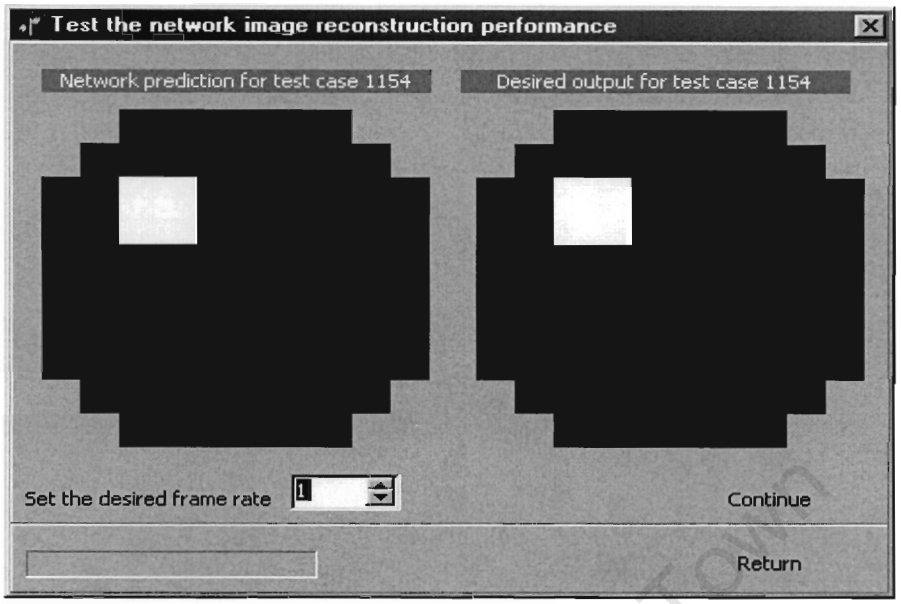

Fig. 5.6 An image reconstruction for case 1154 a 20% air bubble

In figure 5.6 an image reconstruction of the static tank with an air bubble size of 20% of the diameter of the tank, at a different position from fig. 5.4 is shown. The case number is 1154. The frame rate at which the database was viewed had to be slowed down to one frame per second, to allow the picture to be taken. In the picture the network prediction image is the one on the left and the desired output image is the one on the right. A visual comparison can be done to see the position of the air bubble.

Figure 5.7 shows a volume fraction for the same case 1154, which represents an air bubble of size equal to 20% of the diameter of the tank.

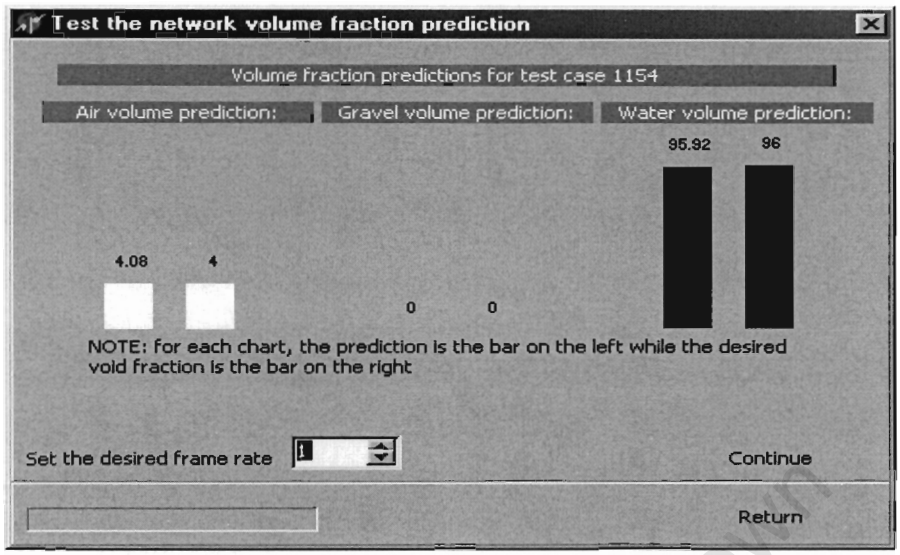

Fig. 5.7 A volume fraction prediction for case 1154

In figure 5.7 a volume fraction prediction of the static tank with 4% air and 96% water is shown. The case number is 1154. The frame rate at which the database was viewed had to be slowed down to one frame per second, to allow the picture to be taken. The picture shows two bars side by side for each case (air, gravel and water volume prediction). The network prediction bar is the one on the left and the desired output bar is the one on the right; in this case a quantitative, numeric interpretation or comparison can be done.

This picture shows that: the volume prediction of air is 4.08%, when the desired output of air is 4%; the volume prediction of gravel is 0, when the desired output of gravel is 0; and the volume prediction of water is 95.92%, when the desired output of water is 96%.

From the static performance results, it was clear that a volume fraction prediction should be pursued rather than image reconstruction, because the volume fraction has quantitative, numeric information that can be used for further processing.

5.2. DYNAMIC PERFOMANCE

Under dynamic performance the results achieved with a hydrocyclone operating with water only are discussed.

The hydrocyclone was assembled with its cylindrical section containing the sensor unit the vortex finder size was set to 22.5 mm and the spigot to 5.4 mm giving a ratio of the underflow diameter (apex) to the overflow diameter (vortex) (d_u/d_o) of 0.24.

The hydrocyclone rig is composed of a pump (with a 1430 rpm motor), a recycling reservoir, and the hydrocyclone. The speed of the motor was controlled with a variable speed drive (PowerFlex70 by Allen-Bradley) [28].

As the speed increases and the hydrocyclone fills with water, the exit from the underflow is a rope-like discharge and nothing comes out the overflow. At a pump speed of about 340 rpm the air core starts to form and some water starts to exit from the overflow. As the pump speed increases further, so does the size of the air core, and the underflow takes the form of a spray discharge (umbrella like form). The angle of the discharge also increases as the air core increases, and so does the overflow contents. The shape the air core takes changes from a faint line into a full grown helical cone (approximating a spiralling cone), which rotates with the liquid about the centre line of the hydrocyclone.

The air core increases until its top end is almost the size of the overflow (vortex), being the size of the vortex finder which is 22.5 mm, and the bottom end is almost the size of its underflow (apex), in this case the size of the spigot which is 5.4 mm. This is in contradiction with both limit numbers from the works Concha et al [16] and Bustamente et. al. (as stated in the work of Concha et. al. [16]). According with both works an air core should not exist (section 2.1.1). Below is picture of the captured air core.

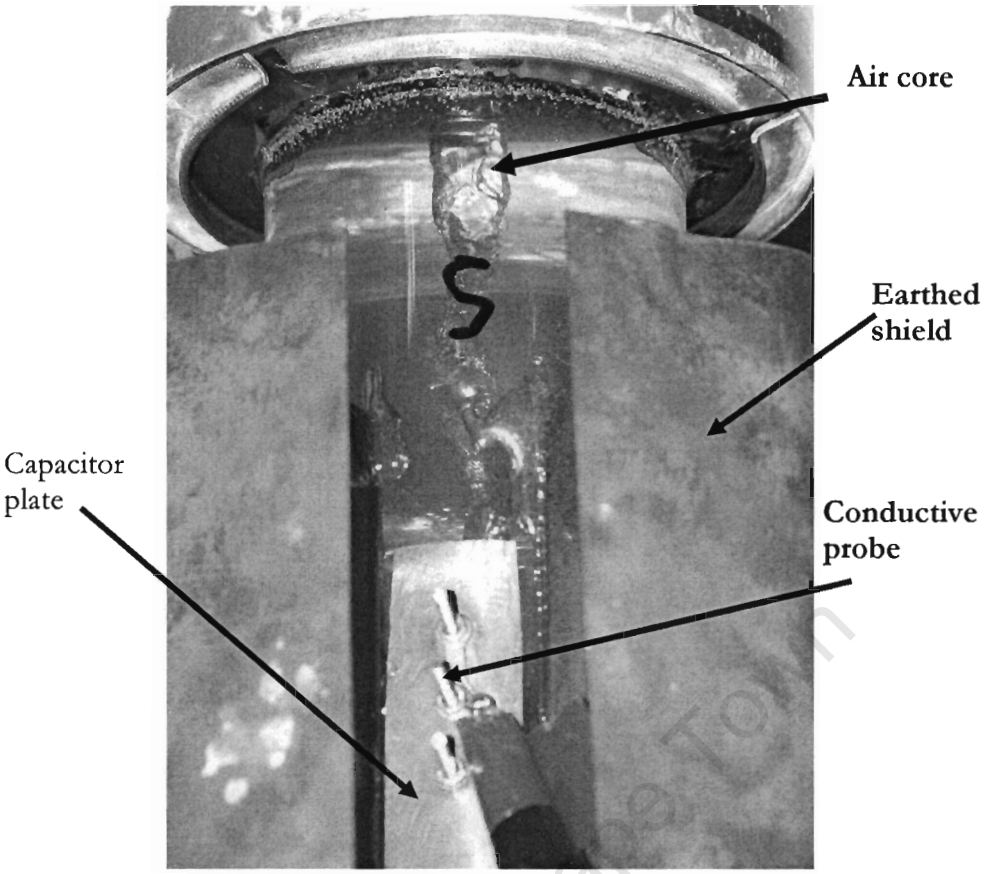

Fig. 5.8 A picture of the helical air core

Figure 5.8 shows a picture of the helical air core, the earthed shield, a capacitor plate, and the conductive probes can be seen as well.

Increasing the pump speed even more, the shape of the sides of the helical cone starts oscillate and become discontinuous (pulses are seen). This is due to the internal forces acting inside the hydrocyclone, as for a brief moment there exists a conflict between the water and the air core as they take turns while exiting from the overflow, as more water tries to exit from the underflow where the air for the air core is entering. The air core is an unstable cone (see appendix B for air core and system pictures).

Then at a pump speed of about 715 rpm, the air core starts to decrease. The spray discharge angle also starts to decrease. This is because more and more water is trying to exit from both the overflow and the underflow. Increasing the pump speed even more, the air core collapses and the discharge at the underflow takes a rope like form again.

According to literature [3, 8, 16], the optimal point to operate a hydrocyclone is at the transitional point from spray to roping, just before the discharge takes the rope like form, i.e. when the air core is about to collapse.

This happened at a pump speed of 715 rpm so the variable speed drive was set to drive the pump at that speed to emulate the optimal conditions.

Initially it was decided to record a testing database at the optimal point and use it to test a static training database. However during the dynamic test it came clear that the system would perform better if both databases (training and testing) were recorded from the dynamic test to minimise the introduction of errors due to differences in electrical properties of polystyrene and air, as well as the electrical properties of the water used in both tests.

From the static performance section it was clear that only the volume fraction prediction should be considered.

The resulting volume fractions predictions are very good. Below are three cases of volume fractions predictions (see appendix C for the whole volume fraction predictions).

Figure 5.9 shows a volume fraction for case 578, which represents an air core.

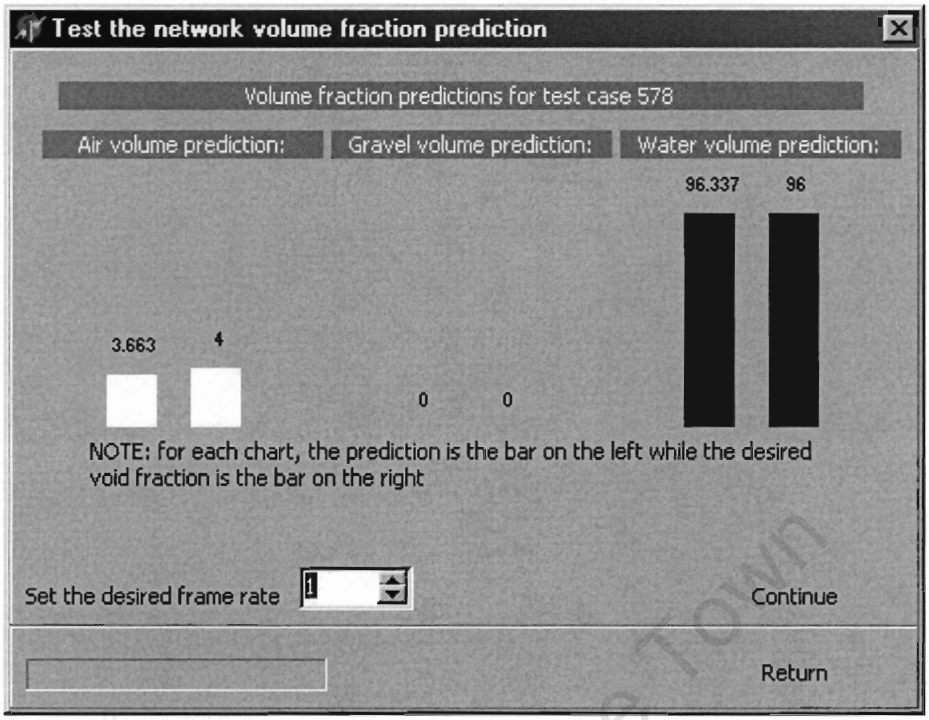

Fig. 5.9 A volume fraction prediction for case 578

In figure 5.9 a volume fraction prediction of the hydrocyclone operating with an air core approximated as 4% air and 96% water is shown. The case number is 578. The frame rate at which the database was viewed had to be slowed down to one frame per second, to allow the picture to be taken. The picture shows two bars side by side for each case (air, gravel and water volume prediction). The network prediction bar is the one on the left and the desired output bar is the one on the right; in this case a quantitative, numeric interpretation or comparison can be done.

This picture shows that: the volume prediction of air is 3.663%, when the desired output of air is 4%; the volume prediction of gravel is 0, when the desired output of gravel is 0; and the volume prediction of water is 96.336%, when the desired output of water is 96%.

Figure 5.10 shows a volume fraction for case 585, which represents an air core.

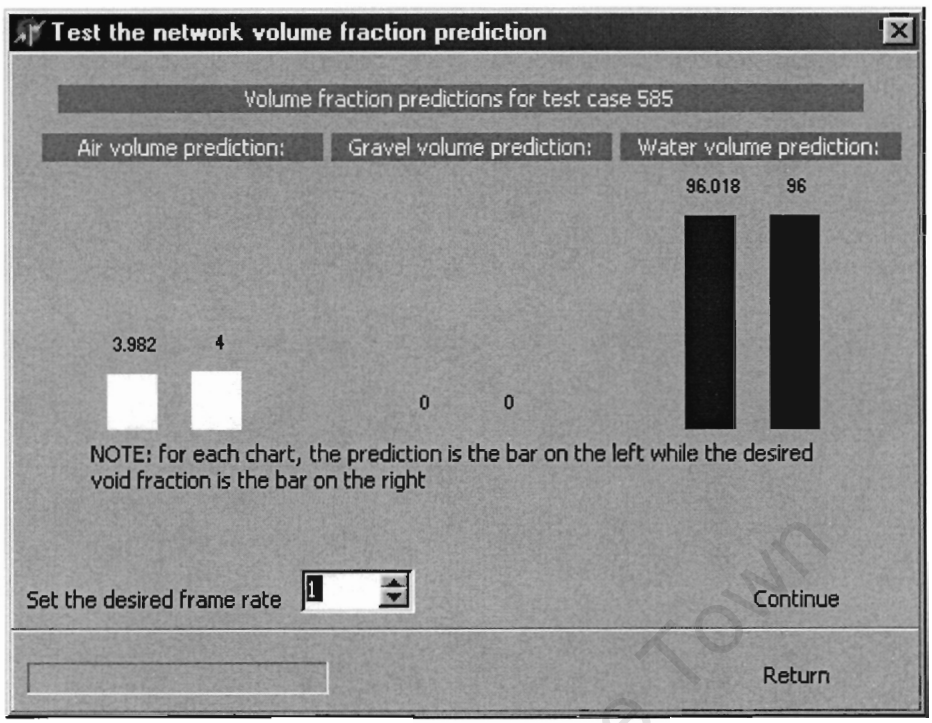

Fig. 5.10 A volume fraction prediction for case 585

In figure 5.10 a volume fraction prediction of the hydrocyclone operating with an air core approximated as 4% air and 96% water is shown. Te case number is 585. The frame rate at which the database was viewed had to be slowed down to one frame per second, to allow the picture to be taken. The picture shows two bars side by side for each case (air, gravel and water volume prediction). The network prediction bar is the one on the left and the desired output bar is the one on the right; in this case a quantitative, numeric interpretation or comparison can be done.

This picture shows that: the volume prediction of air is 3.982%, when the desired output of air is 4%; the volume prediction of gravel is 0, when the desired output of gravel is 0; and the volume prediction of water is 96.018%, when the desired output of water is 96%.

Figure 5.11 shows a volume fraction for case 593, which represents an air core.

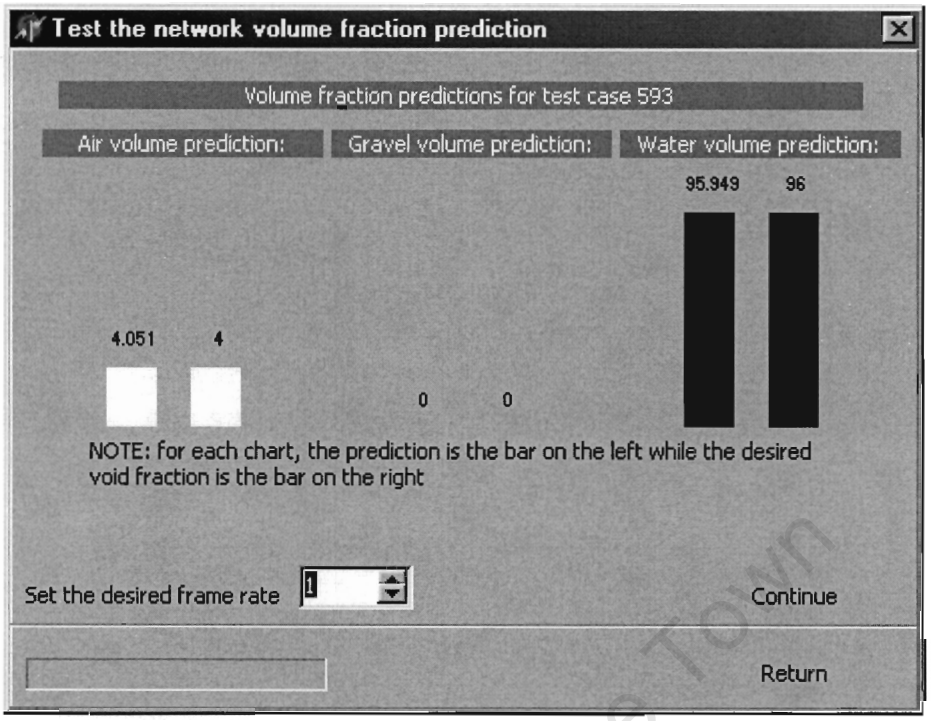

Fig. 5.11 A volume fraction prediction for case 593

In figure 5.11 a volume fraction prediction of the hydrocyclone operating with an air core approximated as 4% air and 96% water is shown. The case number is 593. The frame rate at which the database was viewed had to be slowed down to one frame per second, to allow the picture to be taken. The picture shows two bars side by side for each case (air, gravel and water volume prediction). The network prediction bar is the one on the left and the desired output bar is the one on the right; in this case a quantitative, numeric interpretation or comparison can be done.

This picture shows that: the volume prediction of air is 4.051%, when the desired output of air is 4%; the volume prediction of gravel is 0, when the desired output of gravel is 0; and the volume prediction of water is 95.949%, when the desired output of water is 96%.

CHAPTER 6

MONITORING OF THE HYDROCYCLONE

6. Monitoring Hydrocyclones

The principle of centrifugal force through which hydrocylones operate presents a way that FDM EIT can be used to optimise and monitor the operational point of a hydrocyclone. This is done by keeping track of the size of the air core which can be achieved by looking at the volume fraction prediction, as shown in the previous chapter.

From the dynamic performance (section 5.2), the air core may increase from 0% to approximately 4% volume of the contents of the hydrocyclone. This increase of the air core is picked up by the FDM EIT as a volume fraction of the air core to volume fraction of water. As the air core forms and grows, a graph of air core volume fraction vs. flow rate can be plotted. Note that the pump speed in revolutions per minute (rpm) is used to illustrate the flow rate of the liquid.

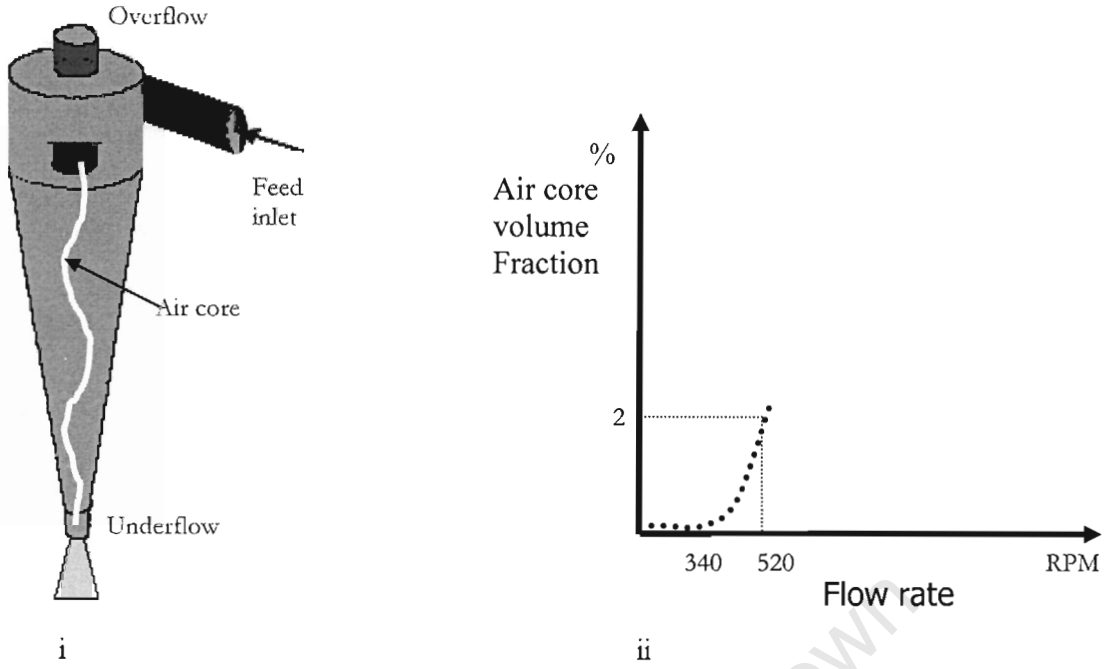

Fig. 6.1 Air core formation underflow (i **adapted from the web page: cyclone.html [35])**

An operating hydrocyclone with the air core at an early stage about 2% of the volume of the content of the hydrocyclone is shown in fig 6.1 i. Note the spray type discharge at the underflow. The corresponding development graph of air core volume fraction vs. flow rate, up to the point where the air core is about 2% of the volume of the content of the hydrocyclone and the flow rate is around 520 rpm, is shown in fig 6.1 ii. The air core starts to form at a flow rate of about 340 rpm.

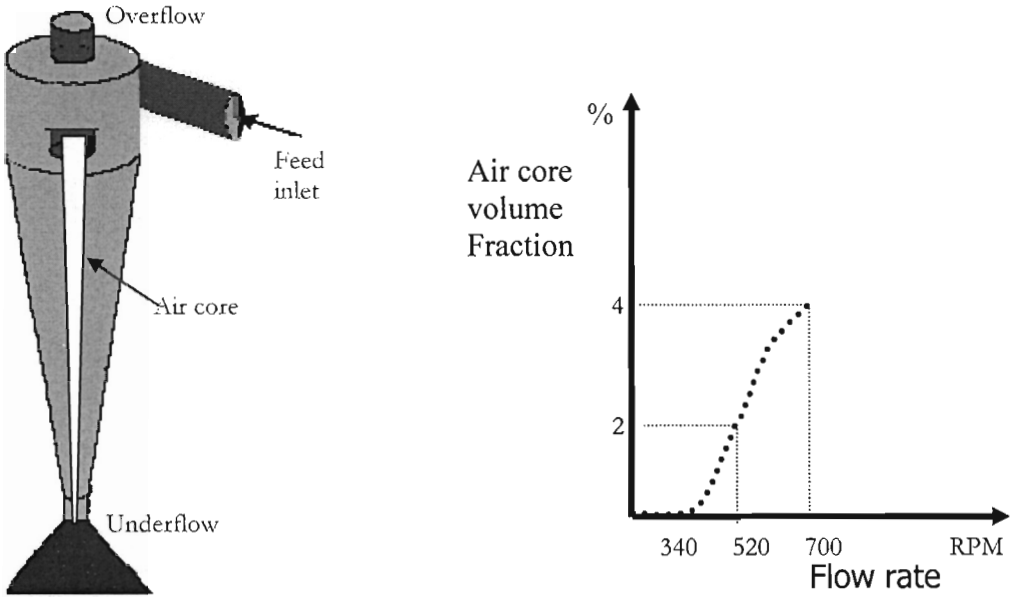

i ii

Fig. 6.2 Air core formation detected as volume fraction of air underflow (i **adapted from the web page: cyclone.html [35])**

An operating hydrocyclone at the stage where the air core reaches about 4% of the volume of the content of the hydrocyclone is shown in fig 6.2 i. Note the spray type discharge at the underflow. The corresponding development graph of air core volume fraction vs. flow rate, up to the point where the air core is about 4% of the volume of the content of the hydrocyclone and the flow rate is around 700 rpm, is shown in fig. 6.2 ii.

In order to fine tune the classification of the hydrocyclone the flow rate will be increased. This will result in the air core shrinking, until the apex saturates and the air core collapses, as in fig 6.3.

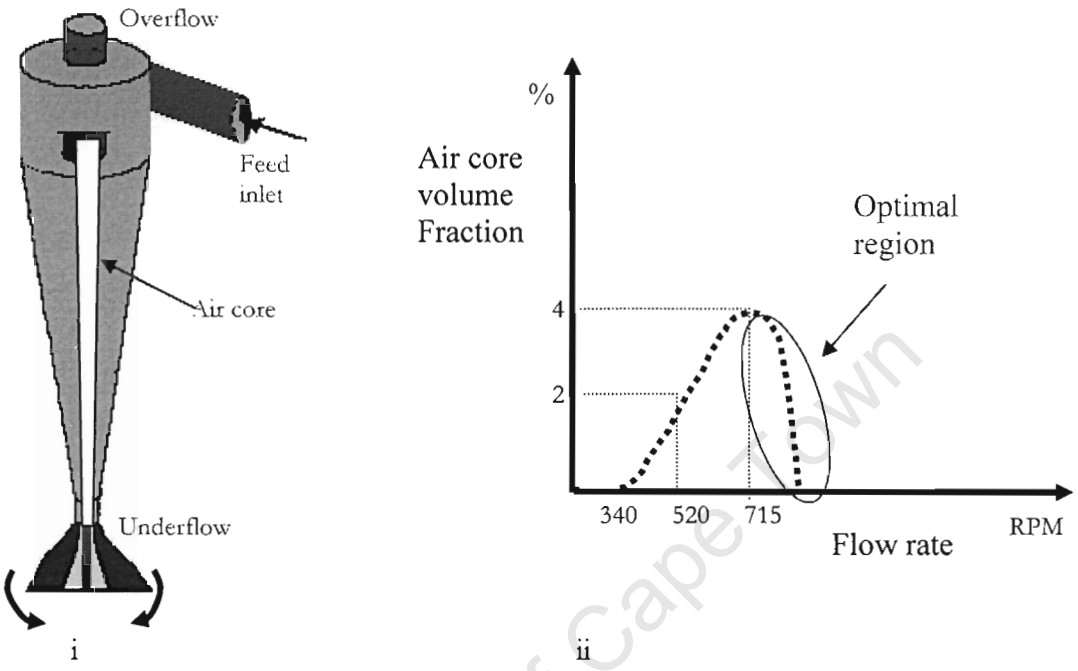

Fig. 6.3 Air core collapse; note behaviour at the underflow (i adapted from the web page: cyclone.html [35])

An operating hydrocyclone at the various stages of the air core is shown in fig. 6.3 i .Note that the angle of discharge changes at the underflow as the air core shrinks while passing the critical flow rate. The spray type (in brown and yellow) discharge at the underflow disappears into a rope like discharge (in red) as the arrows indicate. The corresponding development graph of air core volume fraction vs. flow rate, for the entire operational range of the volume fraction of the air core in the hydrocyclone, is shown in fig. 6.3 ii. The air core remains at 4% for a short while from 700 rpm until passing the critical flow rate of about 715 rpm when it starts to decrease.

The optimal region of operation happens when the discharge is about to change from spray to roping. This can be seen from the changes in the air core (the air core is shrinking); therefore by monitoring the volume fraction of the air core with the FDM EIT, and feeding back the necessary information, commands and actions, to the actuator variable speed drive (VSD) and the pump that feeds the hydrocyclone, control of the hydrocyclone can be achieved. This is shown in the diagram below:

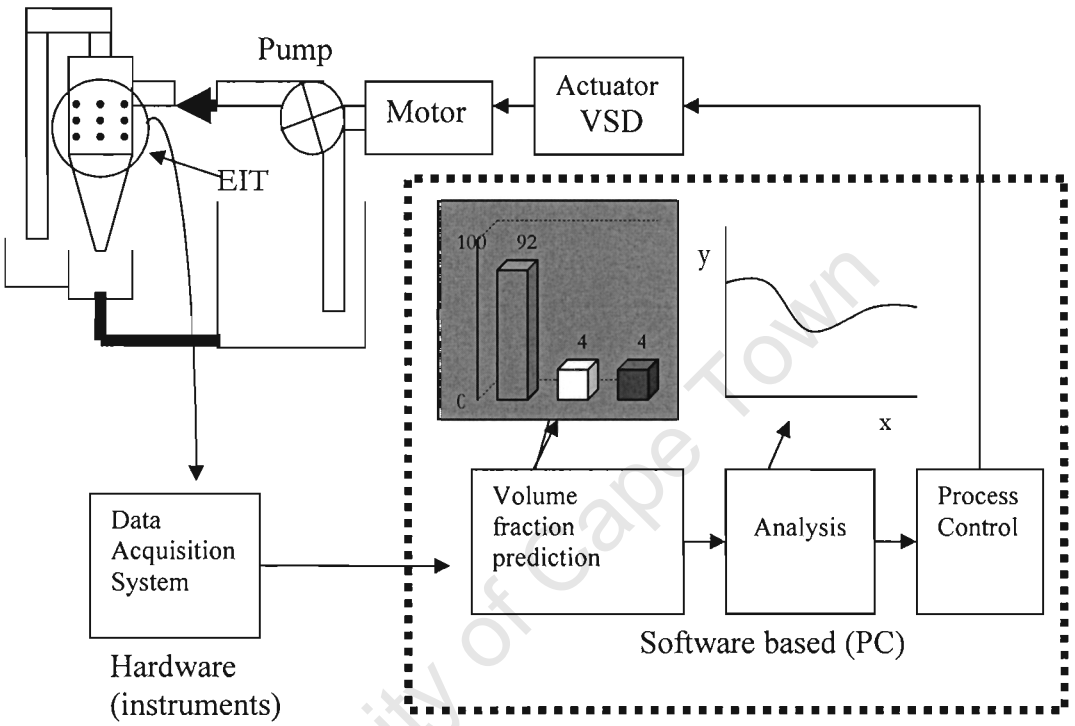

Fig. 6.4 Closed loop hydrocyclone controlling system (Adapted from M.S. Beck and R.A. Williams [29, 32])

A different approach, would be to try to get variable size valves and use them to vary the ratio of the underflow diameter (apex) to the overflow diameter (vortex) (d_u/d_o). However this can only be achieved after more studies can be done to establish the true relationship between air core and the ratio of the underflow diameter (apex) to the overflow diameter (vortex) (d_u/d_o).

CHAPTER 7

CONCLUSIONS

7. CONCLUSIONS

Based on the performance of the FDM EIT, the following conclusions may be drawn:

7.1. The air core is a good indicator for the performance of a hydrocyclone.

The air core behaviour does determine the operational point of the hydrocyclone; hence it determines the separation quality of products.

7.2. The FDM EIT system does detect the air core.

The FDM EIT system can perform both image reconstructions and volume fraction predictions of the air core inside of an operating hydrocyclone.

7.3. The volume fraction prediction should be used rather than an image reconstruction.

When volume fraction prediction is performed, a quantitative, numeric, interpretation or comparison can be done regarding the behaviour of the air core.

7.4. Monitoring and controlling a hydrocyclone can be achieved using a FDM EIT system.

By capturing and monitoring the air core using FDM EIT to measure volume fraction, and using the qualitative information obtained as input to the control software or hardware system that is linked to a set of actuators that control valves and the pump, control of a hydrocyclone can be achieved.

CHAPTER 8

RECOMMENDATIONS

8. RECOMMENDATIONS

Based on the performance of the FDM EIT system and on the conclusions, the following recommendations can be made:

8.1. A larger size hydrocyclone should be used.

For further research a larger hydrocyclone should be used to facilitate the placement of the sensors, and also to be able to expand the FDM EIT system to 16 electrodes to try to obtain more readings and a higher spatial resolution.

8.2. Extend the FDM EIT system to 16 electrodes.

In theory the more readings taken, the better would be the image resolution and volume fraction prediction. With the increase in size of the hydrocyclone a project on increasing to a 16 electrode FDM EIT system should be undertaken, to introduce more frequencies and to investigate the above theory.

8.3. The reconstruction software should be modified.

The reconstruction software was designed to perform flow measurements only, making it difficult to obtain online reconstructions of an operating hydrocyclone.

8.4. The training strategy needs to change.

While obtaining the training and testing databases of an operating hydrocyclone, the actual size of the air core can not be determined. At moment only mathematical assumptions and a visual approximation are available.

8.5. Graphs of air core vs. flow rate, pressure, slurry concentration and ratio of underflow diameter to overflow diameter should be plotted.

Experiments should be conducted using an online FDM EIT, to obtain graphs and charts relating air core to pressure, slurry concentration, and the ratio of the underflow diameter to overflow diameter d_u/d_o.

REFERECES

1. R.A. Williams, F.J. Dickin, J.A Gutiérrez, T. Dyakowski and M.S. Beck*: Using electrical impedance tomography for controlling hydrocyclone underflow discharge.* Control Eng. Practice. 5 (1997) pp 253-256
2. R.A. Williams, X. Jia, R.M. West, M. Wang, J.C. Cullivan, J. Bond, I. Faulks, T. Dyakowski, S.J. Wang, N. Climpson, J.A. Kostuch and D. Payton*: Industrial monitoring of hydrocyclone operation using electrical resistance tomography.* Min. Eng. 12 (1999) pp 1245-1252
3. T. Dyakowski and R.A. Williams: *Prediction of air core size and shape in a hydrocyclone.* Int. J. Miner. Process. 43 (1995) pp 1-14
4. J. Romero, R. Sampaio and R.S. da Gama: *Numerical simulation of flow in a hydrocyclone.* Latin America Applied Research 34 (2004) pp 1-9
5. A. Barrientos, R. Sampaio and F. Concha*: Effect of the air core on performance of hydrocyclone.* International Mineral Processing Congress (18th: 1993: Sidney, N.S.W.) 1 (1993) pp 267-270
6. J.A Gutiérrez,. T. Dyakowski, M.S. Beck, R.A. Williams*: Using electrical impedance tomography for controlling hydrocyclone underflow discharge.* Powder Tech. 108 (2000) pp 180-184
7. M.A. Bennett and R.A. Williams: *Monitoring the operation of an oil/ water separator using impedance the tomography.* Min. Eng. 17 (2004) pp 605-614
8. Th. Neesse, M. Schneider, J. Dueck, V. Golyk, S. Buntenbach and H. Tiefel: *Hydrocyclone operation at the transition point rope spray discharge.* Min. Eng. 17 (2004) pp 733-737
9. J.C. Cullivan, R.A. Williams, T. Dyakowski and C. R. Cross: *New understanding of a hydrocyclone flow field and separation mechanism from computational fluid dynamics* Min. Eng. 17 (2004) pp 651-660
10. B. Firth: *Hydrocyclones in dewatering circuits.* Min. Eng. 16 (2003) pp 115-120
11. G. Teague, J. Tapson and Q. Smit: *Neural network reconstruction for tomography of a gravel-air-seawater mixture.* Meas. Sci. Technol. 12 (2001) pp 1102-1108
12. B. Chiné and F. Concha: *Flow patterns in conical and cylindrical hydrocyclones.* Chen. Eng. J. 80 (2000) pp 267-273

13. R.A. Williams, O.M. Ilyas, T. Dyakowski, F.J. Dickin, J.A Gutiérrez, M. Wang, M.S. Beck, C. Shah, and A. Rushton: *Air core imaging in cyclonic Separators: implications for separator design and modelling.* Chem. Eng. J. 56 (1995) pp 135-141
14. T.C. Monredon, K.T. Hsieh and R.K. Rajamani: *Fluid flow of the hydrocyclone: an investigation of the device dimensions.* Int. J. Miner. Process. 35 (1992) pp 65-83
15. M. Cheney, D. Isaacson and J.C. Newellwski: *Electrical impedance tomography.* SIAM Review 41, (1999) pp 85-101
16. F. Concha, A. Barrientos, J. Montero and R. Sampaio: *Air core and roping in hydrocyclones.* Int. J. Miner. Process. 44-45 (1996) pp 743-749
17. P.R. Steffens, W.J. Whiten, S. Appleby and J. Hitchins: *Prediction of air core diameter for hydrocyclones.* Int. J. Miner. Process. 39 (1993) pp 61-74
18. J.B. Yianatos, M.A. Lisboa and D.R. Baeza: *Grinding capacity enhancement by solid concentration control of hydrocyclone underflow.* Min. Eng. 15 (2002) pp 317-323
19. Prof. G, Tarján: *Contribution to the analytics of medium flow and pressure drop in hydrocyclones.* Institute of Mineral Dressing, Technical University, Miskolc (1960)
20. B. Dabir and C.A. Petty: *Laser doppler anemometry measurements of tangential and axial velocities in a hydrocyclone operating without an air core.* Paper A2, 2nd International Conference on Hydrocyclones, Bath, England: 19-21 September 1984.
21. K.A. Percieous, N. Rhodes and G.W. Cutting: *A mathematical model for predicting the flow field in a hydrocyclone classifier.* Paper B11, 2nd International Conference on Hydrocyclones, Bath, England: 19-21 September 1984.
22. E.M. Sevilla and R.M.R. Branion: *The fluid dynamics of hydrocyclones.* Journal of Pulp and Paper Science. 23 (2004) pp J85-J93
23. L.R. Plitt, B.C. Flintoff and T.J. Stuffco: *Roping in hydrocyclones.* Paper A3, 3rd International Conference on Hydrocyclones, Oxford, England: 30th September – 2nd October 1987.
24. T. Dyakowski and R.A. Williams*: Prediction of high solids concentration regions within hydrocyclone.* Powder Tech. 87 (1996) pp 43-47
25. G. Teague: *Mass flow measurement of multi-phase mixtures by means of tomography.* PhD Thesis, Department of Electrical Engineering, University of Cape Town, (2002).
26. A. Giannopoulos: *Electrical impedance tomography systems.* MSc. Thesis, Department of Electrical Engineering, University of Cape Town, (2003).

27. Q. Smit: *Material phase detection using capacitance tomography.* MSc. Thesis, Department of Electrical Engineering, University of Cape Town, (2000).
28. Rockwell Automation: *Adjustable frequency AC drive.* Power flex70 user manual Allen-Bradley (also at www.abpowerflex.com)
29. M.S. Beck and R.A. Williams: *Process tomography: a European innovation and its applications.* Meas. Sci. Technol. 7 (1996) pp 215-224
30. N. Reinecke and D. Mewes: *Recent developments and industrial/ research applications of capacitance tomography.* Meas. Sci. Technol. 7 (1996) pp 233-246
31. F. Dickin and M. Wang: *Electrical resistance tomography for process applications.* Meas. Sci. Technol. 7 (1996) pp 247-260
32. R.A. Williams and M.S. Beck. *Process tomography: principles, techniques and applications.* UK: Butterwort-Heinemann Ltd, 1995.
33. http://www.psl.bc.ca/downloads/presentations/cyclone/cyclone.html

    Cyclone.html Process Simulations Ltd.
    last accessed on the 22nd March 2005

34. http://www.globalspec.com/industrial-directory/hydrocyclone

    Wanwilai, K.: *The experimental study of the flow within a hydrocyclone*
    last accessed on the 2nd February 2005

35. http://www.vortexventures.com/Products/SpintopHydrocyclone/SpintopHydrocyclone.htm SPINTOP HYDROCYCLONE - The Density Separator That Converts Pressure Energy Into Rotational Momentum In Liquid Applications
    last accessed on the 10th March 2005

Interview

Mr Aubrey Mainza Department of Chemical Engineering University of Cape Town, Personal interview (discussion)

Internet Sites

http://www.vortexventures.com/Products/SpintopHydrocyclone/SpintopHydrocyclone.htm SPINTOP HYDROCYCLONE - The Density Separator That Converts Pressure Energy Into Rotational Momentum In Liquid Applications - So

http://www.psl.bc.ca/
Process Simulations Ltd.

http://www.psl.bc.ca/equipment/hydrocyclone/
Hydrocyclone

http://www.psl.bc.ca/downloads/presentations/cyclone/cyclone.html
http--www.psl.bc.ca-downloads-presentations-cyclone-cyclone.html

http://www.sciencedirect.com
Science Direct - Minerals Engineering, Volume 17, Issue 5, Pages 571-744 (May 2004)
Science Direct - Minerals Engineering Monitoring the operation of an oil-water separator using impedance tomography
Science Direct - Minerals Engineering - List of Issues
Science Direct - Minerals Engineering Industrial monitoring of hydrocyclone operation using electrical resistance tomography1

http://www.mec.puc-rio.br/prof/rsampaio/rsampaio.html
Perfil Tecnologico - Professor Rubens Sampaio - DEM da PUC-RIO

http://www.glossary.oilfield.slb.com/Display.cfm?Term=hydrocyclone
Oilfield Glossary Term 'hydrocyclone'

http://www.natcogroup.com/Content.asp?t=ProductPage&ProductID=114
MOZLEY SANDSPIN Solid-Liquid Hydrocyclone - NATCO Group

http://www.tomography.umist.ac.uk/ecci.shtml
Monitoring Industrial Hydrocyclone Performance using electrical resistance and ultrasound.

http://www.min-eng.com/
Minerals Engineering International Online - mineral processing & extractive metallurgy information

http://www.krebs.com/products.php/category/1/Hydrocyclones
Krebs Hydrocyclones

http://www.saj.usace.army.mil/nav/hydrocyclone.htm
Hydrocyclone technology

http://www.odisfiltering.com/phydro.html
Hydrocyclone Separators

http://www.nalusda.gov/ttic/tektran/data/000007/32/0000073285.html
HYDROCYCLONE SEPARATION OF DRY-MILLED CORN

http://www.chemindustry.com/chemnames/H/hydrocyclone.asp
Hydrocyclone at ChemIndustry.com

http://www.enductive.com/pdf/paper_hydrocyc_2003.pdf
http--www.enductive.com-pdf-paper_hydrocyc_2003.pdf

http://www.ab.com/drives/
Allen-Bradley Drives Home page

http://www.afrlhorizons.com/Briefs/Sept02/ML0205.html
Air Sparged Hydrocyclone Technology

APPENDICES

TABLE OF CONTETS

APPENDIX A

Drawings of the cylindrical and conical sections

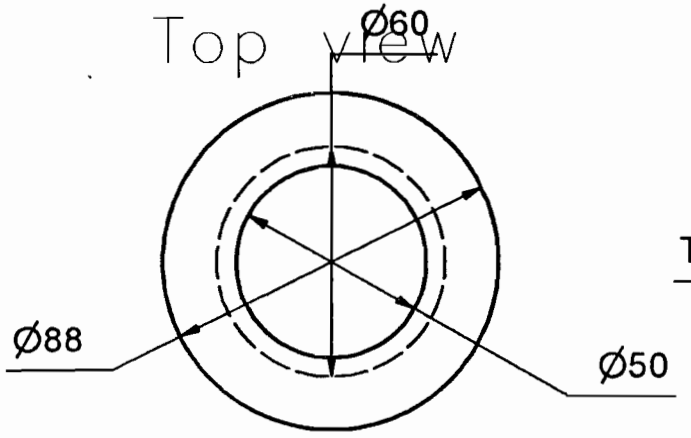

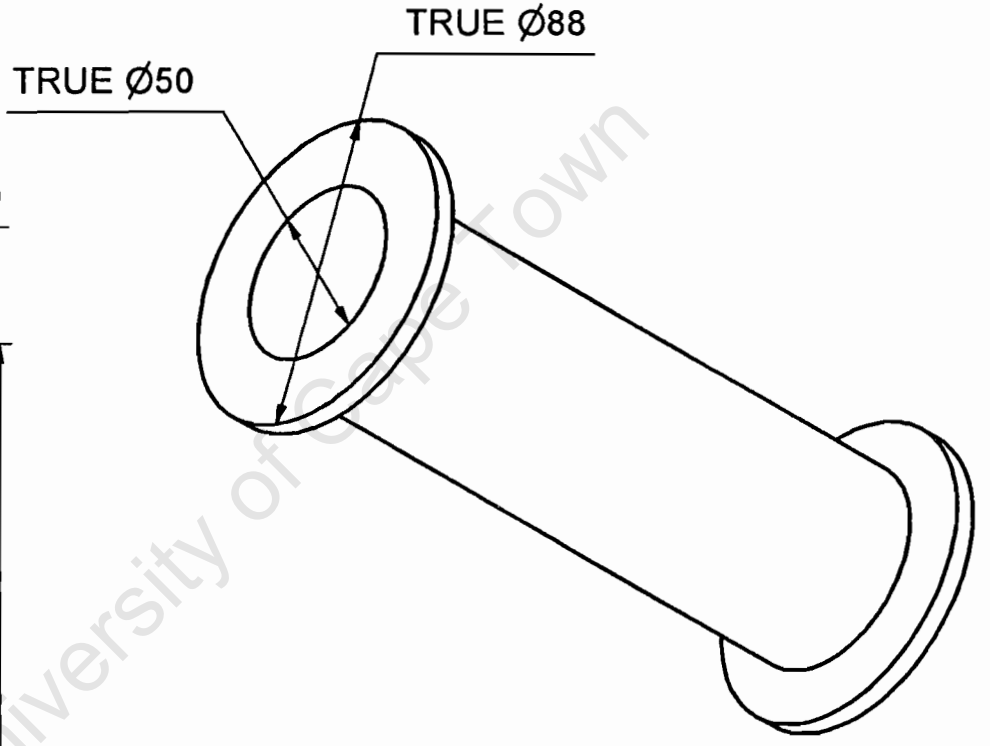

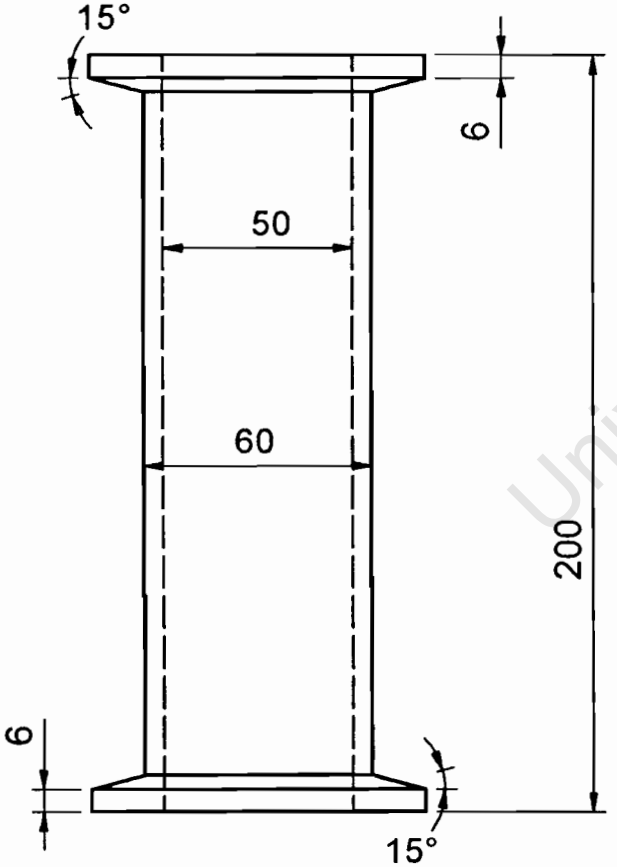

	UNIVERSITY OF CAPE TOWN Department of Mechanical Engineering	
	Title Hydrocyclone	
Dimentions in mm Tolerance U.O.S	Scale	Date 01/08/03 Sheet 1 of 2
	Drawn By Vladimir Capindisso	Drawing Number 1

Top view

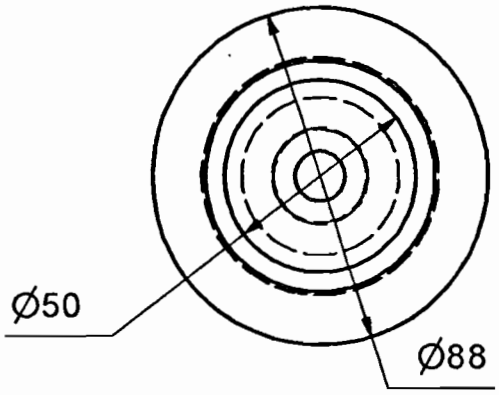

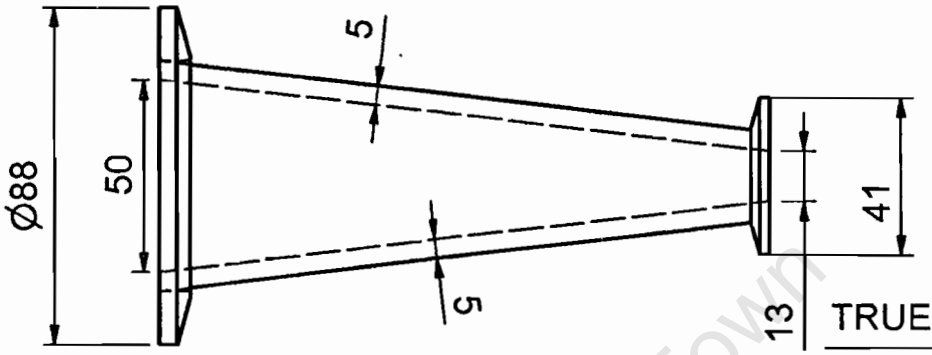

Botton view

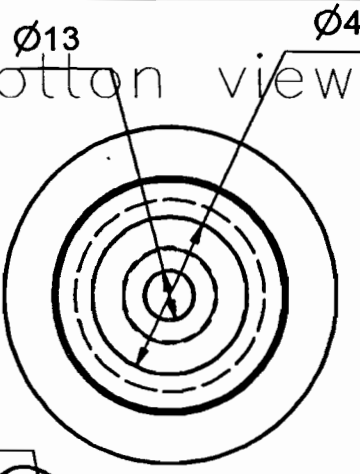

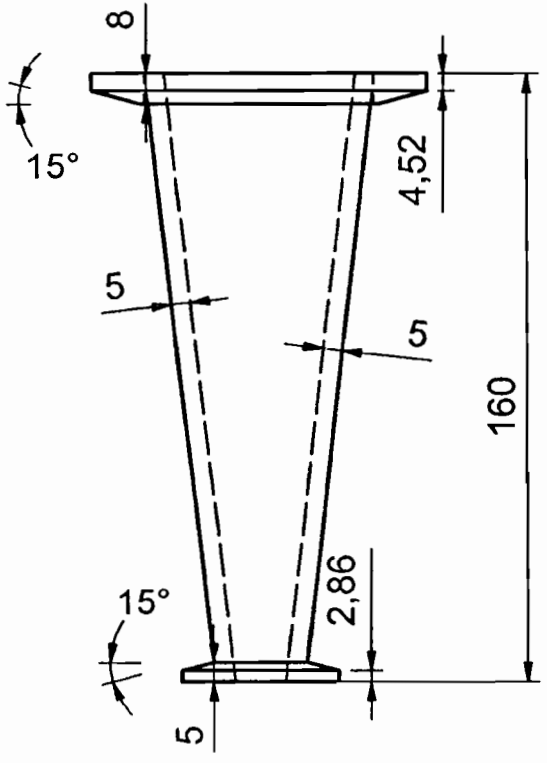

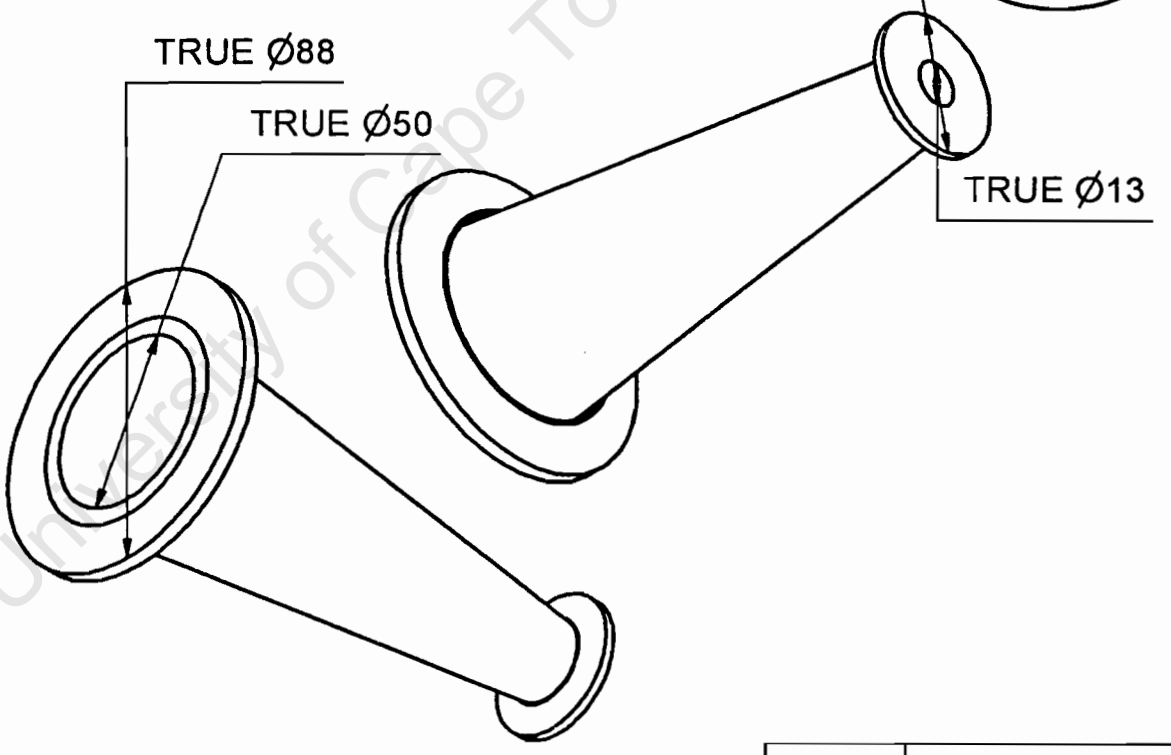

	UNIVERSITY OF CAPE TOWN Department of Mechanical Engineering
	Title: Hydrocyclone
Dimentions in mm Tolerance U.O.S	Scale Date 01/08/03 Sheet 2 of 2
	Drawn By Vladimir Capindisso Drawing Number 2

APPENDIX B

Pictures of the FDM EIT system and of the air core

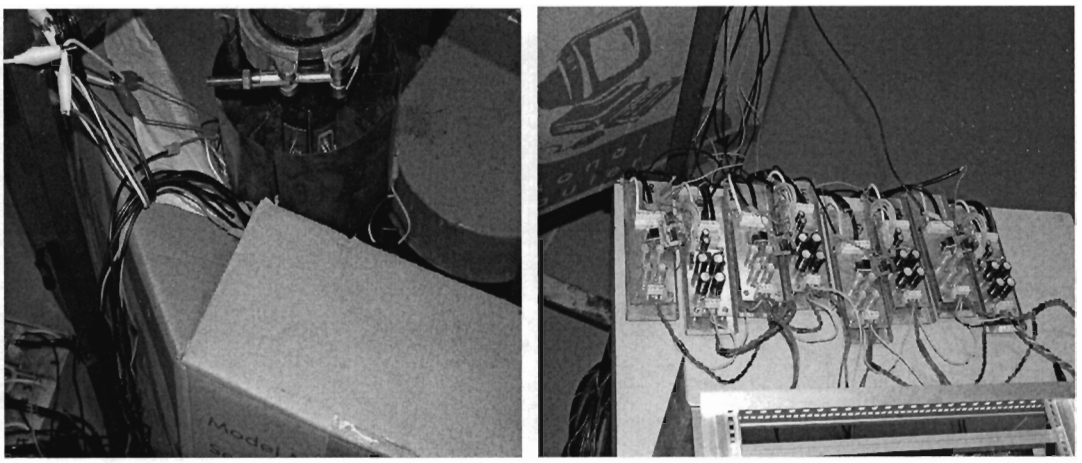

Fig. B-1 Pictures of the transmitter and receiver boards and cable connections

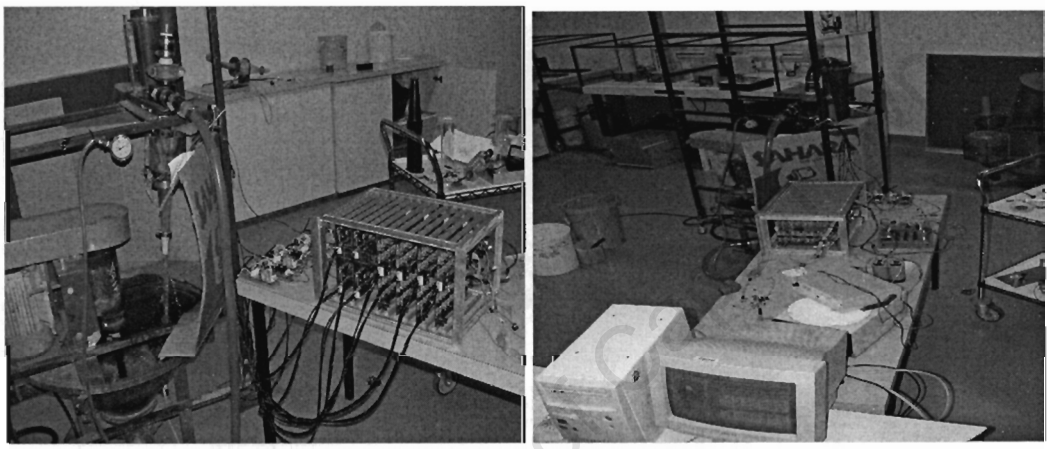

Fig. B-2 Pictures of the FDM EIT system

Fig. B-3 Pictures of the reconstruction computer and the FDM EIT system

Fig. B-4 Pictures of the FDM EIT system setup

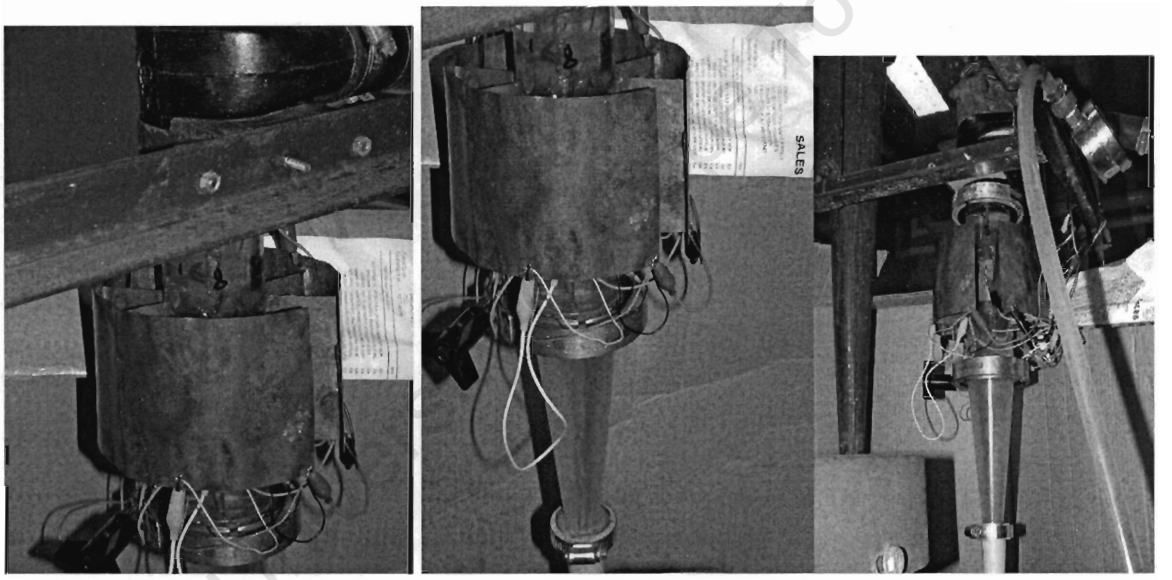

Fig. B-5 Pictures of the hydrocyclone with the sensor unit

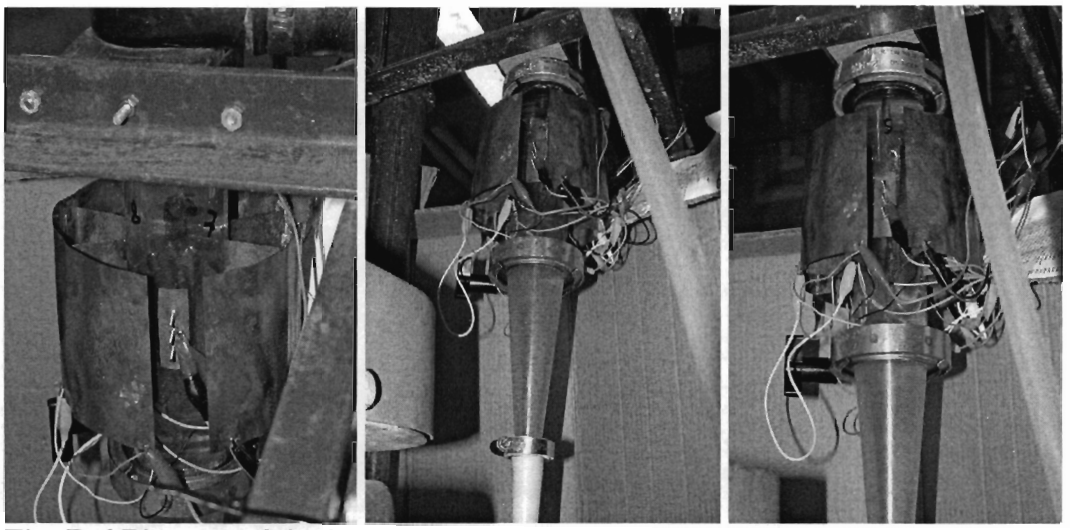

Fig. B-6 Pictures of the hydrocyclone with the sensor unit

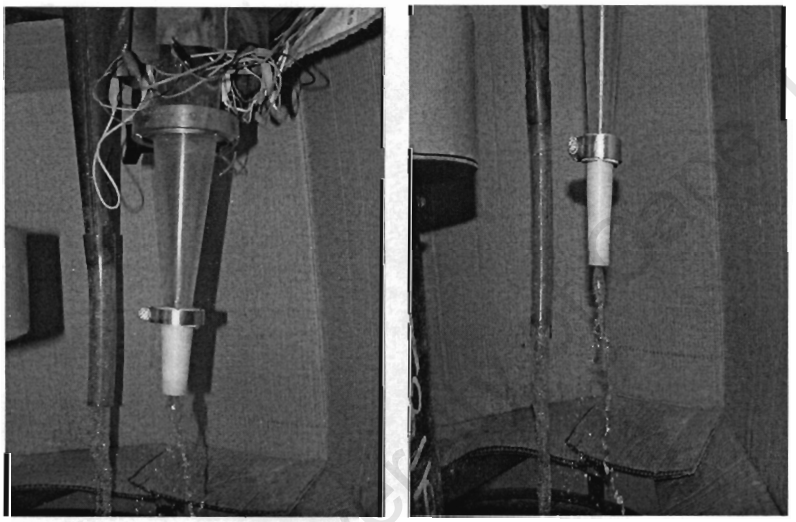

Fig. B-7 Pictures of the hydrocyclone discharge

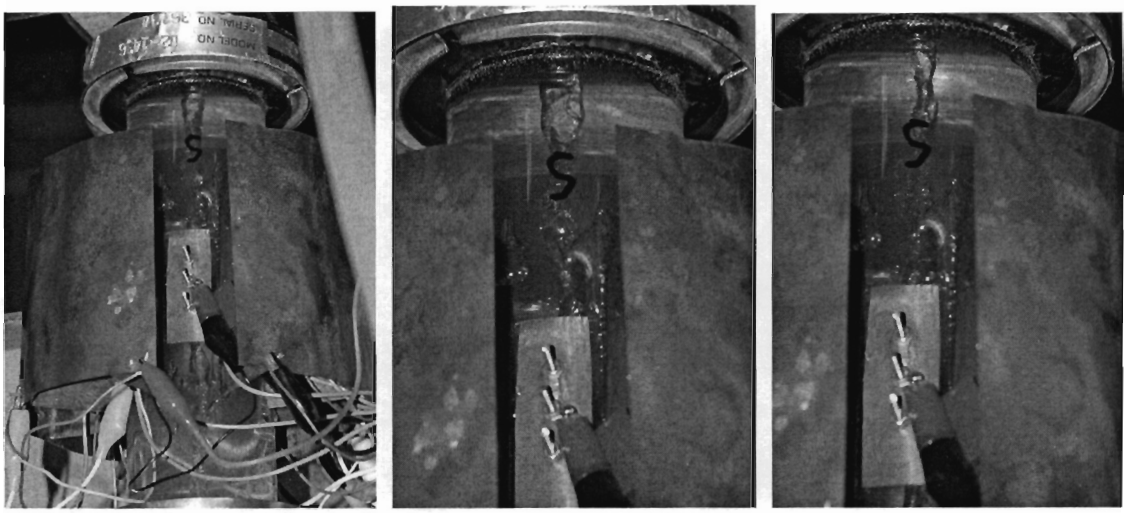

Fig. B-8 Pictures of the helical air core

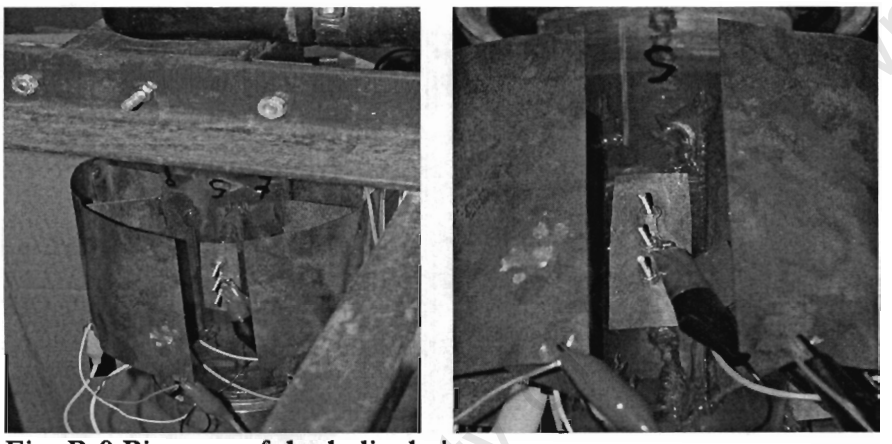

Fig. B-9 Pictures of the helical air core

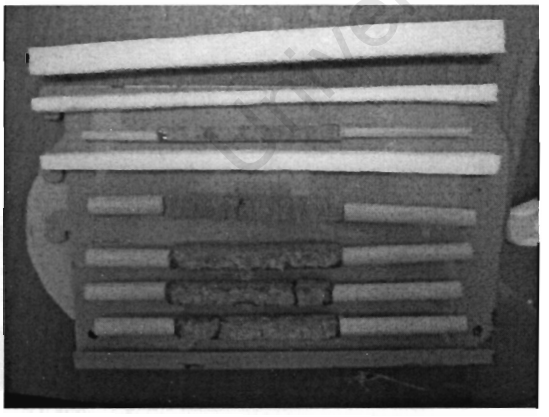

Fig. B-10 Picture of Air and Gravel Samples

APPENDIX C

Volume fraction predictions

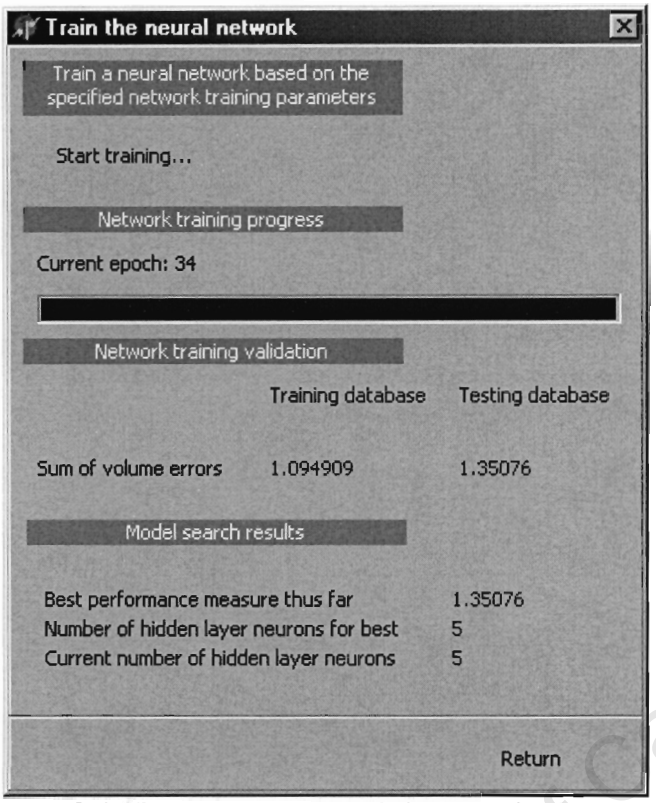

A neural network training results for volume fraction prediction of the hydrocyclone operating with an air core approximated as 4% air and 96% water is shown. The picture shows the number of the current epoch also the sum of the volume errors for training and testing databases and the number of hidden layers in use.

Fig. C-1 Neural network training results for volume fraction prediction

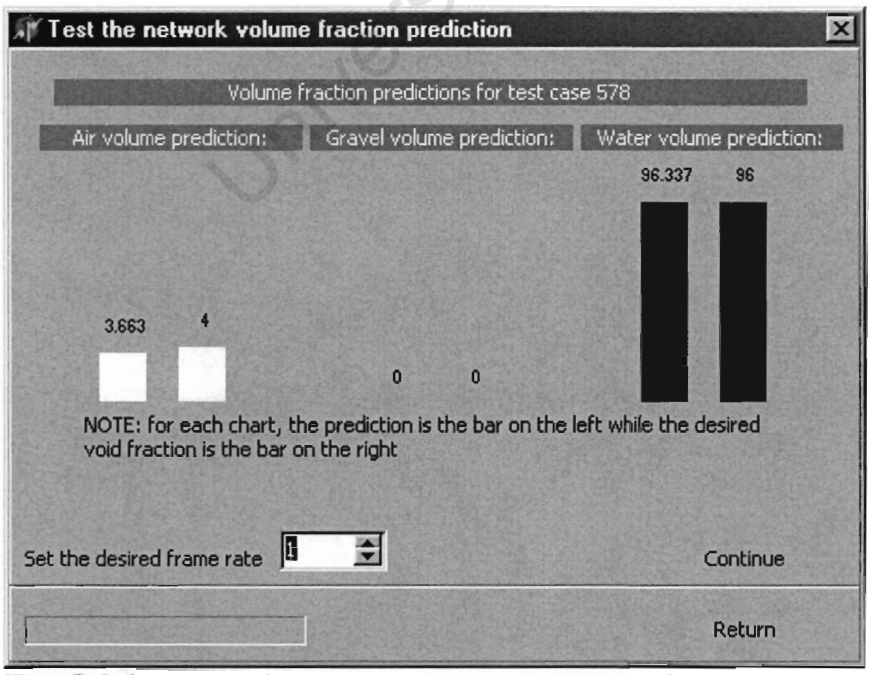

A volume fraction prediction of the hydrocyclone operating with an air core approximated as 4% air and 96% water is shown. The case number is 578. The frame rate at which the database was viewed had to be slowed down to one frame per second, to allow the picture to be taken. The picture shows two bars side by side for each case (air, gravel and water volume prediction). The network prediction bar is the one on the left and the desired output bar is the one on the right

Fig. C-2 A volume fraction prediction for case 578

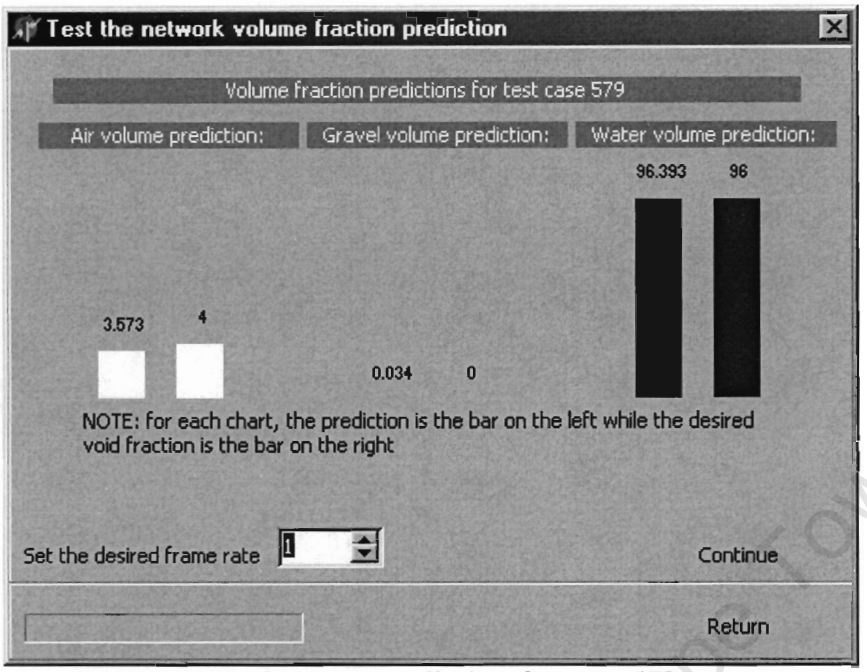

Fig. C-3 A volume fraction prediction for case 579

A volume fraction prediction of the hydrocyclone operating with an air core approximated as 4% air and 96% water is shown. The case number is 579. The frame rate at which the database was viewed had to be slowed down to one frame per second, to allow the picture to be taken. The picture shows two bars side by side for each case (air, gravel and water volume prediction). The network prediction bar is the one on the left and the desired output bar is the one on the right

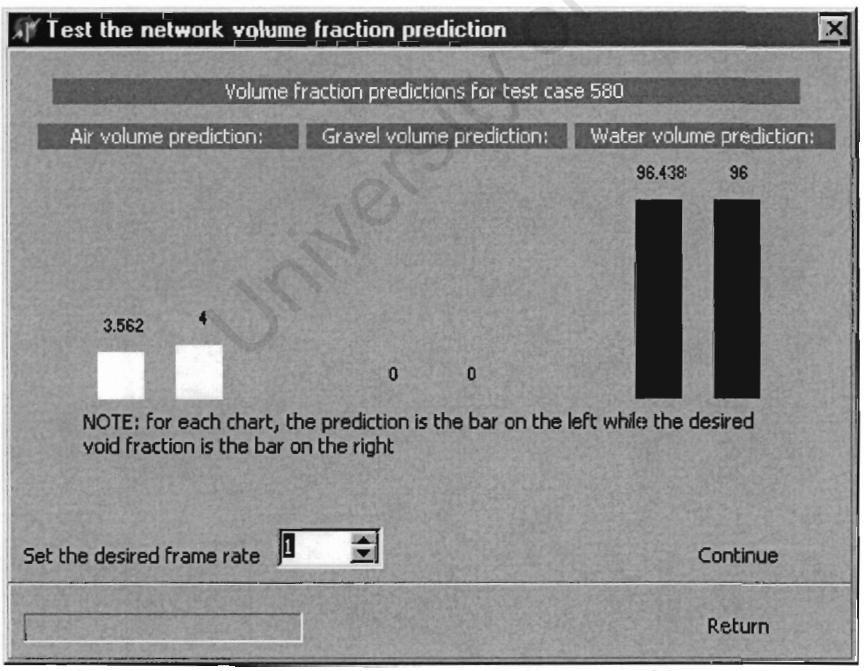

Fig. C-4 A volume fraction prediction for case 580

A volume fraction prediction of the hydrocyclone operating with an air core approximated as 4% air and 96% water is shown. The case number is 580. The frame rate at which the database was viewed had to be slowed down to one frame per second, to allow the picture to be taken. The picture shows two bars side by side for each case (air, gravel and water volume prediction). The network prediction bar is the one on the left and the desired output bar is the one on the right

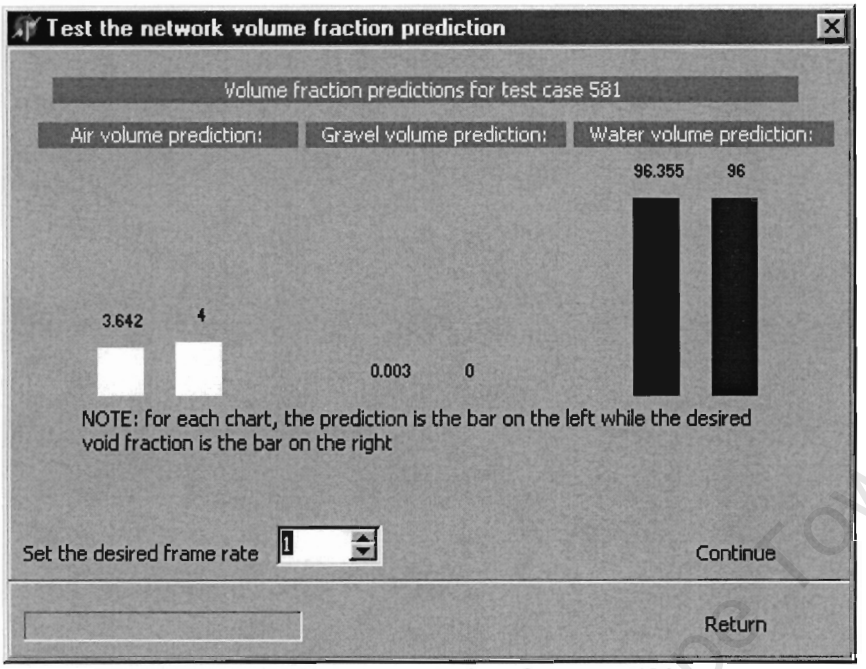

Fig. C-5 A volume fraction prediction for case 581

A volume fraction prediction of the hydrocyclone operating with an air core approximated as 4% air and 96% water is shown. The case number is 581. The frame rate at which the database was viewed had to be slowed down to one frame per second, to allow the picture to be taken. The picture shows two bars side by side for each case (air, gravel and water volume prediction). The network prediction bar is the one on the left and the desired output bar is the one on the right

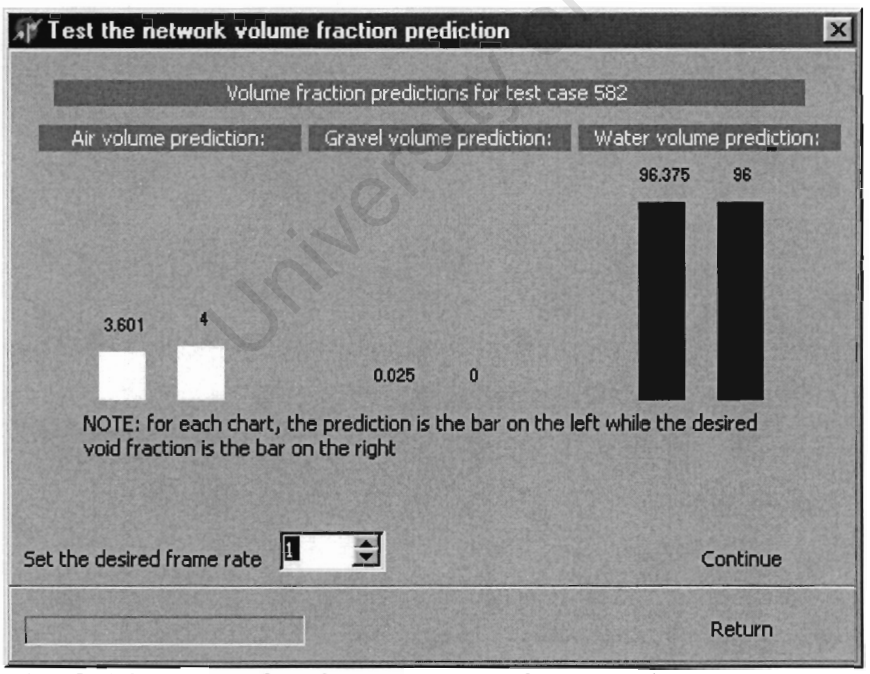

Fig. C-6 A volume fraction prediction for case 582

A volume fraction prediction of the hydrocyclone operating with an air core approximated as 4% air and 96% water is shown. The case number is 582. The frame rate at which the database was viewed had to be slowed down to one frame per second, to allow the picture to be taken. The picture shows two bars side by side for each case (air, gravel and water volume prediction). The network prediction bar is the one on the left and the desired output bar is the one on the right

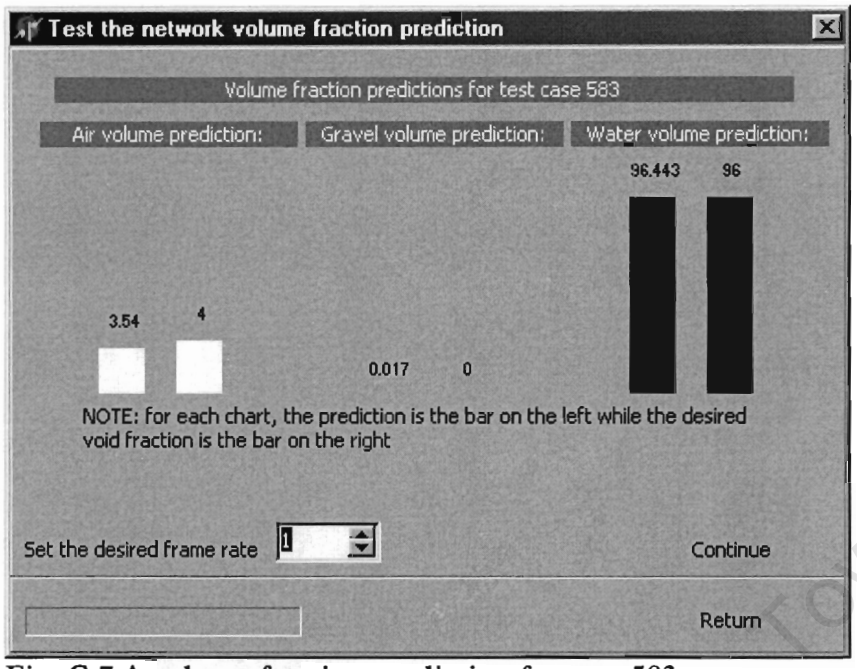

Fig. C-7 A volume fraction prediction for case 583

A volume fraction prediction of the hydrocyclone operating with an air core approximated as 4% air and 96% water is shown. The case number is 583. The frame rate at which the database was viewed had to be slowed down to one frame per second, to allow the picture to be taken. The picture shows two bars side by side for each case (air, gravel and water volume prediction). The network prediction bar is the one on the left and the desired output bar is the one on the right

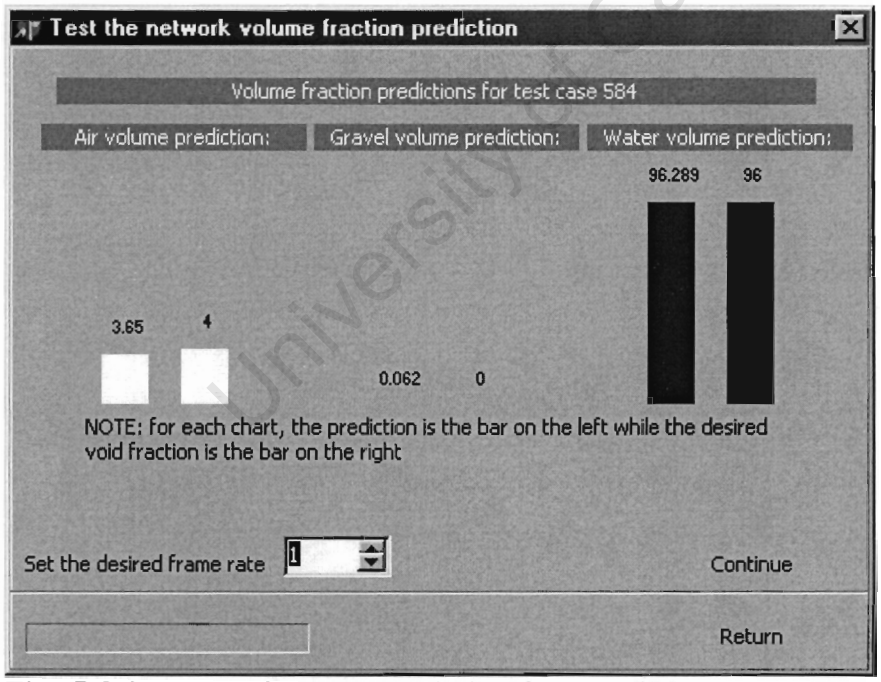

Fig. C-8 A volume fraction prediction for case 584

A volume fraction prediction of the hydrocyclone operating with an air core approximated as 4% air and 96% water is shown. The case number is 584. The frame rate at which the database was viewed had to be slowed down to one frame per second, to allow the picture to be taken. The picture shows two bars side by side for each case (air, gravel and water volume prediction). The network prediction bar is the one on the left and the desired output bar is the one on the right

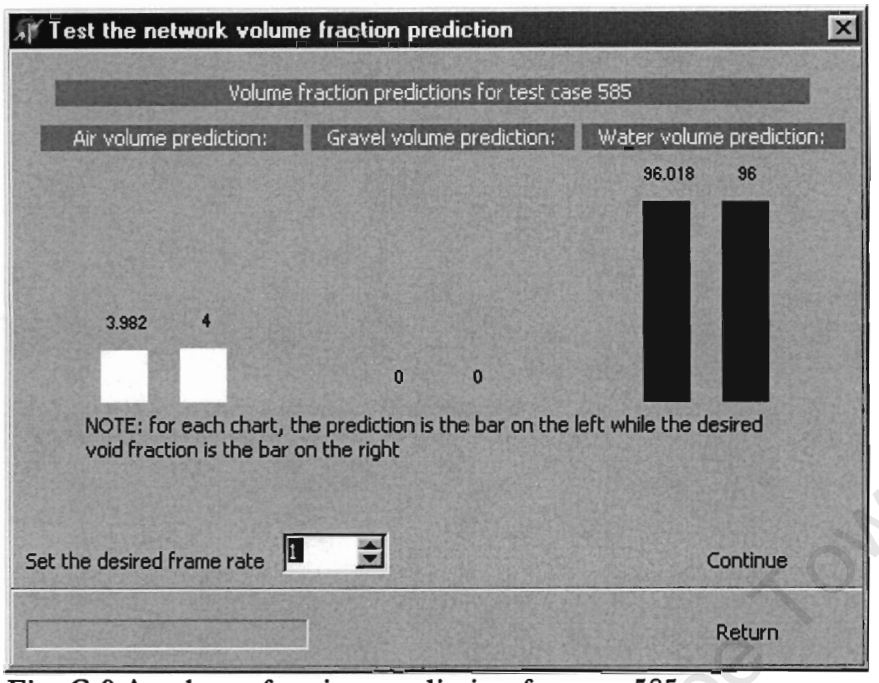

A volume fraction prediction of the hydrocyclone operating with an air core approximated as 4% air and 96% water is shown. The case number is 585. The frame rate at which the database was viewed had to be slowed down to one frame per second, to allow the picture to be taken. The picture shows two bars side by side for each case (air, gravel and water volume prediction). The network prediction bar is the one on the left and the desired output bar is the one on the right

Fig. C-9 A volume fraction prediction for case 585

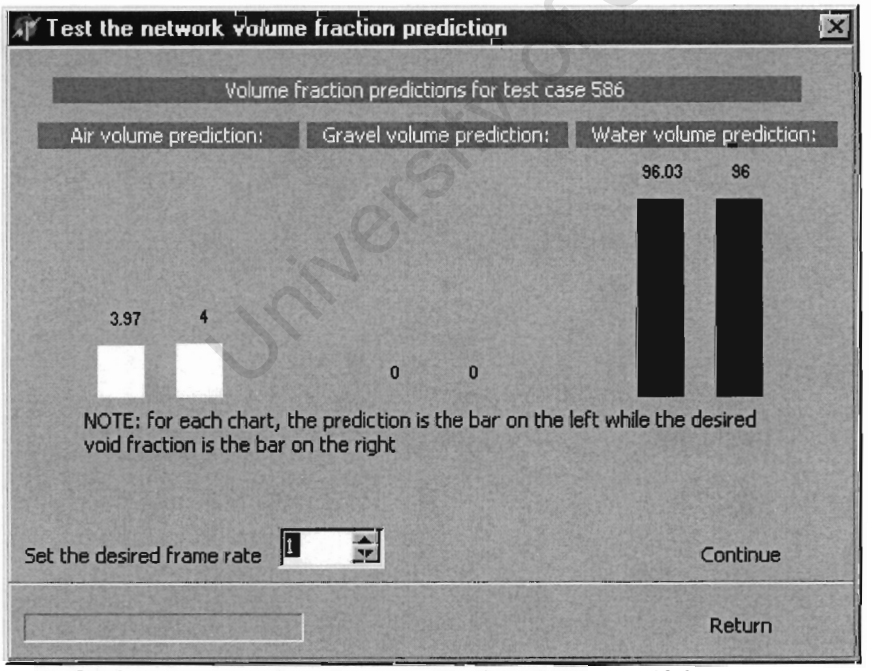

A volume fraction prediction of the hydrocyclone operating with an air core approximated as 4% air and 96% water is shown. The case number is 586. The frame rate at which the database was viewed had to be slowed down to one frame per second, to allow the picture to be taken. The picture shows two bars side by side for each case (air, gravel and water volume prediction). The network prediction bar is the one on the left and the desired output bar is the one on the right

Fig. C-10 A volume fraction prediction for case 586

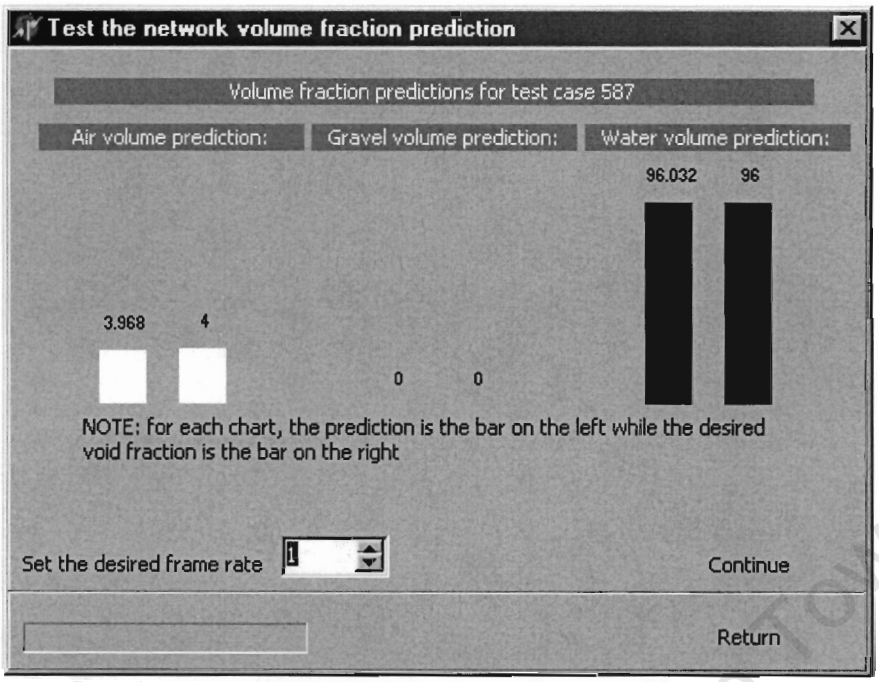

A volume fraction prediction of the hydrocyclone operating with an air core approximated as 4% air and 96% water is shown. The case number is 587. The frame rate at which the database was viewed had to be slowed down to one frame per second, to allow the picture to be taken. The picture shows two bars side by side for each case (air, gravel and water volume prediction). The network prediction bar is the one on the left and the desired output bar is the one on the right

Fig. C-11 A volume fraction prediction for case 587

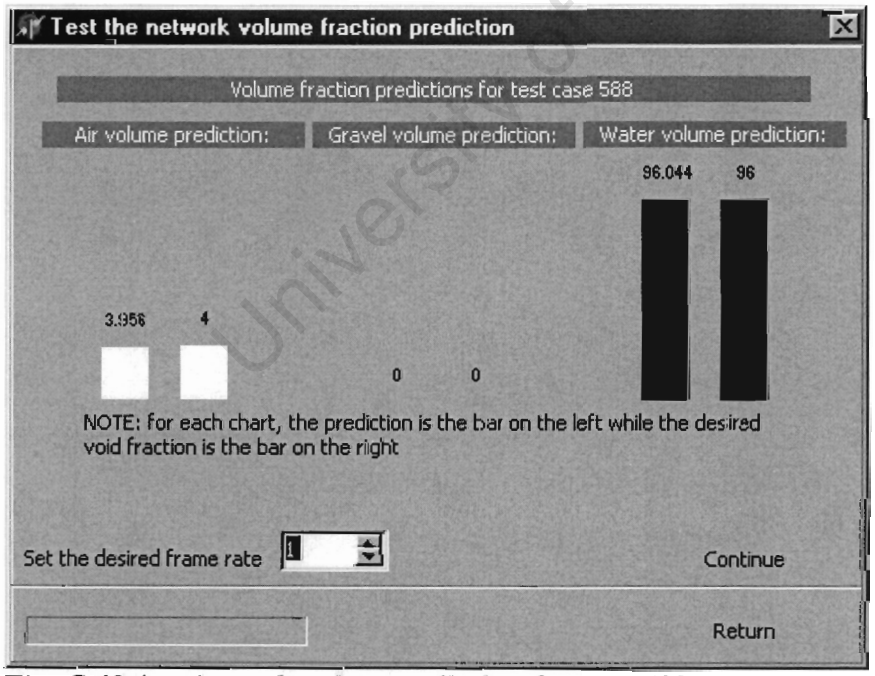

A volume fraction prediction of the hydrocyclone operating with an air core approximated as 4% air and 96% water is shown. The case number is 588. The frame rate at which the database was viewed had to be slowed down to one frame per second, to allow the picture to be taken. The picture shows two bars side by side for each case (air, gravel and water volume prediction). The network prediction bar is the one on the left and the desired output bar is the one on the right

Fig. C-12 A volume fraction prediction for case 588

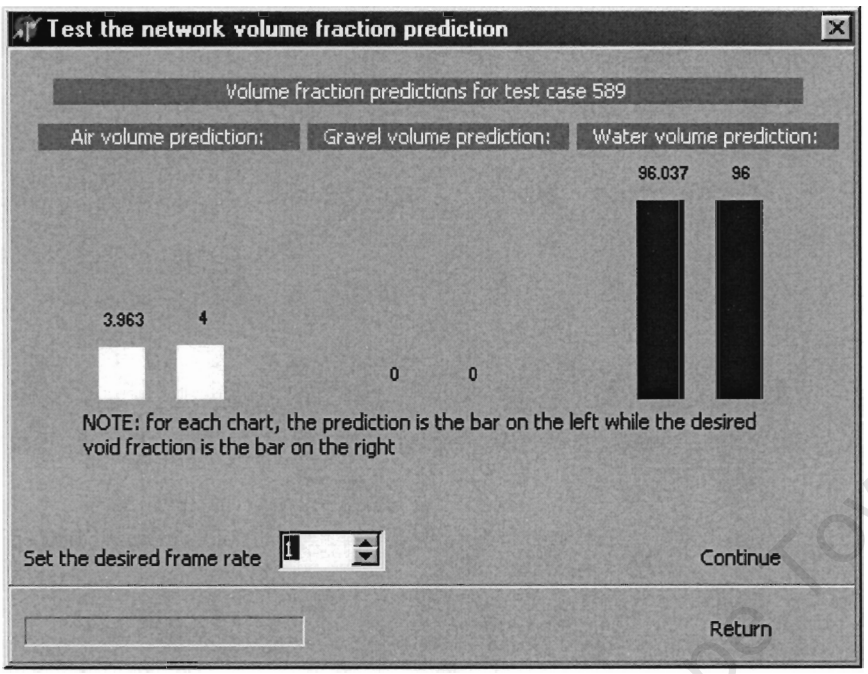

Fig. C-13 A volume fraction prediction for case 589

A volume fraction prediction of the hydrocyclone operating with an air core approximated as 4% air and 96% water is shown. The case number is 589. The frame rate at which the database was viewed had to be slowed down to one frame per second, to allow the picture to be taken. The picture shows two bars side by side for each case (air, gravel and water volume prediction). The network prediction bar is the one on the left and the desired output bar is the one on the right

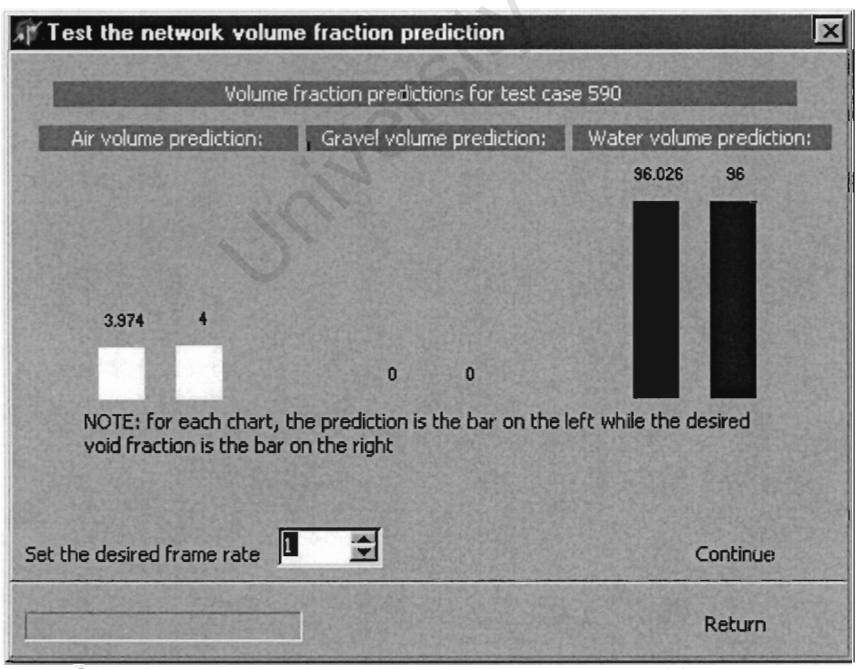

Fig. C-14 A volume fraction prediction for case 590

A volume fraction prediction of the hydrocyclone operating with an air core approximated as 4% air and 96% water is shown. The case number is 590. The frame rate at which the database was viewed had to be slowed down to one frame per second, to allow the picture to be taken. The picture shows two bars side by side for each case (air, gravel and water volume prediction). The network prediction bar is the one on the left and the desired output bar is the one on the right

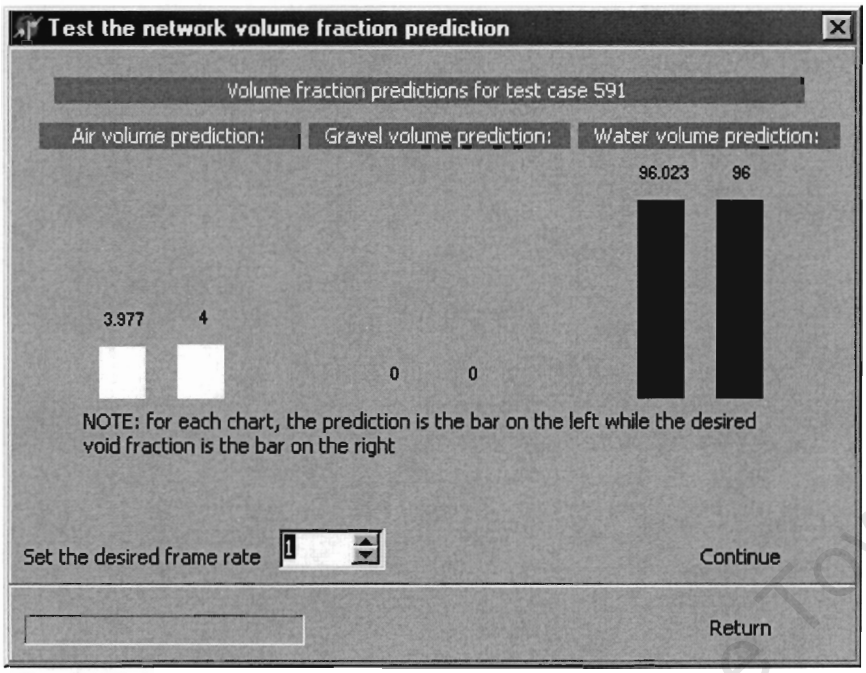

A volume fraction prediction of the hydrocyclone operating with an air core approximated as 4% air and 96% water is shown. The case number is 591. The frame rate at which the database was viewed had to be slowed down to one frame per second, to allow the picture to be taken. The picture shows two bars side by side for each case (air, gravel and water volume prediction). The network prediction bar is the one on the left and the desired output bar is the one on the right

Fig. C-15 A volume fraction prediction for case 591

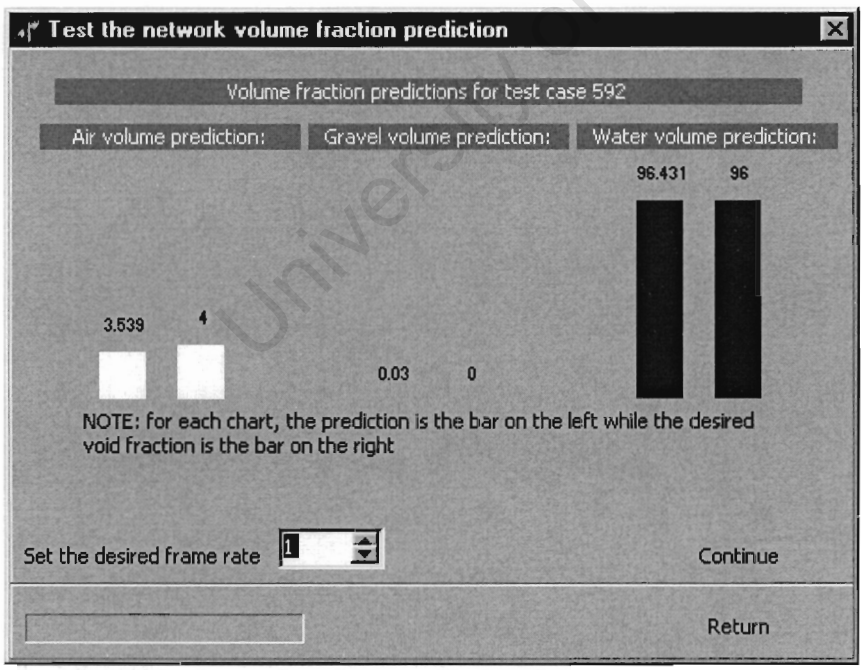

A volume fraction prediction of the hydrocyclone operating with an air core approximated as 4% air and 96% water is shown. The case number is 592. The frame rate at which the database was viewed had to be slowed down to one frame per second, to allow the picture to be taken. The picture shows two bars side by side for each case (air, gravel and water volume prediction). The network prediction bar is the one on the left and the desired output bar is the one on the right

Fig. C-16 A volume fraction prediction for case 592

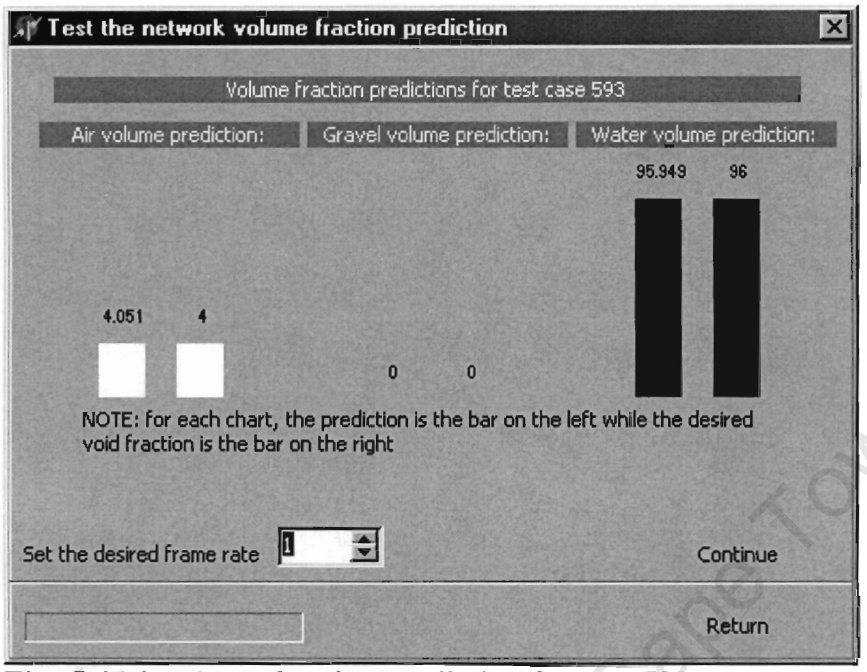

A volume fraction prediction of the hydrocyclone operating with an air core approximated as 4% air and 96% water is shown. The case number is 593. The frame rate at which the database was viewed had to be slowed down to one frame per second, to allow the picture to be taken. The picture shows two bars side by side for each case (air, gravel and water volume prediction). The network prediction bar is the one on the left and the desired output bar is the one on the right

Fig. C-17 A volume fraction prediction for case 593

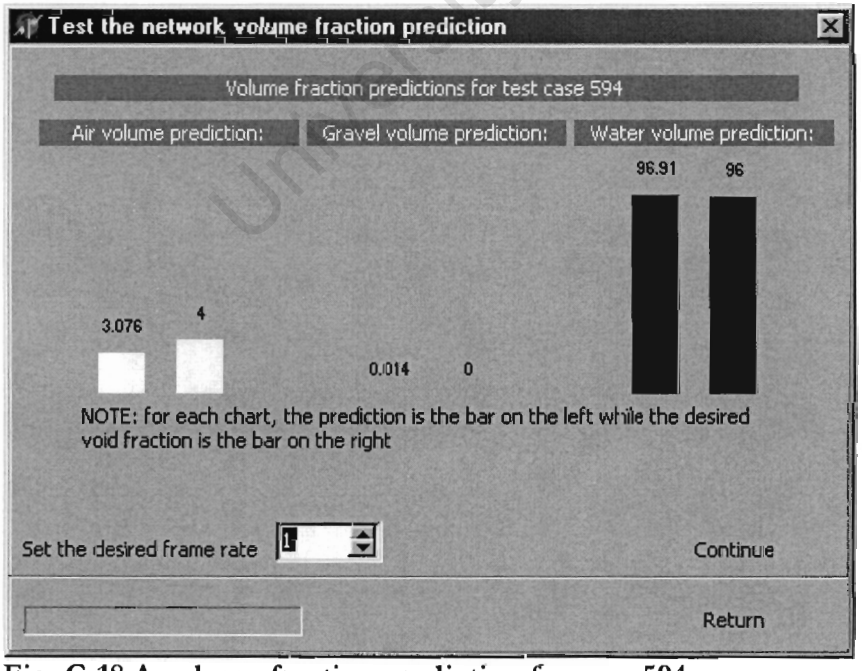

A volume fraction prediction of the hydrocyclone operating with an air core approximated as 4% air and 96% water is shown. The case number is 594. The frame rate at which the database was viewed had to be slowed down to one frame per second, to allow the picture to be taken. The picture shows two bars side by side for each case (air, gravel and water volume prediction). The network prediction bar is the one on the left and the desired output bar is the one on the right

Fig. C-18 A volume fraction prediction for case 594

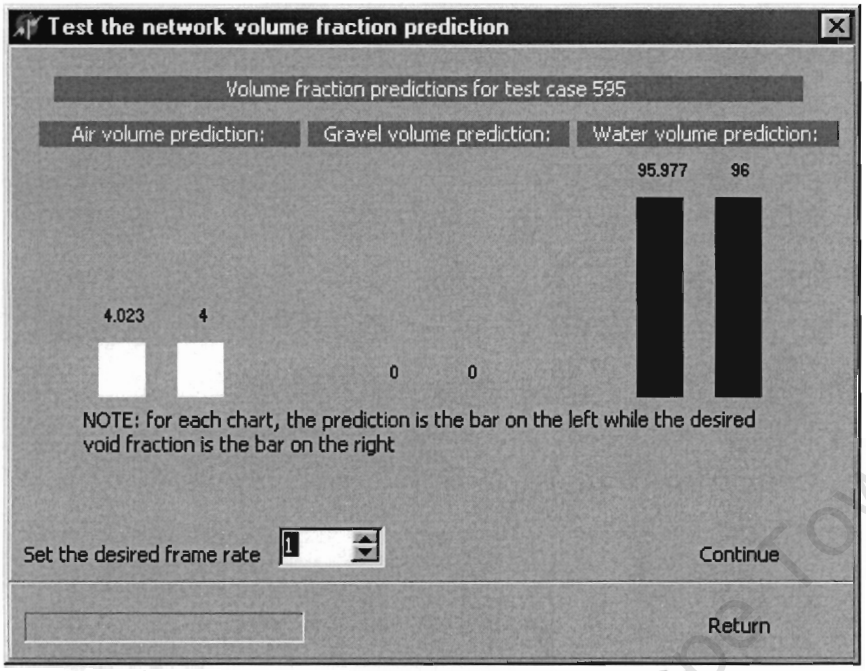

A volume fraction prediction of the hydrocyclone operating with an air core approximated as 4% air and 96% water is shown. The case number is 595. The frame rate at which the database was viewed had to be slowed down to one frame per second, to allow the picture to be taken. The picture shows two bars side by side for each case (air, gravel and water volume prediction). The network prediction bar is the one on the left and the desired output bar is the one on the right

Fig. C-19 A volume fraction prediction for case 595

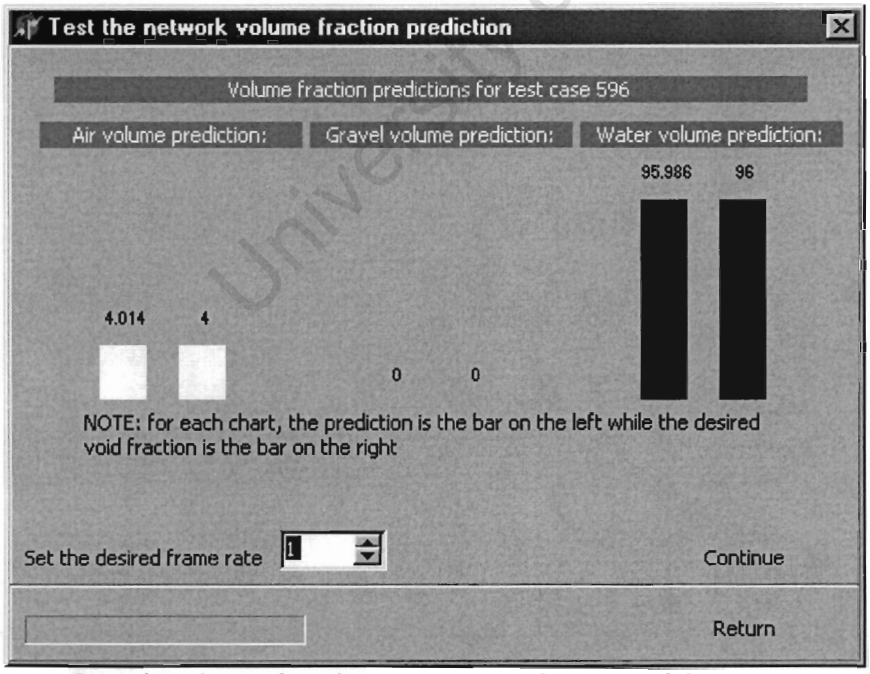

A volume fraction prediction of the hydrocyclone operating with an air core approximated as 4% air and 96% water is shown. The case number is 596. The frame rate at which the database was viewed had to be slowed down to one frame per second, to allow the picture to be taken. The picture shows two bars side by side for each case (air, gravel and water volume prediction). The network prediction bar is the one on the left and the desired output bar is the one on the right

Fig. C-20 A volume fraction prediction for case 596

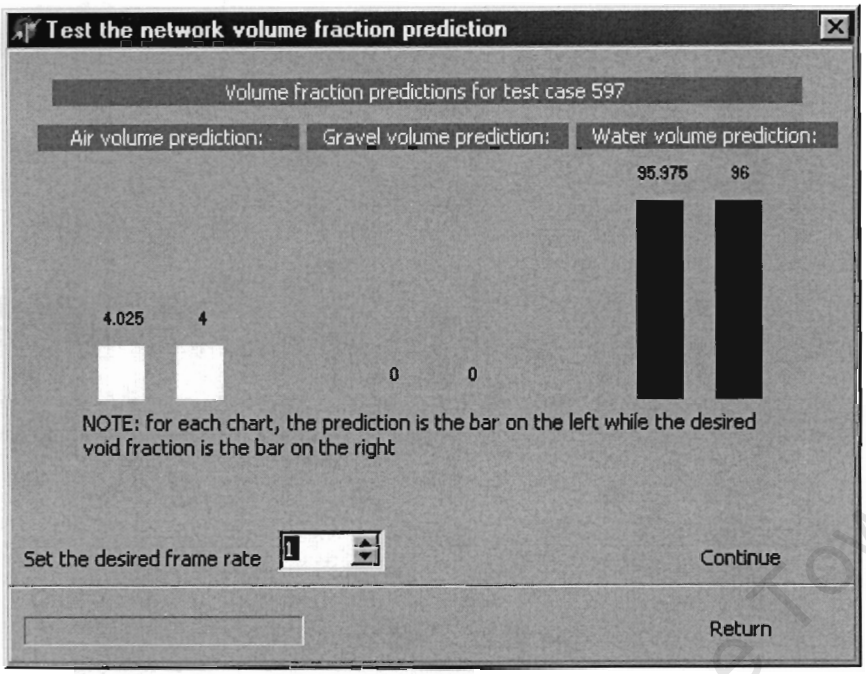

A volume fraction prediction of the hydrocyclone operating with an air core approximated as 4% air and 96% water is shown. The case number is 597. The frame rate at which the database was viewed had to be slowed down to one frame per second, to allow the picture to be taken. The picture shows two bars side by side for each case (air, gravel and water volume prediction). The network prediction bar is the one on the left and the desired output bar is the one on the right

Fig. C-21 A volume fraction prediction for case 597

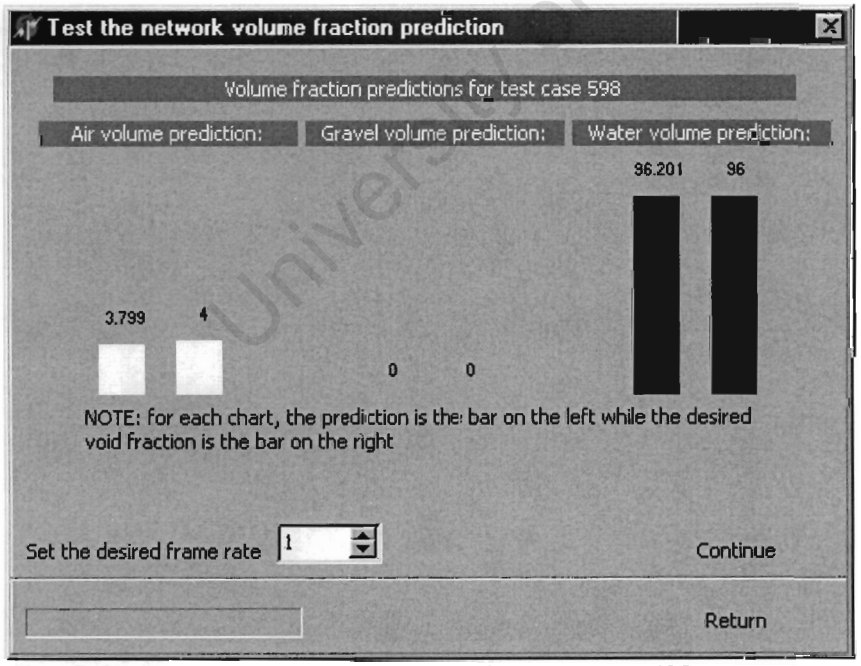

A volume fraction prediction of the hydrocyclone operating with an air core approximated as 4% air and 96% water is shown. The case number is 598. The frame rate at which the database was viewed had to be slowed down to one frame per second, to allow the picture to be taken. The picture shows two bars side by side for each case (air, gravel and water volume prediction). The network prediction bar is the one on the left and the desired output bar is the one on the right

Fig. C-22 A volume fraction prediction for case 598

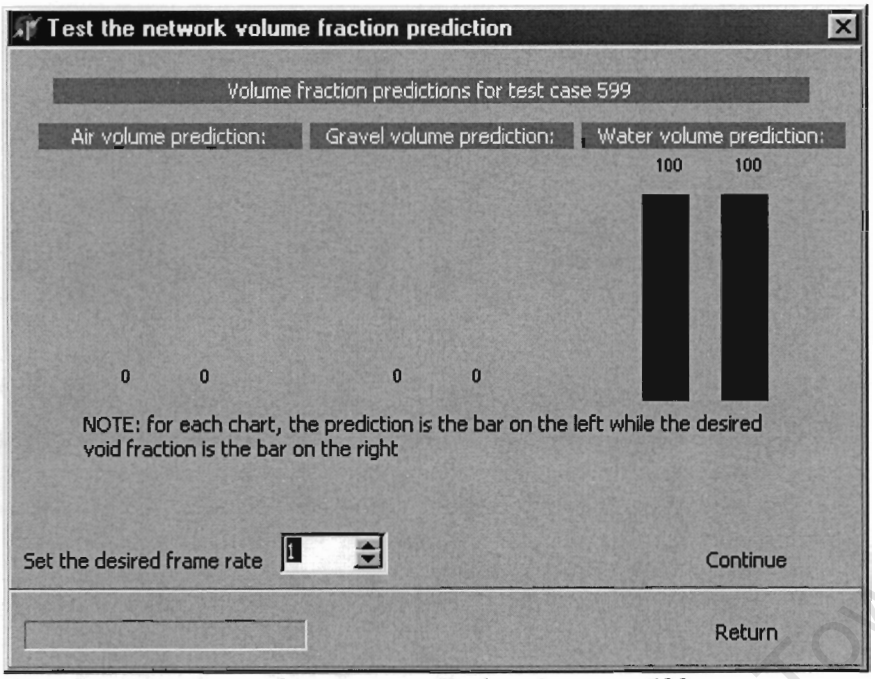

A volume fraction prediction of the hydrocyclone operating with an air core approximated as 4% air and 96% water is shown. The case number is 599. The frame rate at which the database was viewed had to be slowed down to one frame per second, to allow the picture to be taken. The picture shows two bars side by side for each case (air, gravel and water volume prediction). The network prediction bar is the one on the left and the desired output bar is the one on the right

Fig. C-23 A volume fraction prediction for case 599

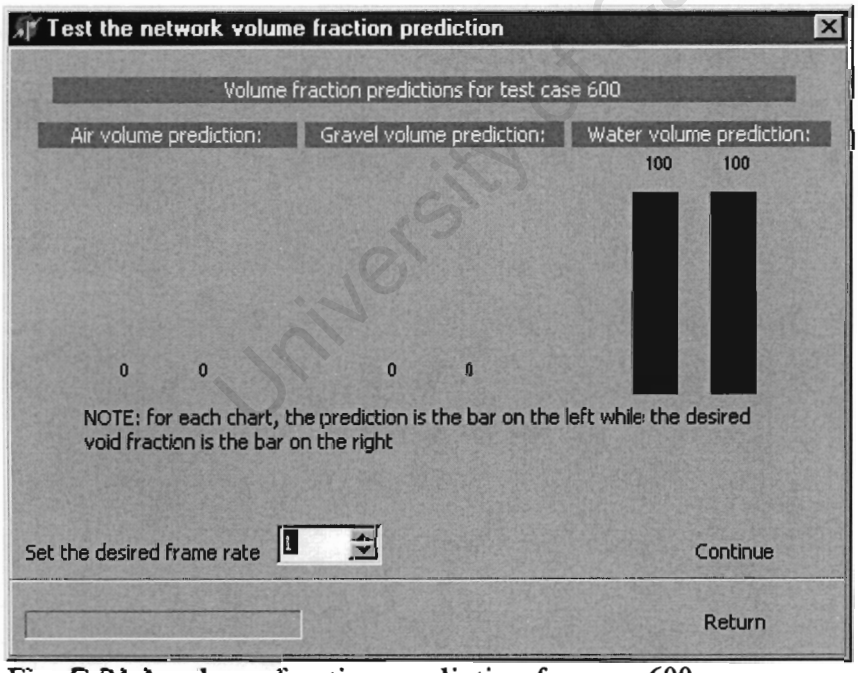

A volume fraction prediction of the hydrocyclone operating with an air core approximated as 4% air and 96% water is shown. The case number is 600. The frame rate at which the database was viewed had to be slowed down to one frame per second, to allow the picture to be taken. The picture shows two bars side by side for each case (air, gravel and water volume prediction). The network prediction bar is the one on the left and the desired output bar is the one on the right

Fig. C-24 A volume fraction prediction for case 600

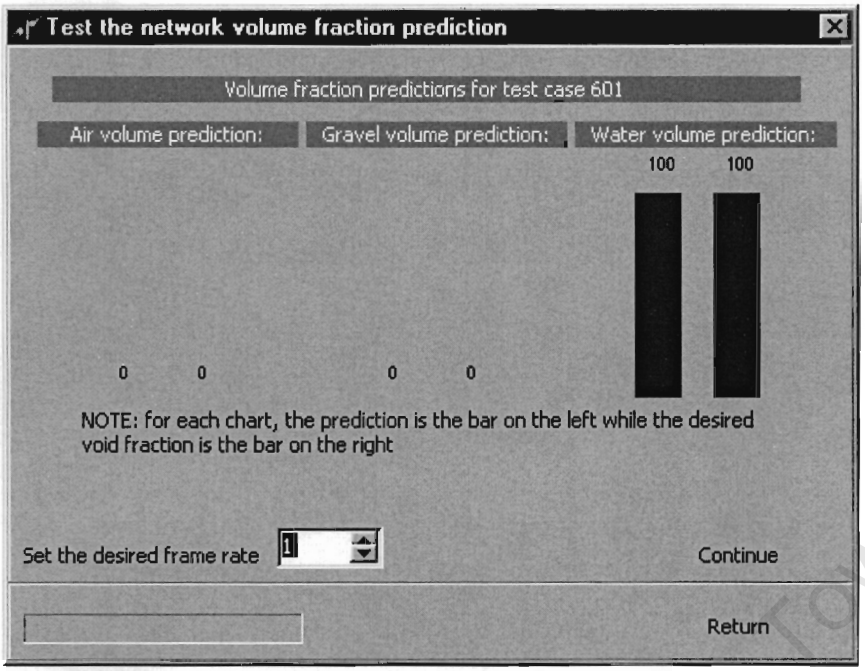

A volume fraction prediction of the hydrocyclone operating with an air core approximated as 4% air and 96% water is shown. The case number is 601. The frame rate at which the database was viewed had to be slowed down to one frame per second, to allow the picture to be taken. The picture shows two bars side by side for each case (air, gravel and water volume prediction). The network prediction bar is the one on the left and the desired output bar is the one on the right

Fig. C-25 A volume fraction prediction for case 601

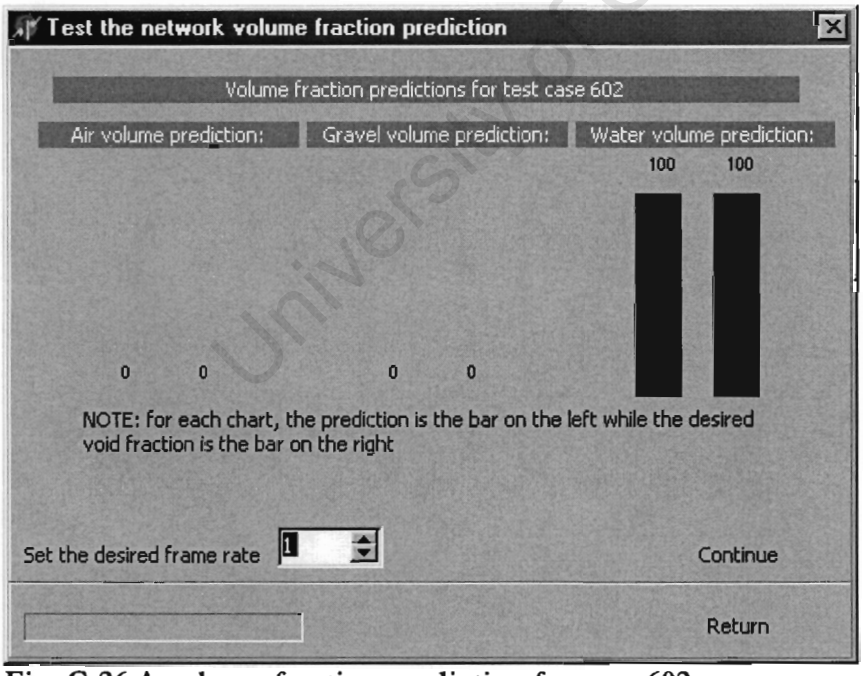

A volume fraction prediction of the hydrocyclone operating with an air core approximated as 4% air and 96% water is shown. The case number is 602. The frame rate at which the database was viewed had to be slowed down to one frame per second, to allow the picture to be taken. The picture shows two bars side by side for each case (air, gravel and water volume prediction). The network prediction bar is the one on the left and the desired output bar is the one on the right

Fig. C-26 A volume fraction prediction for case 602